

Cross-Sectional Stiffness Properties of Complex Drone Wings

Neeharika Muthirevula

This thesis is submitted to the faculty of the Virginia Polytechnic Institute and State University in partial fulfillment of the requirements for the degree of

Master of Science
In
Aerospace Engineering

Rakesh.K.Kapania
Mayuresh.J.Patil
Kevin.G.Wang

September 27, 2016
Blacksburg, VA

Keywords: Composites, Timoshenko beam, Cross-sectional Analysis, Drones, stress recovery, strain recovery.

Cross-Sectional Stiffness Properties of Complex Drone Wings

Neeharika Muthirevula

ABSTRACT

The main purpose of this thesis is to develop a beam element in order to model the wing of a drone, made of composite materials. The proposed model consists of the framework for the structural design and analysis of long slender beam like structures, e.g., wings, wind turbine blades, and helicopter rotor blades, etc. The main feature consists of the addition of the coupling between axial and bending with torsional effects that may arise when using composite materials and the coupling stemming from the inhomogeneity in cross-sections of any arbitrary geometry. This type of modeling approach allows for an accurate yet computationally inexpensive representation of a general class of beam-like structures.

The framework for beam analysis consists of main two parts, cross-sectional analysis of the beam sections and then using this section analysis to build up the finite element model. The cross-sectional analysis is performed in order to predict the structural properties for composite sections, which are used for the beam model.

The thesis consists of the model to validate the convergence of the element size required for the cross-sectional analysis. This follows by the validation of the shell models of constant cross-section to assess the performance of the beam elements, including coupling terms. This framework also has the capability of calculating the strains and displacements at various points of the cross-section. Natural frequencies and mode shapes are compared for different cases of increasing complexity with those available in the papers. Then, the

framework is used to analyze the wing of a drone and compare the results to a model developed in NASTRAN.

Cross-Sectional Stiffness Properties of Complex Drone Wings

Neeharika Muthirevula

GENERAL AUDIENCE ABSTRACT

This thesis is based on developing framework for structural design and analysis of long slender beam-like structures, e.g., airplane wings, helicopter blades, wind turbine blades or any UAVs. The framework is used for the generation of beam finite element models which correctly account for effects stemming from material anisotropy and inhomogeneity in cross sections of arbitrary geometry.

The framework for beam analysis consists of main two parts, cross-sectional analysis of the beam sections and then using this section analysis to build up the finite element model. The cross-sectional analysis is performed in order to predict the structural properties for composite sections, which are used for the beam model. This type of modelling approach allows for an accurate yet computationally inexpensive representation of a general class of beam-like structures.

Acknowledgements

I would like to thank my advisor, Dr. Rakesh K. Kapania, for giving me the opportunity to work as part of his group. Thank you for your support, guidance, patience and most importantly, for having faith in me. My special thanks to Wei Zhao, for giving me a great start in this project and always being able to answer my work related questions.

I would like to acknowledge NASA NRA, —Lightweight Adaptive Aeroelastic Wing for Enhanced Performance across the Flight Envelope, NRA NNX14AL36A, Mr. John Bosworth Technical Monitor, for funding this research.

A big thanks to all my friends for their support throughout the development of my thesis. I would never have even been in a position to complete this work without the loving support of my parents, and my little sister Archana, who have always encouraged me through all of my academic ventures.

Neeharika Muthirevula

Content

ABSTRACT	ii
GENERAL AUDIENCE ABSTRACT.....	iv
Acknowledgements	v
Content	vi
List of Figures	viii
List of Tables.....	xi
1. Introduction	1
1.1.Introduction:	1
1.2.Motivation:	2
1.3.Objectives:.....	4
1.4. Overview:.....	4
2. Literature review	6
2.1. Cross-sectional Analysis:.....	7
2.2. Beam Formulations Review:.....	8
2.2.1 Beam Formulations (Analytical expressions):.....	9
2.2.1 Beam Formulations (Finite Element method):.....	12
2.3. Scope:	18
3. Cross-sectional Analysis Theory.....	19
3.1. Cross-Sectional Analysis:	19
3.2. Equilibrium equations for cross-section:	20
3.3. Solutions for the Equilibrium equations for any cross-section:.....	26
3.4. Shear Center and Elastic Center:.....	27
3.4.1. Shear Center:	27
3.4.2. Elastic Center:	28
3.5. Implementation:	29
3.6. Cross-sectional mass matrix:.....	33
3.7.Strain and stress recovery:	34

4. Beam Formulations.....	38
4.1. Introduction:	38
4.2. Beam finite element model.....	39
5. Validation	44
5.1. Convergence Test:.....	45
5.2. Validation –Shear Center:	49
5.2.1. C- Channel Section:	49
5.2.2. I- Channel Section:.....	51
5.2.3 Box Beam Section:.....	52
5.3. Validation –Cross-sectional Analysis:	54
5.3.1. Square Cross-section:	54
5.3.2. Cylindrical Shell:.....	56
5.3.3. Three Cell Cross-section:	60
5.4. Validation –Timoshenko Beam Analysis:	64
5.4.1. Elliptical Beam:	64
5.4.2. Rectangular Box Beam:	68
5.4.3. Airfoil Section:	71
5.5. Stress – Strain Validation:.....	75
6. Natural Frequencies of a Drone.....	78
7. Conclusion	88
References:	90
Appendix:	99

List of Figures

Figure.1.1. Application of the beam modeling [1]	1
Figure.1.2. Drone (mAEWing1) used in the PAAW project, (Credit: University of Minnesota).	3
Figure.3.1. Cross-section analysis and design processes	20
Figure.3.2. Cross-section Forces, Moments in cross-sectional coordinate system [5]	21
Figure.3.3. Total deformation of the c/s is the sum of reference coordinate system of the c/s rigid body motions and warping deformations [5].	22
Figure.3.4. Example of the two dimensional finite element mesh of a box beam section using four node isoparametric finite elements.	30
Figure.3.5. Isoparametric coordinate system, nodal positions and position of Gauss points for the four node isoparametric plane finite element. [5]	30
Figure.3.6. Determination of the material constitutive matrix at each finite element of the cross-section mesh. (a) Definition of the cross-section coordinate system $XY Z$ and element coordinate system xyz . (b) Convention adopted for the rotation of the element coordinate system xyz into the fiber plane coordinate system $x'y'z'$. (c) Convention adopted for the rotation of the fiber plane coordinate system $x'y'z'$ into the material coordinate system 123 [4,5]	35
Figure.4.1. General Beam Element with external forces [1].	39
Figure.4.2. Beam kinematics for stiffness matrix (in red) and reference systems: global $\{O, X-X, Y-Y, Z-Z\}$, local for stiffness matrix $\{T, X'-X', Y'-Y', Z'-Z'\}$ and local for	

mass matrix $\{G, X''-X'', Y^*-Y^*, Z^*-Z^*\}$ [1, 3, 6-10]	40
Figure5.1. Cross-section coordinate system [5]	44
Figure 5.2. Rectangular box beam cross-section of the geometry.	46
Figure.5.3. Plot of stiffness components with respect to number of elements	48
Figure.5.4. C- Section (Open section)	49
Figure.5.5. I- Section (Open section)	51
Figure.5.6. Rectangular Box Beam Section (Closed section)	53
Figure.5.7. Square Cross-section	54
Figure.5.8. Square Cross-section warping displacements	56
Figure.5.9. Cylindrical shell Cross-section with isotropic materials.	57
Figure.5.10. Circular Cross-section warping displacements	59
Figure.5.11 Three cell cross-section which has the top-bottom face of orthotropic material (P1) oriented at 45o and the vertical webs as isotropic material (P2).	60
Figure.5.12. Three cell Cross-section warping displacements	63
Figure.5.13. Elliptical Cross-section cantilevered beam.	64
Figure.5.14. First six mode shapes of an elliptical cantilevered beam	67
Figure.5.15. Rectangular box beam Cross-section [20o/-70o/20o/-70o/-70o/20o] layups with T300/5208 Graphite	68
Figure.5.16. First six mode shapes of a cantilevered beam with box beam cross-section...	71
Figure.5.17. Mesh of the airfoil model in NASTRAN	72
Figure.5.18. Cross-section mesh of the airfoil section used in the framework.	72

Figure.5.19. Mode shapes for the airfoil c/s.	74
Figure.5.20. Square cross-section cantilevered beam	75
Figure.5.21. Fiber Plane coordinate system of the square cross-section.	75
Figure.5.22. Stress contour of the cross-section. The light shaded lines are from the cross-sectional analysis tool, the dark lines indicate the stress from the NASTRAN model.	77
Figure.6.1. Geometry of the maewing1 model	78
Figure.6.2. Depiction of the materials for the wing section of maewing1	79
Figure.6.3. Depiction of the cross-section segments considered while modeling the beam.....	82
Figure.6.4. Airfoil mesh of maewing1 section 18.	82
Figure.6.5. Airfoil mesh of maewing1 section 36 which is the intersection of the outer wing and inner wing.	83
Figure.6.6. Six mode shapes of maewing1 WS#1	85
Figure.6.7. Six mode shapes of maewing1 WS#3	87

List of Tables

Table.5.1. Dimensions and Material properties for the c/s in the figure 5.2	46
Table.5.2. Different data sets for Cross-sectional Properties of the box beam geometry in figure 5. 2.....	47
Table.5.3. Cross-sectional Properties of the box beam geometry in figure 5.2.	47
Tabel.5.4. Dimensions and Material properties for the cross section shown in fig.5.4	50
Table.5.5. Comparison of shear center for the C-section	51
Table.5.6. Dimensions & Material properties for the I- c/s.	52
Table.5.7. Comparison of shear center for the I-section.	52
Table.5.8. Material properties for the cross section shown in figure 5.6.	53
Table.5.9. Comparison of shear center for the cross section shown in figure 5.6	53
Table.5.10. Material properties for the square cross section shown in figure 5 .7	55
Table.5.11. Cross-sectional properties for the cross section shown in figure 5.7	55
Table.5.12. Material properties for the cross section shown in figure 5.9	57
Table.5.13. Cross-sectional properties for the cross section shown in figure 5.9.	58
Table 5.14. Material properties for the cross section shown in figure 5.11.	61
Table.5.15. Comparison of cross-sectional properties for the cross section shown in figure 5.11	62
Table.5.16. Comparison of mass properties for the cross section shown in figure 5.11 ...	62

Table.5.17. Dimension & material properties for the cross section shown in fig.5.13....	65
Table.5.18. Cross-sectional properties for the cross section shown in figure 5.13	65
Table.5.19. Comparison of natural frequencies with respect to NASTRAN for the cross section shown in figure 5.13	66
Table.5.20. Material properties for the cross section shown in figure 5.15	69
Table.5.21. Comparison of the cross-sectional properties for the cross section shown in figure 5.15	69
Table.5.22. Comparison of the natural frequency for the cross section shown in figure.5.15.	70
Table.5.23. Comparison of the cross-sectional properties for the airfoil cross section. ...	73
Table.5.24. Comparison of the natural frequencies for the airfoil cross section.	73
Table.6.1. Material properties of <i>maewing1</i>	81
Table.6.2. Cross-sectional properties of section12 of <i>maewing1</i>	83
Table.6.3. Comparison of natural frequencies of the model with wingset WS#1	84
Table.6.4. Comparison of natural frequencies of the model with wingset WS#3.	86

1. Introduction

1.1.Introduction:

Beams are structures having one dimension much larger than the other two. Beam models are often used in design, because they can provide valuable insight into the behavior of the structures with much less effort than more complex models. Beam theories have several engineering applications and are often used to model helicopter rotor blades, wind turbine blades, aircraft wings, robot arms, bridges, etc. as shown in Fig.1.1.



Figure.1.1.Application of the beam modeling [1].

When working with beam models it is assumed that the geometry of the solid is represented by the geometry of its cross-sections and that the beam is represented by the line that goes through the reference points of these sections. The analysis of the beam is separated into two parts. The first part concerns the two-dimensional analysis of the crosssection properties while the second regards the one-dimensional analysis of the global response of the beam. This separation allows for a reduction in the problem size that makes beam models a suitable alternative for computationally intensive applications like optimal design frameworks.

Some assumptions must be observed when working with beam models. It is assumed that the reference line presents a certain degree of continuity. Moreover, the section geometry, when not constant along the length of the beam is restricted to moderate variations. The same holds for the structural properties. Namely, the material properties and applied loads should also vary smoothly along the length of the beam. Consequently, the resulting displacements, strains and stresses will also present a smooth variation. These geometrical and structural restrictions do not apply in the cross-section face along the width and height directions. The cross-section geometry can be arbitrarily defined and the materials with distinct mechanical properties may be distributed inhomogeneous in the cross-section [1-3].

1.2.Motivation:

An unmanned aerial vehicle (UAV), commonly known as a drone is an aircraft which can be controlled remotely without any human pilot aboard. These are often used in military applications, although their use is expanding in commercial, scientific, recreational, and agricultural. A typical unmanned aircraft is made of light composite materials to reduce weight and increase maneuverability. This composite material strength allows drones to cruise at extreme maneuver loads. The geometry of the drone is varyingly complex with different composite materials integrated in to the system.

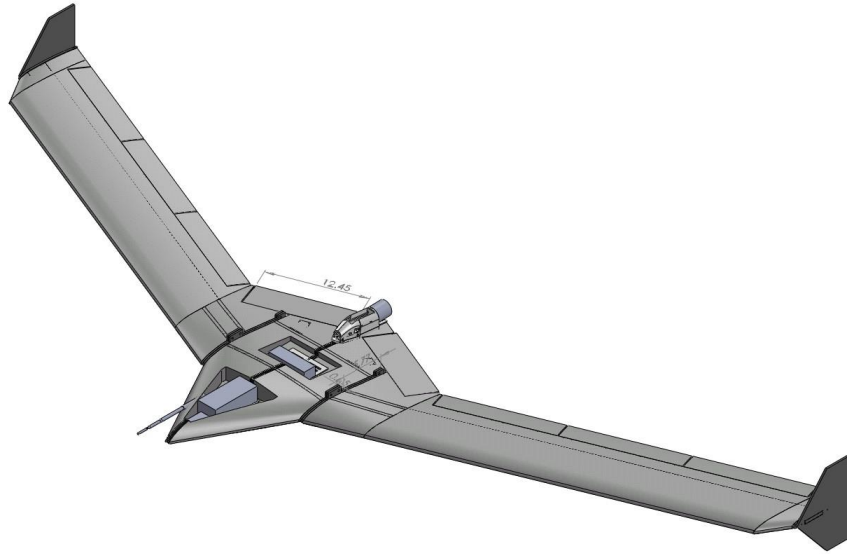


Figure.1.2. Drone (*mAEWing1*) used in the PAAW project, (Credit: University of Minnesota).

The generation of the beam finite element matrices for such complex geometries entails the determination of the cross-section stiffness and mass properties. For isotropic beams with simple geometries the determination of these properties is usually easy. However, the development of accurate beam models to represent the wings of a composite drone is not so simple. The wings have complex geometries and are made of combinations of different composite materials with different degrees of anisotropy. Simplified approaches have been used in the past to estimate the wing crosssection properties by taking the equivalent stiffness values from static tests to represent the stiffness distribution of the complex composite drone. However, this model with equivalent test stiffness properties does not meet the desired level of accuracy for the implementation in the aeroelastic or control models. These models moreover do not capture the coupling effects arising due to the composite structure.

This project is motivated to provide a robust beam model to capture the dynamic behavior of wing of a drone by utilizing the anisotropic properties of composite materials in an intelligent manner. To obtain this objective, one of the main building blocks needed is a general, fully coupled and validated beam element. Also needed are effective and exact methods for determination of stiffness and mass

coefficients of the cross-section which can be used for the fully coupled beam element based on 3D geometry and material data for the wing. The main purpose of the project described in this report is to develop such a beam element with exact prediction of stiffness and mass coefficients. This model will be used in the framework for multidisciplinary optimization of a drone wing.

1.3.Objectives:

The main purpose of this thesis is to develop a 3D beam element in order to model the wing of a drone. The wing includes various coupling effects that may arise when using composite materials and also geometric arbitrarily shape.

The main objective is further divided into two main objectives. The extraction of the cross-sectional properties of an arbitrarily geometrically shaped cross-section made of composite material and development of a 3D beam element model using these extracted properties.

The model is taken with the input of arbitrary geometry and the material properties. Then this model is discretized into different sections to build a model for cross-sectional analysis. Then for each cross-section, the sectional properties are determined. These sectional properties are then used for a beam element formulation.

1.4. Overview:

Literature review and the formulation used in the beam model are described in Chapter 2.

This chapter describes the structural beam model used in this thesis. The beam model is developed in a finite element context. The cross-section stiffness and mass properties are estimated using a finite element cross-section analysis formulation which is able to correctly estimate the effects of material anisotropy and inhomogeneity. Chapter 3 underlines the theory behind the cross-sectional

analysis of any arbitrary cross-section. Chapter 4 discusses the theory used in the formulation of the Timoshenko beam.

To validate the formulation used in the framework, several cases have been studied and their results are compared to data available in research papers, this is given in Chapter 5. Chapter 6 focuses on the implementation of the framework on the wing of a drone. Finally, Chapter 7 briefly summarizes the work done in this thesis and presents the conclusions.

2. Literature review

The fiber-reinforced composite materials are ideal for structural applications where high specific strength-to-weight and specific stiffness-to-weight ratios are required. Composite materials can be tailored to meet the particular requirements of stiffness and strength by altering lay-up and fiber orientations. The ability to tailor a composite material to its function is one of the most significant advantages of a composite material over an ordinary material. So the research and development of composite materials in the design of aerospace, mechanical and civil structures has grown tremendously in the past few decades. It is essential to know the vibration characteristics of these structures, which may be subjected to dynamic loads in complex environmental conditions. If the frequency of the loads variation matches one of the resonance frequencies of the structure, large translation/torsion deflections and internal stresses can occur, which may lead to failure of structure components.

A variety of structural components made of composite materials such as aircraft wing, helicopter blade, vehicle axles, and turbine blades can be approximated as laminated composite beams, which requires a deeper understanding of the vibration characteristics of the composite beams. The practical importance and potential benefits of the composite beams have inspired continuing research interest. Beams are structures which have one dimension (length) much larger than the other two (the cross-section dimensions). Crosssection analysis tool computes the sectional properties of beams in three phases: define the geometry, generate the mesh, and perform finite element analysis. The literature review on cross-sectional analysis and beam modeling is given below in two different sections.

2.1. Cross-sectional Analysis:

About the cross-sectional analysis, there have been many theories developed over the years. Two of the most accurate and efficient beam theories that have emerged from a desire to incorporate composites as well as higher-order warping effects into the design process have been developed by Hodges [2] and Giavotto et al. [4]. These two main theories are applicable to various sections of arbitrary geometry and anisotropic materials. The adhoc approach is used in the earlier days for the analytical cross-sectional analysis of blades made of isotropic materials. The different theories are discussed below.

The Hodges beam theory VABS (Variational Asymptotic Beam Sectional analysis) is the more well-known theory as it is used extensively in industry, and has been highly verified. Its development over the past ten years is described in [6–10]. VABS can perform a classical analysis for beams with initial twist and curvature with arbitrary reference crosssections. VABS is also capable of capturing the trapeze and Vlasov effects, which are useful for specific beam applications. VABS is now able to calculate the 1-D stiffness matrix with transverse shear refinement for any initially twisted and curved, inhomogeneous, anisotropic beam with arbitrary geometry and material properties. Finally, VABS can recover the 3-D stress and strain fields, if required, such as finding stress concentrations, interlaminar stresses, etc.

While Giavotto et al.'s formulation was used to develop a code called NABSA (Nonhomogeneous Anisotropic Beam Section Analysis), it has been used less extensively. Giavotto et al. [4] can be easily implemented in any conventional general purpose finite element program without any undue approximation and without the need to develop special

elements. Recently, it was implemented in the development of the code BECAS (Beam Cross-sectional Analysis Software) by Blasques [5]. Despite the excellence both of these tools present, neither of them are commercially available.

The ad hoc approach is based on the assumptions about the displacement or stress field. Ad hoc is the introduction of a set of kinematics assumptions which enables us to express the 3D displacements in terms of the 1D beam displacements, the 3D strain field in terms of 1D beam strains. Assumptions of the stress field are also used to relate the 3D stress field with the 3D strain field. The ad hoc analyses have been discussed in the papers by Smith and Chopra [72], Pai and Nayfeh [73], Song and Librescu [74], Loughlan and Ata [75], Massa and Barbero [76], Johnson et al. [77], and Jung et al.[78]. All of these are restricted to the thin-walled cases except Jung et al. [78]. The most accurate and powerful of the ad hoc methods to date appears to be Jung et al. (2002); although it is only applicable to specific cross-sectional geometries, it yields results that compare favorably with those from finite-element-based analyses. However, the ad hoc analyses generally invoke assumptions that do not hold in the general case, such as ignoring the hoop stress or hoop moment, or ignoring shell bending measures. So, in general cases of arbitrary geometry and anisotropic material ad hoc approach does not yield better results as compared to the approaches of Giavotto [4] and VABS [1,3, 6-10]

2.2. Beam Formulations Review:

Many researchers have developed numerous solution methods in last 20 years for the dynamic representation of engineering applications such as rotor blades, wind turbines,

landing gear, wings, etc. Some of the key points pertaining to each paper have been noted below.

2.2.1 Beam Formulations (Analytical expressions):

There have been many papers in which the exact solutions of composite beams have been derived analytically. Discussion about the various papers used in the derivation of the analytical expressions of the composite beams is given below.

Raciti and Kapania [10] surveyed various of developments in the vibration analysis of laminated composite beams. First, a review of the recent studies on the free-vibration analysis of symmetrically laminated beams is given. These studies have been conducted for various geometric shapes and edge conditions. Both analytical (closed-form, Galerkin, Rayleigh-Ritz) and numerical methods have been used. Because of the importance of unsymmetrically laminated structural components in many applications, a detailed review of the various developments in the analysis of unsymmetrically laminated beams and plates also is given. This paper is great source of information on the development of various theories for the vibration analysis of composite beams.

Chandrashekhara et al. [11] found the accurate solutions based on first order shear deformation theory including rotary inertia for symmetrically laminated beams. The laminated beams are constructed by a systematic reduction of the constitutive relations of the three-dimensional anisotropic body. They have derived the basic equations based on the parabolic shear deformation theory. The detailed explanations and assumptions used in the theory are given by Bhimaraddi and Chandrashekhara [12]. However, these equations and derivations are found for simple geometrical laminated beam.

A third-order shear deformation theory for static and dynamic analysis of an orthotropic beam is given by Soldatos and Elishakoff [13]. They mainly discuss about incorporating the impact of transverse shear and transverse normal deformations in the beam modeling. This is done for a specific cross-section and have not been implemented for arbitrary geometry.

Abramovich [14] derived analytically the exact solutions for symmetrically laminated composite beams with 10 different boundary conditions. This theory also considers shear deformation and rotary inertia.

Krishnaswamy et al. [15] used the hamilton's principle to calculate the dynamic equations governing the free vibration of laminated composite beams. The impacts of transverse shear deformation and rotary inertia were included in the formulation. However, analytical solutions by applying the Lagrange multipliers method were obtained only for the unsymmetrical laminated beams.

Khadeir and Reddy [18] studied the analytical solutions of various beam theories to study the free vibration behavior of cross-ply rectangular beams with arbitrary boundary conditions. However, the analytical solutions are provided only for a specific crosssection. The analytical solutions for laminated beams based on first-order shear deformation theory including rotary inertia is obtained by Eisenberger et al. [20]. In this, the equation of motion for the beam including the rotary inertia has been derived using Hamilton's principle. But, this is done only for specific boundary conditions to derive the analytical solution for the beam element.

Banerjee and Williams [21] studied the exact dynamic stiffness matrix for a uniform, straight, bending–torsion coupled, composite beam without the effects of shear deformation and rotary inertia included. However, in the subsequent papers, Banerjee[23] have derived the analytical solution for laminated composite beam with the shear effects and rotary inertia. Banerjee [39-40] reported the exact expressions for the frequency equation and mode shapes of composite Timoshenko beams with cantilever end conditions. The impacts of material coupling between the bending and torsional modes of deformation together with the effects of shear deformation and rotary inertia was taken into account when formulating the theory. But, the derivations are only provided for few examples and are not done for complex sections.

Kant [24,61] has derived an analytical solution to the dynamic analysis of the laminated composite beams using a higher order refined theory. This theory also includes the effect of transverse normal strain. However, this model fails to satisfy the traction- free surface conditions at the top and bottom of the beam.

Shimpi and Ainapure [25] presented the free vibration of two-layered laminated cross-ply beams using the variation ally consistent layer wise trigonometric shear deformation theory. But, this is done only for the two layered composite beam.

A complete set of equations governing the dynamic behavior of pre-twisted composite space rods under isothermal conditions based on the Timoshenko beam theory was formulated. The anisotropy of the rod material, the curvatures of the rod axis, and the effects of the rotary inertia, the shear, axial deformations and Poisson effect were considered in the formulation reported by Yildirim [38]. Yildirim et al. [26-28] also analyzed the in-plane and out-of-plane free vibration problem of symmetric cross-ply laminated composite beams using the transfer matrix method. This examines the impacts of rotary inertia, axial and

shear deformations on the in-plane free vibration of symmetric cross-ply laminated beams.

However, Yildirim have only considered few cases.

These above papers have used the Hamilton's principle and equation of motion to derive the solution for the dynamic displacement of beam elements. However these papers are for specific examples and cannot be used for arbitrary cross-section and different boundary conditions of the laminated beam

2.2.1 Beam Formulations (Finite Element method):

The beam formulation based on the adhoc theories, small strain approximation, asymptotic beam theories, and engineering beam theories based on truncation method have been extensively researched. Discussions based on these papers are given below.

Friedmann et al. [3] and Hodges et al. [1] developed a nonlinear beam model including elastic flap- edge dynamics of a rotating beam. The analytical nonlinear beam equation of motion, coupling bending and torsion, becomes very long and complicated. Therefore, ordering schemes are introduced [6-8,62]. However, the derivation of the equation of motion with an ordering scheme is not consistent. It is very dependent on who conducts the analyses and which nonlinear effects produced by higher order terms are neglected.

Therefore, an exact beam theory which does not rely on an ordering scheme was introduced by Hodges [63]. The kinematics of this theory are exact. Simo[64], Simo et al.

[65], and Hodges [66] introduced a mixed formulation which is given in first order form.

The mentioned advanced beam theories focus on improving the kinematic representation of the beam motion. However, it is still assumed that beams are constructed from

homogeneous, isotropic materials, and linearly elastic. This does not fit with a composite beam model which must consider anisotropic material effects and warping effects Hodges and his colleagues [1, 6, and 66] introduced a finite element based cross-section analysis method using the variational asymptotic method to reduce a general three-dimensional nonlinear anisotropic elasticity problem into a two-dimensional linear cross-sectional analysis and a one-dimensional nonlinear beam analysis. Three-dimensional warping functions are asymptotically computed by two-dimensional cross-section analysis. The constitutive model for the one-dimensional nonlinear beam analysis is obtained as well. This approach is able to compute any initially twisted and curved, inhomogeneous, anisotropic beam with arbitrary cross-sectional geometries. But, the framework is not readily available for commercial use.

The static analysis of smart beams by using two finite elements with piezoelectric sensors/actuators is presented in the paper by Yu, et al. [19] and the elements used in this analysis are adhoc smart beam element (ADSBE) and variational asymptotic smart beam element (VASBE). A numerical integration method using the VABS program is used for taking the benefits of the discretized cross-section of the beam. A two-dimensional electromechanical cross-sectional analysis and a one-dimensional beam analysis are decoupled by the original three-dimensional electromechanical problem by using Timoshenko theory. The adhoc smart beam element presents considerable errors and, therefore, should not be used. Variational asymptotic smart beam element can show the error less than 8% for the prediction of the 3D results.

The free vibration behavior of laminated composite beams by the conventional finite element analysis using a higher-order shears deformation theory. The Poisson effect,

coupled extensional - bending deformations and rotary inertia are considered in the formulation studied by Chandrashekhara and Bangera [16]. However, this was only done for a simple geometry.

Teboub and Hajela [22] applied the symbolic computation technique to analyze the free vibration of generally layered composite beam on the basis of a first-order shear deformation theory. However, the model used did not consider the coupled extensional, bending and torsional deformations.

Ghugal and Shimpi [30] conducted a review of displacement and stress-based refined theories for isotropic and anisotropic laminated beams and discussed various equivalent single layer and layer wise theories for laminated beams. Higher-order mixed theory for determining the natural frequencies of a diversity of laminated Simply-Supported beams was presented by Rao et al. [31].

However, this paper only provides the formulation for simply supported beams.

Chakraborty et al. [32] used new refined first-order shear deformable finite element to analyze composite beams. This method is demonstrated in solving free vibration and wave propagation problems of laminated composite beam structures with symmetric as well as asymmetric ply stacking. But, this method does not consider the rotary inertia in its implementation.

A new approach combining the state space method and the differential quadrature method for freely vibrating laminated beams based on two-dimensional theory of elasticity was proposed by Chen et al. [34-35,43]. However, only straight beams with rectangular crosssections are considered.

Ruotolo [36] proposed a spectral element for anisotropic, laminated composite beams. The axial - bending coupled equations of motion were derived under the assumptions of the first-order shear deformation theory. But, this paper doesn't consider the coupling due to torsional deformation.

Raveendranath et al. [37] proposed a two-node curved composite beam element with three degrees of freedom per node for the analysis of laminated beam structures. The coupling between the flexural - extensional deformations together with transverse shear deformation based on first-order shear deformation theory was incorporated in the formulation. Also, the Poisson effect was incorporated in the formulation in the beam constitution equation.

Bassiouni et al. [41] proposed a finite element model to investigate the natural frequencies and mode shapes of the laminated composite beams. The transverse shear deformation was included in the formulation. However, the model needed that all lamina to have the same lateral displacement at a typical cross-section, but allowed each lamina to rotate a different amount from the other.

A new variational consistent finite element formulation for the free vibration analysis of composite beams based on the third-order beam theory was proposed by Shi and Lam [42]. The vibration analysis of cross-ply laminated beams with different sets of boundary conditions based on a third degree shear deformable beam theory was performed. The Ritz method was adopted to determine the free vibration frequencies and was presented by Aydogdu [44].

The free vibration behavior of symmetrically laminated fiber reinforced composite beams with different boundary conditions. The impacts of shear deformation and rotary inertia were considered and the finite-difference method was used to solve the partial differential equations describing the free vibration motion analyzed by Numayr et al. [46].

Subramanian [47] performed the free vibration analysis of laminated composite beams using two higher-order shear deformation theory and finite elements based theory. Both theories considered a quintic and quartic variation of in plane and transverse displacements

in the thickness coordinates of the beams, respectively, and satisfied the zero transverse shear strain- stress conditions at the top and bottom surfaces of the beams. But, this paper only considers straight beams with simple cross-sections.

A new layer wise beam theory for generally laminated composite beam and contrasted the analytical solutions for static bending and free vibration with the three-dimensional elasticity solution of cross-ply laminates in cylindrical bending and with three-dimensional finite element analysis for angle-ply laminates developed by Tahani [48] .

Finite elements have also been developed based on Timoshenko beam theory [50]. Most of the finite element models developed for Timoshenko beams possess a two node-two degree of freedom structure based on the requirements of the variation principle for the Timoshenko's displacement field. A Timoshenko beam element showing that the element converged to the exact solution of the elasticity equations for a simply supported beam provided that the correct value of the shear factor ,proposed by Davis et al. [51] , was used. However, this paper does not consider the coupling effects arising due to the arbitrary geometry.

Thomas et al. [52] proposed a new element of two nodes having three degrees of freedom per node, the nodal variables being transverse displacement, shear deformation and rotation of cross-section. The rates of convergence of a number of the elements were compared by calculating the natural frequencies of two cantilever beams. Further this paper gave a brief summary of different Timoshenko beam elements, but only for simple straight beams.

For the first time a finite element model with nodal degrees of freedom which could satisfy all the forced and natural boundary conditions of Timoshenko beam was developed by Thomas and Abbas [53]. The element has degrees of freedom as transverse deflection, total

slope (slope due to bending and shear deformation), bending slope and the first derivative of the bending slope.

A second-order beam theory requiring two coefficients, one for cross-sectional warping and the other for transverse direct stress, was developed by Stephen and Levinson [54]. Later Bickford [56] represented Levinson theory using a variational principle and also showed how one could obtain the correct and variationally consistent equations using the vectorial approach. Thus the resulting differential equation for consistent beam theory is of the sixth order; whereas that for the inconsistent beams theory it is of the fourth-order.

Krishnamurthy [57] proposed an improved theory in which the in-plane displacement was assumed to be cubic variation in the thickness coordinate of the beam whereas the transverse displacement was assumed to be the sum of two partial deflections, one due to bending and other due to transverse shear. However, this theory does not take in to account the effect of transverse normal strain and does not satisfy the zero strain-stress conditions at the top and bottom surfaces of the beam.

Bauchau[67-69] expanded Euler-Bernoulli beam theory including a transverse shear and a warping displacement. He extended the beam theory to orthotropic materials.

Heyliger and Reddy [58] also propose a higher order beam finite element for bending and vibration analysis of the beams. In this formulation, the theory assumes a cubic variation of the in-plane displacement in thickness coordinate and a parabolic variation of the transverse shear stress across the thickness of the beam. Further the theory satisfies the zero shear strain conditions at the top and bottom surfaces of the beam. But, it neglects the effect of the transverse normal strain.

However, there have been several drawbacks among these. There are difficulties in the formulation of appropriate one-dimensional constitutive laws in terms of known

threedimensional elastic constants; and they rely heavily on rather abstract tensor analysis, which can be troublesome for applications-oriented engineers

2.3. Scope:

By using the anisotropic properties of composite materials, bend-twist and other couplings can be built into the model. The bend-twist coupling causes the model to twist under the bending load and can be designed in a manner where the angle of attack decreases with increasing bending load. In order to understand the effect of the couplings in the preliminary stage, we need to find the stiffness matrix of the cross-section with all the coupling terms which are generally neglected. So, the framework used in this thesis is based on Giavotto et al. [4]. This module has been extensively verified against results from VABS and NASTRAN for its capabilities in cross-sectional analysis, and normal mode beam analysis, as well as 3D stress recovery. In the following Chapters, the derivations for the cross-sectional analysis formulation and the Timoshenko beam finite element model will be discussed.

3. Cross-sectional Analysis Theory

3.1. Cross-Sectional Analysis:

In any beam model, the cross-sectional analysis is a crucial part and will need a precise assessment of the cross-section properties, which includes the effort of the coupling, terms due to geometric or material anisotropy. Hodges [1] has presented a comprehensive and thorough historical overview of the developments in the beam-modeling field. Furthermore, Jung et al. [2] and Volovoi et al. [3] present an assessment of the different cross-section analysis formulations and include comparative results which highlight the advantages and limitations of each. The theory underlying the development of tool is mainly based on the formulation from Giovanni et al. [4].

The overall cross-sectional analysis process is shown in Fig.3.1. The analysis processes can be broken into three phases: model definition phase, computational phase, and post processing phase. The geometry and material properties are defined in model definition phase. Computational phase has two steps: mesh generation and finite element analysis phases. Finite element analysis is performed for computing the sectional properties and stress distributions over the cross-section. The final, post-processing phase provides the visualization of the computed stress fields. The entire process is integrated into a design environment that includes the definition of the cross-section, the analysis and the visualization of the results.

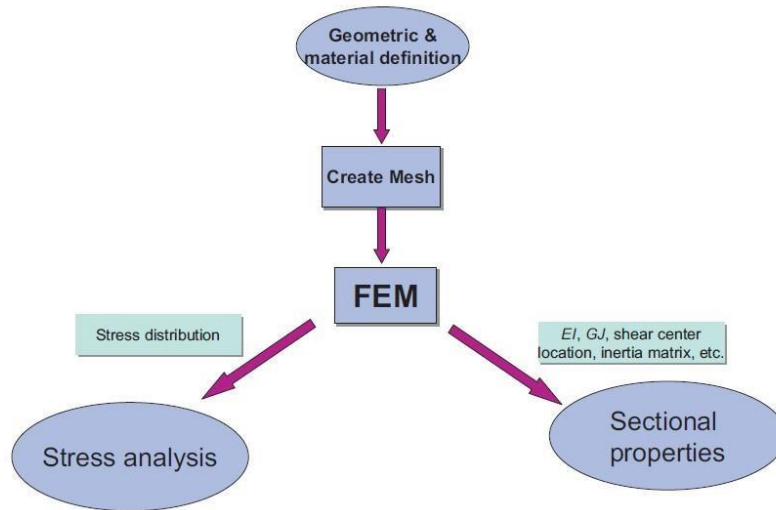


Figure.3.1. Cross-section analysis and design processes

The theory presented in the next sections is valid only for long slender structures which has certain level of geometric and structural continuity. Thus, there should not be any abrupt variations of the cross-section geometry and material properties along the beam length. Finally, the theory is based on the assumptions of small displacements and rotations. The equilibrium equation needed for the analysis is presented in the following sections.

3.2. Equilibrium equations for cross-section:

The displacement of a point in the section $s = [s_x \ s_y \ s_z]^T$ is defined with respect to the cross-section coordinate system x, y, z . The strain and stress, ϵ and ζ , are given as

$$\epsilon^T = [\epsilon_{xx} \ \epsilon_{yy} \ 2\epsilon_{xy} \ 2\epsilon_{xz} \ 2\epsilon_{yz} \ \epsilon_{zz}]$$

$$\sigma^T = [\sigma_{xx} \ \sigma_{yy} \ \sigma_{xy} \ \sigma_{xz} \ \sigma_{yz} \ \sigma_{zz}]$$

The stress and strain relate through Hooke's law

$$\zeta = Q \epsilon$$

where Q is the material constitutive matrix. It is assumed that the material is linear elastic, otherwise there are no restrictions regarding the level of anisotropy. The ordering of the entries in ϵ and δ is such that the tractions or the components of stress acting on the cross-section face, can be easily isolated as

$$p^T = [\sigma_{xx} \ \sigma_{yz} \ \sigma_{zz}]$$

The tractions p acting upon the cross-section face is statically equivalent to a force T and moment M as shown in Fig.3.2

$$T = \iint p \, dA ; \quad M = \iint n^T p \, dA ;$$

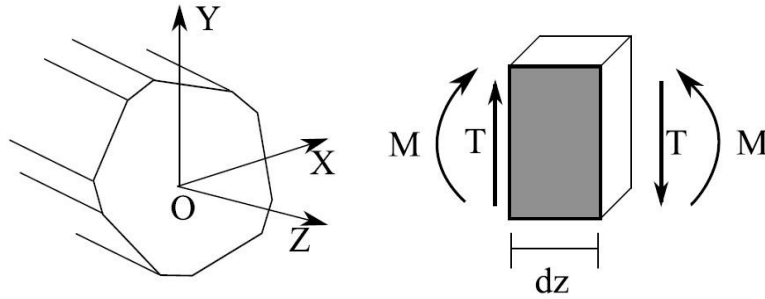


Figure.3.2. Cross-section Forces, Moments in cross-sectional coordinate system [5].

So, for the given cross-section, the forces is given by

$$H = [T^T \ M^T];$$

$$H = \int_A Z^T p \, dA \quad ; \quad Z = [I_3 | n^T]; \text{ Where } n \text{ is the position vector.}$$

The theory assumes that the cross-section deformation is defined by a superimposition of the reference coordinate system rigid body motions (i.e., the translations and rotations in the reference frame) and warping deformations g . This shown in Fig.3.3 [4]. So,

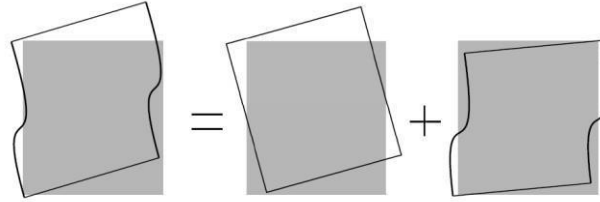


Figure.3.3. Total deformation of the c/s is the sum of reference coordinate system of the c/s rigid body motions and warping deformations [5].

$$s = v + g$$

Where $v = [v_x, v_y, v_z]^T$ is the vector of displacements associated with the rigid body translation and rotation of the cross-section. The vector $g = [g_x, g_y, g_z]^T$ is the vector of warping displacements associated with the cross-section .

Assuming small displacements and rotations, the rigid displacements v can be obtained as

$v = Zr$, a linear combination of the components of $r = [\chi^T \ \varphi^T]$. The components of $\chi(z) = [\chi_x \ \chi_y \ \chi_z]^T$ represent the translations of the cross-section reference point, while $\varphi(z) = [\varphi_x \ \varphi_y \ \varphi_z]^T$ are the cross-section rotations. The total displacement can be rewritten as

$$s = Zr + g$$

Using the strain displacement relations and also the above relations, we get

$$\epsilon = Bs + S \frac{\partial s}{\partial z}$$

Where, B and S are given as

$$\begin{bmatrix} \epsilon_{xx} \\ \epsilon_{yy} \\ 2\epsilon_{xy} \\ 2\epsilon_{xz} \\ 2\epsilon_{yz} \\ \epsilon_{zz} \end{bmatrix} = \begin{bmatrix} \partial/\partial x & 0 & 0 \\ 0 & \partial/\partial y & 0 \\ \partial/\partial y & \partial/\partial x & 0 \\ 0 & 0 & \partial/\partial x \\ 0 & 0 & \partial/\partial y \\ 0 & 0 & 0 \end{bmatrix} \begin{bmatrix} s_x \\ s_y \\ s_z \end{bmatrix} + \begin{bmatrix} 0 & 0 & 0 \\ 0 & 0 & 0 \\ 0 & 0 & 0 \\ 1 & 0 & 0 \\ 0 & 1 & 0 \\ 0 & 0 & 1 \end{bmatrix} \begin{bmatrix} \frac{\partial s_x}{\partial z} \\ \frac{\partial s_y}{\partial z} \\ \frac{\partial s_z}{\partial z} \end{bmatrix}$$

$$\epsilon = BZr + Bg + S \frac{\partial g}{\partial z} + SZ \frac{\partial r}{\partial z};$$

$$\psi = T_r r + \frac{\partial r}{\partial z};$$

Where

$$T_r = \begin{bmatrix} 0 & 0 & 0 & 0 & -1 & 0 \\ 0 & 0 & 0 & 1 & 0 & 0 \\ 0 & 0 & 0 & 0 & 0 & 0 \\ 0 & 0 & 0 & 0 & 0 & 0 \\ 0 & 0 & 0 & 0 & 0 & 0 \\ 0 & 0 & 0 & 0 & 0 & 0 \end{bmatrix}$$

Then,

$$\epsilon = SZ \left(T_r r + \frac{\partial r}{\partial z} \right) + Bg + S \frac{\partial g}{\partial z};$$

$$\epsilon = SZ(\psi) + Bg + SN \frac{\partial g}{\partial z};$$

The warping displacements g are discretized as $g(x, y, z) = N_i(x, y)u(x_i, y_i, z)$; N are the typical finite element shape functions and u the nodal warping displacements.

$$\epsilon = SZ(\psi) + BNu + SN \frac{\partial u}{\partial z};$$

The total virtual work per unit length W is given as $W = W_i + W_e$. The first variation of the total virtual work per unit length can be written as

$$\delta \frac{\partial W}{\partial z} = \delta \frac{\partial W_i}{\partial z} + \delta \frac{\partial W_e}{\partial z};$$

W_i is the work done by the internal elastic forces, and W_e is the work done by the external forces acting on the cross-section.

Assuming that the surface and the body forces are zero, the axial derivative of the work produced by the section stresses is the only contribution to the external work W_e [4],

$$\delta \frac{\partial W_e}{\partial z} = - \iint \frac{\partial(\delta s^T p)}{\partial z} dA$$

$$\delta \frac{\partial W_e}{\partial z} =$$

$$- \left(\delta r^T \frac{\partial H}{\partial z} - \delta r^T T_r^t H + \delta \psi^T H \right) - \left(\delta \frac{\partial u^T}{\partial z} \iint N^T p dA + \delta u^T \iint N^T \frac{\partial(p^T)}{\partial z} dA \right)$$

$$\delta \frac{\partial W_e}{\partial z} = \begin{bmatrix} \delta \frac{\partial u^T}{\partial z} \\ \delta u \\ \delta \psi \end{bmatrix}^T \begin{bmatrix} \mathbf{P} \\ \frac{\partial \mathbf{P}}{\partial z} \\ H \end{bmatrix} - \delta r^T \left(\frac{\partial H}{\partial z} - T_r^t H \right)$$

$$\mathbf{P} = \iint N^T p dA; \frac{\partial \mathbf{P}}{\partial z} = \iint N^T \frac{\partial p^T}{\partial z} dA$$

\mathbf{P} , stress resultants in the cross-section finite element discretization as it represents the discretized stresses acting on the cross-section face.

The internal work or the work done by the elastic strain energy per unit length can be written as [4]

$$\delta \frac{\partial W_i}{\partial z} = \iint \delta \epsilon^T \sigma \, dA$$

$$\delta \frac{\partial W_i}{\partial z} = \iint (\delta \psi^T Z^T S^T + \delta u^T N^T B^T + \delta \frac{\partial u^T}{\partial z} N^T S^T) Q \left(SZ\psi + BNu + SN \frac{\partial u}{\partial z} \right) dA$$

$$\delta \frac{\partial W_i}{\partial z} = \begin{bmatrix} \delta \frac{\partial u}{\partial z} \\ \delta u \\ \delta \psi \end{bmatrix}^T \begin{bmatrix} \mathbf{M} & \mathbf{C} & \mathbf{L} \\ \mathbf{C}^T & \mathbf{E} & \mathbf{R} \\ \mathbf{L}^T & \mathbf{R}^T & \mathbf{A} \end{bmatrix} \begin{bmatrix} \frac{\partial u}{\partial z} \\ u \\ \psi \end{bmatrix}$$

$$A = \iint Z^T S^T Q S Z \, dA; \quad R = \iint N^T B^T Q S Z \, dA; \quad E = \iint N^T B^T Q B N \, dA$$

$$C = \iint N^T S^T Q B N \, dA \quad ; \quad L = \iint N^T S^T Q S Z \, dA; \quad M = \iint N^T S^T Q S N \, dA$$

Now total work done will be

$$\delta \frac{\partial W}{\partial z} = \delta \frac{\partial W_i}{\partial z} + \delta \frac{\partial W_e}{\partial z}$$

$$\delta \frac{\partial W}{\partial z} = \iint \delta \epsilon^T Q \epsilon \, dA - \iint \frac{\partial(\delta s^T p)}{\partial z} \, dA$$

For a general virtual displacement δs and virtual strain $\delta \epsilon$, a necessary and sufficient equilibrium condition is

$$\delta \frac{\partial W}{\partial z} = 0; \\ \iint \delta \epsilon^T Q \epsilon \, dA = \iint \frac{\partial(\delta s^T p)}{\partial z} \, dA$$

$$\begin{bmatrix} \delta \frac{\partial u}{\partial z} \\ \delta u \\ \delta \psi \end{bmatrix}^T \begin{bmatrix} \mathbf{M} & \mathbf{C} & \mathbf{L} \\ \mathbf{C}^T & \mathbf{E} & \mathbf{R} \\ \mathbf{L}^T & \mathbf{R}^T & \mathbf{A} \end{bmatrix} \begin{bmatrix} \frac{\partial u}{\partial z} \\ u \\ \psi \end{bmatrix} = \begin{bmatrix} \delta \frac{\partial u^T}{\partial z} \\ \delta u \\ \delta \psi \end{bmatrix}^T \begin{bmatrix} \mathbf{P} \\ \frac{\partial \mathbf{P}}{\partial z} \\ H \end{bmatrix} - \delta r^T \left(\frac{\partial H}{\partial z} - T_r^T H \right)$$

Now, the equilibrium equations for a cross-section are given as [4]

$$M \frac{\partial^2 u}{\partial z^2} + (C - C^T) \frac{\partial u}{\partial z} + L \frac{\partial \psi}{\partial z} - Eu - R\psi = 0$$

$$L^T \frac{\partial u}{\partial z} + R^T u - A\psi = H$$

$$\frac{\partial H}{\partial z} = T_r^T H$$

3.3. Solutions for the Equilibrium equations for any cross-section:

Consider the case where the cross-section equilibrium equations are solved for different right-hand sides each corresponding to setting one of the entries of \mathbf{H} to unity and the remaining to zero. This procedure is similar to the stiffness method in the finite element method. It can be realized by replacing the cross-section load vector \mathbf{H} by the 6x6 identity matrix $[\mathbf{I}]$ and solving the following set of equations [4]

$$(C - C^T) \frac{\partial X}{\partial z} + L \frac{\partial Y}{\partial z} - EX - RY = 0$$

$$-L^T \frac{\partial X}{\partial z} + I_6 = R^T X + AY$$

$$E \frac{\partial X}{\partial z} + R \frac{\partial Y}{\partial z} = 0$$

$$T_r^T = R^T \frac{\partial X}{\partial z} + A \frac{\partial Y}{\partial z}$$

Where the resulting solution matrices \mathbf{u} , $\mathbf{du/dz}$, ψ and $\mathbf{d}\psi/\mathbf{dz}$ have six columns each corresponding to each of the six right-hand sides. Using the solutions from the system of linear equations above and based on the complimentary form of the internal virtual energy

of the cross-section it is possible to determine the cross-section compliance matrix $[F_s]$ defined as[4]

$$F_s = \begin{bmatrix} X \\ \frac{\partial X}{\partial Z} \\ Y \end{bmatrix}^T \begin{bmatrix} E & C & R \\ C^T & M & L \\ R^T & L^T & A \end{bmatrix} \begin{bmatrix} X \\ \frac{\partial X}{\partial Z} \\ Y \end{bmatrix}$$

Then, the corresponding stiffness matrix is computed as

$$K_s = F_s^{-1}$$

This result can be used to generate beam finite element models for which the strains can be exactly described by the six strain parameters in ψ . The material may be anisotropic, inhomogeneously distributed, and the reference coordinate system may be arbitrarily located. The stiffness matrix $[K_s]$ will correctly account for any geometrical or material couplings [4, 5].

3.4. Shear Center and Elastic Center:

The expressions for the positions of the shear and elastic center are presented next.

3.4.1. Shear Center:

The shear center is defined as the point at which a load applied parallel to the plane of the section will produce no torsion (i.e., $\kappa z = 0$). Hence, assume that two transverse forces, T_x and T_y are applied at a point (x_s, y_s) at a given cross-section. The moments induced by the two forces are

$$M_x = -T_y(L - z)$$

$$M_y = T_x(L - z)$$

$$M_z = -T_x * y_s + T_y * x_s$$

The aim is to find the position (x_s, y_s) for which the curvature associated with the twist $\kappa_z = 0$. Thus, taking into account the cross-section constitutive relation

$$\psi = F_s * H$$

The following holds

$$\begin{aligned} \kappa_z &= F_{s,61} * T_x + F_{s,62} * T_y + F_{s,64} * M_x + F_{s,65} * M_y + F_{s,66} * M_z = 0 \\ [F_{s,61} + F_{s,62} * (L - z) - F_{s,66} * y_s] T_x + [F_{s,62} - F_{s,64} * (L - z) + F_{s,66} * x_s] T_y \\ &= 0 \end{aligned}$$

Since the above has to be valid for any T_x and T_y ,

$$\begin{aligned} x_s &= \frac{-(F_{s,62} - F_{s,64} * (L - z))}{F_{s,66}} \\ y_s &= \frac{(F_{s,61} + F_{s,65} * (L - z))}{F_{s,66}} \end{aligned}$$

From the previous equation it can be seen that the shear center is not a property of the cross-section. Instead, in the case where the entries $F_{s,64}$ and $F_{s,65}$ associated with the bending-twist coupling are not zero, the position of the shear center varies linearly along the beam length .

3.4.2. Elastic Center:

The expressions for the position of the elastic center can be determined in the same manner.

The elastic center is defined as the point where a force applied normal to the cross-section will produce no bending curvatures (i.e., $\kappa_x = \kappa_y = 0$). Thus, assume that a load T_z is applied at the point (x_t, y_t) in the cross-section. The moments induced by this force are

$$\begin{aligned} M_x &= T_z * y_t \\ M_y &= -T_z * x_t \end{aligned}$$

We look for the positions (x_t, y_t) for which $\kappa_x = \kappa_y = 0$. From the cross-section constitutive relation, we get

$$\kappa_x = F_{s,43} * T_z + F_{s,44} * M_x + F_{s,45} * M_y = 0$$

$$\kappa_y = F_{s,53} * T_z + F_{s,54} * M_x + F_{s,55} * M_y = 0$$

Since the previous equation must be valid for any force T_z , then

$$F_{s,43} + F_{s,44} * y_t - F_{s,45} * x_t = 0$$

$$F_{s,53} + F_{s,54} * y_t - F_{s,55} * x_t = 0$$

Then,

$$x_t = \frac{-(-F_{s,44} * F_{s,53} + F_{s,45} * F_{s,43})}{F_{s,44} * F_{s,55} - F_{s,45}^2}$$

$$y_t = \frac{-(F_{s,43} * F_{s,55} - F_{s,45} * F_{s,53})}{F_{s,44} * F_{s,55} - F_{s,45}^2}$$

Thus, the elastic center and shear center are found

3.5. Implementation:

The first step in the evaluation of the cross-section properties is the generation of a two dimensional finite element mesh of the cross-section. An example of a discretized profile section using Q4 elements is presented in Fig.3.4. The material properties, fiber plane orientation and fiber directions are defined at each element of the finite element mesh. Thus, a layer of a certain material is defined using a layer of elements. Having defined the cross-section mesh and material properties, the subsequent step concerns the derivation of each of the matrices.

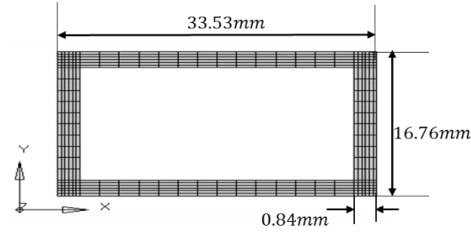


Figure.3.4. Example of the two dimensional finite element mesh of a box beam section using four node isoparametric finite elements.

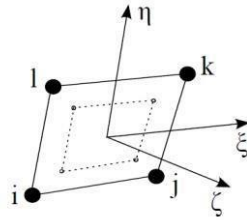


Figure.3.5. Isoparametric coordinate system, nodal positions and position of Gauss points for the four node isoparametric plane finite element.[5]

The node numbering and isoparametric coordinate system for element QUAD4 are presented in Fig.3.5. The shape functions employed in the derivation of the four node isoparametric finite element are

$$N_1 = \left(\frac{1}{4}\right) (1 - \xi)(1 - \eta)$$

$$N_2 = \left(\frac{1}{4}\right) (1 + \xi)(1 - \eta)$$

$$N_3 = \left(\frac{1}{4}\right) (1 + \xi)(1 + \eta)$$

$$N_4 = \left(\frac{1}{4}\right) (1 - \xi)(1 + \eta)$$

The position of a point in the element is given by interpolation of the nodal positions as

$$x = \sum_{i=1}^{n_q} N_i(\xi, \eta) x_i$$

$$y = \sum_{i=1}^{n_q} N_i(\xi, \eta) y_i$$

$$z = \sum_{i=1}^{n_q} N_i(\xi, \eta) z_i$$

where n_q is the number of nodes in the element, and (x_i, y_i, z_i) are the nodal positions. In matrix form for the four node element

$$N = [N_1 I_3 \quad N_2 I_3 \quad N_3 I_3 \quad N_4 I_3]$$

The integration is performed with respect to the element coordinate system although the integrals are defined with respect to the cross-section coordinate system. To account for the change of coordinates we employ the following transformation

$$\begin{bmatrix} \frac{\partial}{\partial \xi} \\ \frac{\partial}{\partial \eta} \\ \frac{\partial}{\partial \zeta} \end{bmatrix} = J \begin{bmatrix} \frac{\partial}{\partial x} \\ \frac{\partial}{\partial y} \\ \frac{\partial}{\partial z} \end{bmatrix}$$

Where J is

$$J = \begin{bmatrix} \frac{\partial x}{\partial \xi} & \frac{\partial y}{\partial \xi} & \frac{\partial z}{\partial \xi} \\ \frac{\partial x}{\partial \eta} & \frac{\partial y}{\partial \eta} & \frac{\partial z}{\partial \eta} \\ \frac{\partial x}{\partial \zeta} & \frac{\partial y}{\partial \zeta} & \frac{\partial z}{\partial \zeta} \end{bmatrix}$$

Using the inverse of the Jacobian matrix we can find the the strain operator B as

$$B(\xi, \eta) = B_\xi \frac{\partial}{\partial \xi} + B_\eta \frac{\partial}{\partial \eta}$$

The strain operator is then applied in the derivation of the matrix product

$$BN = B_{\xi} \frac{\partial N}{\partial \xi} + B_{\eta} \frac{\partial N}{\partial \eta}$$

$$\frac{\partial N}{\partial \xi} = \left[\frac{\partial N_1}{\partial \xi} I_3 \quad \frac{\partial N_2}{\partial \xi} I_3 \quad \frac{\partial N_3}{\partial \xi} I_3 \quad \frac{\partial N_4}{\partial \xi} I_3 \right]$$

$$\frac{\partial N}{\partial \eta} = \left[\frac{\partial N_1}{\partial \eta} I_3 \quad \frac{\partial N_2}{\partial \eta} I_3 \quad \frac{\partial N_3}{\partial \eta} I_3 \quad \frac{\partial N_4}{\partial \eta} I_3 \right]$$

The integration is performed at the element level and hence the element matrices are evaluated as

$$A_e = \iint Z^T S^T Q S Z dx dy = \iint Z^T S^T Q S Z |J| d\xi d\eta$$

$$R_e = \iint N^T B^T Q S Z dx dy = \iint N^T B^T Q S Z |J| d\xi d\eta$$

$$E_e = \iint N^T B^T Q B N dx dy = \iint N^T B^T Q B N |J| d\xi d\eta$$

$$C_e = \iint N^T S^T Q B N dx dy = \iint N^T S^T Q B N |J| d\xi d\eta$$

$$L_e = \iint N^T S^T Q S Z dx dy = \iint N^T S^T Q S Z |J| d\xi d\eta$$

$$M_e = \iint N^T S^T Q S N dx dy = \iint N^T S^T Q S N |J| d\xi d\eta$$

where the integration is performed using a four point Gauss quadrature. The global matrices are subsequently assembled following typical finite element procedures

$$A = \sum_{i=1}^{n_e} A_e;$$

$$R = \sum_{i=1}^{n_e} R_e;$$

$$E = \sum_{i=1}^{n_e} E_e$$

$$C = \sum_{i=1}^{n_e} C_e$$

$$L = \sum_{i=1}^{n_e} L_e$$

$$M = \sum_{i=1}^{n_e} M_e$$

Where n_e is the number of elements in the cross-section mesh.

The cross-section compliance matrix is then readily obtained by inserting the solutions and the cross-sectional stiffness matrix is obtained by the inverse of the compliance matrix.

3.6. Cross-sectional mass matrix:

The analysis of the cross-section mass properties is significantly simpler than the analysis of the cross-section stiffness parameters. The 6×6 cross-section mass matrix M_s relates the linear and angular velocities in H to the inertial linear and angular momentum in γ through $H = M_s \gamma$. The cross-section mass matrix is given with respect to the cross-section reference point as (cf. Hodges [1]).

$$M_s = \begin{bmatrix} m & 0 & 0 & 0 & 0 & -my_m \\ 0 & m & 0 & 0 & 0 & mx_m \\ 0 & 0 & m & my_m & -mx_m & 0 \\ 0 & 0 & my_m & I_{xx} & -I_{xy} & 0 \\ 0 & 0 & -mx_m & -I_{xy} & I_{yy} & 0 \\ -my_m & mx_m & 0 & 0 & 0 & I_{xx} + I_{yy} \end{bmatrix}$$

Where m is the mass per unit length of the cross-section. The cross-section moments of inertia with respect to x and y are given by I_{xx} and I_{yy} , respectively, while I_{xy} is the cross-section product of inertia. The term $I_{xx} + I_{yy}$ is the polar moment of inertia associated

with the torsion of the cross-section. The mass and moments of inertia are obtained through integration of the mass properties on the cross-section finite element mesh and defined as

$$\begin{bmatrix} m & 0 & 0 \\ 0 & I_{xx} & I_{xy} \\ 0 & 0 & I_{yy} \end{bmatrix} = \iint \begin{bmatrix} 1 & 0 & 0 \\ 0 & y^2 & xy \\ 0 & 0 & x^2 \end{bmatrix} \rho \, dA$$

The off-diagonal terms are associated with the offset between the mass center position $m_c = (x_m, y_m)$ and the cross-section reference point. The position of the mass center m_c is given as

$$x_m = \left(\sum_{e=1}^{n_e} x_{c_e} v_e \rho_e \right) / \left(\sum_{e=1}^{n_e} v_e \rho_e \right)$$

$$y_m = \left(\sum_{e=1}^{n_e} y_{c_e} v_e \rho_e \right) / \left(\sum_{e=1}^{n_e} v_e \rho_e \right)$$

Where (x_{m_e}, y_{m_e}) , v_e and ρ_e are the coordinates of the centroid, volume and density of element e , and n_e is the number of the elements in the cross-sectional mesh.

3.7. Strain and stress recovery:

In this section, it is assumed that the cross-section forces and moments H and M have been previously determined. This can be obtained from the solution to the 1D beam problem or from simple static equilibrium considerations. It is also assumed that the warping solutions to the unit loads X , $\partial X / \partial z$, and Y have been previously determined and are readily available. Then, the element strains in the global coordinate system ϵ_g are calculated as

$$\epsilon_{g,e} = S_e Z_e Y_e H_0 + B_e N_e X_e H_0 + S_e N_e \frac{\partial X_e}{\partial z} H_0$$

where the subscript e indicates the element number. The strains may be evaluated at different positions in each element. In the current implementation the strains and stresses are evaluated at both element centers and Gauss points. That is, the matrices S_e , Z_e , B_e and N_e are evaluated at this positions. The arrays X_e , $\partial X_e/\partial z$, and Y_e are obtained by extracting the degrees of freedom of element e from the corresponding arrays.

The element strains in the material coordinate system ϵ_m are obtained by rotation, writing the strains ϵ_g in matrix format yields

$$\epsilon_g = \begin{bmatrix} \gamma_{xxg} & 0.5\gamma_{xyg} & 0.5\gamma_{xzg} \\ 0.5\gamma_{yxg} & \gamma_{yyg} & 0.5\gamma_{zyg} \\ 0.5\gamma_{zxx} & 0.5\gamma_{zyg} & \gamma_{zzg} \end{bmatrix}$$

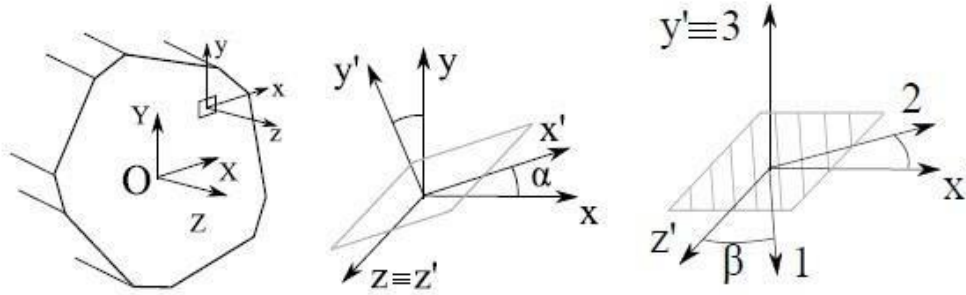


Figure.3.6. Determination of the material constitutive matrix at each finite element of the cross-section mesh. (a) Definition of the cross-section coordinate system XYZ and element coordinate system xyz. (b) Convention adopted for the rotation of the element coordinate system xyz into the fiber plane coordinate system x'y'z'. (c) Convention adopted for the rotation of the fiber plane coordinate system x'y'z' into the material coordinate system 123[4,5]

The constitutive matrix in the problem coordinate system, Q_p , is obtained by transformation of the material constitutive matrix in the material coordinate system, Q_m . The strains in the material coordinate system (123) are then obtained by

$$\epsilon_{m,\beta} = L_\beta \epsilon_p L_\beta^T$$

$$\epsilon_{m,\beta} = L_\beta \epsilon_p L_\beta^T$$

where replacing L_α or L_β as defined in the above equation correspond to the fiber and fiber plane rotations, respectively. Having determined the strains it is straightforward to determine the stresses. The stresses in global and material coordinate systems ζ_p and ζ_m , respectively are obtained as

$$\sigma_m = Q_m \epsilon_m$$

$$\sigma_p = Q_p \epsilon_p$$

Thus, these equations are used in the extraction of cross-sectional properties for any arbitrary geometry and material.

Cross section load vector H' obtained from a rotation α and translation $p = [p_x \ p_y \ p_z]^T$ of the cross section load vector H from the coordinate system O to coordinate system O' (Fig. 3.6).

The translation matrix T_T is obtained from static considerations and defined in function of the position vector p as follows

$$T_T = \begin{bmatrix} 1 & 0 & 0 & 0 & 0 & 0 \\ 0 & 1 & 0 & 0 & 0 & 0 \\ 0 & 0 & 1 & 0 & 0 & 0 \\ 0 & 0 & -p_y & 1 & 0 & 0 \\ 0 & 0 & p_x & 0 & 1 & 0 \\ p_y & -p_x & 0 & 0 & 0 & 1 \end{bmatrix}$$

The rotation matrix T_r is defined in function of the rotation α as

$$T_r = \begin{bmatrix} \cos(\alpha) & \sin(\alpha) & 0 & 0 & 0 & 0 \\ -\sin(\alpha) & \cos(\alpha) & 0 & 0 & 0 & 0 \\ 0 & 0 & 1 & 0 & 0 & 0 \\ 0 & 0 & 0 & \cos(\alpha) & \sin(\alpha) & 0 \\ 0 & 0 & 0 & -\sin(\alpha) & \cos(\alpha) & 0 \\ 0 & 0 & 0 & 0 & 0 & 1 \end{bmatrix}$$

The transformed vector of cross section forces and moments due to a translation and rotation can be obtained as $H' = T_t H$ and $H' = T_r H$, respectively. For the translation and rotation of a given cross section constitutive matrix M where the transformed version M' is then obtained as $M' = T_t M^T T_t$, and $M' = T_r M^T T_r$.

4. Beam Formulations

4.1. Introduction:

A beam is essentially a solid structural element whose geometry possesses a certain degree of slenderness such that its length is relatively larger than the cross-section dimensions. When working with beam models, it is assumed that the geometry of the solid is represented by the geometry of its cross-sections and that the beam is represented by the line that goes through the reference points of the section. The three-dimensional problem of the analysis of the beam is separated into two parts. The first part concerns the two-dimensional analysis of the cross-section properties while the second regards the one dimensional analysis of the global response of the beam. The deformation of the cross-section is represented by the rigid body translations and rotations of these sections with respect to the reference coordinate system of the section.

This chapter describes the structural beam model used in this thesis. The beam model is developed in a finite element context. The cross-section stiffness and mass properties are estimated using a finite element cross-section analysis tool which is able to correctly estimate the effects of material anisotropy and geometric inhomogeneity.

The beam finite element static and dynamic equations are derived in this section. The kinematics of the beam are established first. The static and dynamic equations are derived next based on the principle of virtual work and using standard finite element techniques.

4.2. Beam finite element model:

Consider the equilibrium of a three-dimensional beam subjected to the external distributed and concentrated forces f_s and f_c , respectively in Fig.4.1. The strains ϵ and stresses ζ acting at a point in the beam slice are given as

$$\epsilon^T = [\epsilon_{xx} \quad \epsilon_{yy} \quad 2\epsilon_{xy} \quad 2\epsilon_{xz} \quad 2\epsilon_{yz} \quad \epsilon_{zz}]$$

$$\sigma^T = [\sigma_{xx} \quad \sigma_{yy} \quad \sigma_{xy} \quad \sigma_{xz} \quad \sigma_{yz} \quad \sigma_{zz}]$$

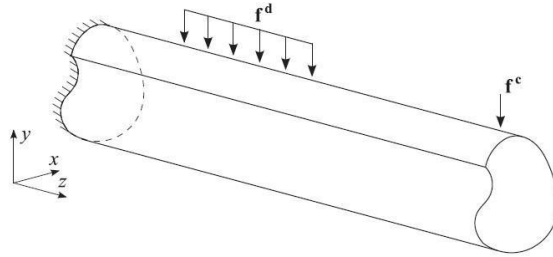


Figure.4.1. General Beam Element with external forces [1].

For linear elastic materials, the stresses and strains are related by the linear constitutive relation

$$\sigma = Q\epsilon$$

Then,

Using the strain displacement relations and principle of virtual work on the cross-section as discussed in the previous chapter, we get the cross-sectional stiffness matrix K_s . In its most general form (considering, e.g., anisotropic and inhomogeneous sections of arbitrary

geometry) K_s may be fully populated and its 21 stiffness parameters will have to be determined to fully describe the deformation of a slice dz of the beam.

Three different Cartesian reference systems are mainly used (see Fig.4.2); Global reference system $\{O, X-X, Y-Y, Z-Z\}$; Local reference system for Stiffness Matrix $\{T, X'-X', Y'-Y', Z'-Z'\}$; Local reference system for Mass Matrix $\{G, X''-X'', Y''-Y'', Z''-Z''\}$. The global axis $X-X$ is chosen parallel to the beam axis. Axes $Y-Y$ and $Z-Z$ will define the cross-section plane and, for the case of a blade, will generally correspond to the lag wise movement direction (or flap wise bending axis) and the flap wise one (or lag wise bending axis), which in general will not be the principal bending directions.

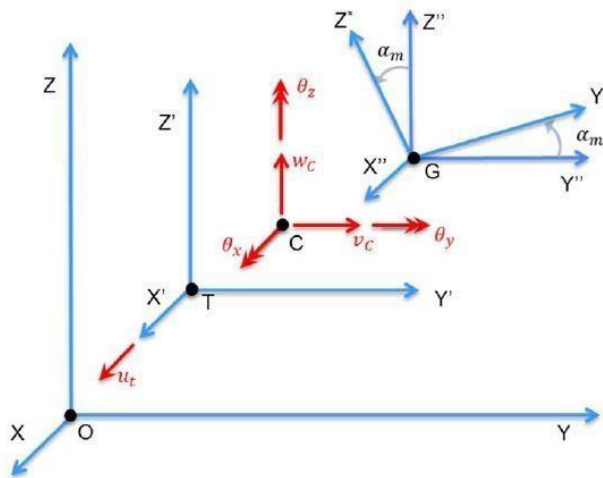


Figure.4.2. Beam kinematics for stiffness matrix (in red) and reference systems: global $\{O, X-X, Y-Y, Z-Z\}$, local for stiffness matrix $\{T, X'-X', Y'-Y', Z'-Z'\}$ and local for mass matrix $\{G, X''-X'', Y''-Y'', Z''-Z''\}$ [1, 3, 6-10]

It is assumed that the cross-section is constant along the element, i.e. the section properties will not vary along $X-X$ axis. The local reference system for the stiffness matrix is parallel to the global one with origin at the tension center (T) of the cross-section (the $X'-X'$ axis

will be the neutral axis). It can be noted that T is generally different from the shear center (C).

Center (G), obtaining the auxiliary system $\{G, X''-X'', Y''-Y'', Z''-Z''\}$, and rotating this system with an angle α_m in order to obtain the mass inertia principal axes $\{Y^*-Y^*, Z^*Z^*\}$. The above reference systems are in accordance with the section properties that can be obtained from cross-sectional tool, which computes section stiffness and mass properties in principal inertia axes.

The elastic energy and the kinetic energy of a beam are considered for deriving stiffness and a mass matrix of a beam, respectively. The stiffness matrix is derived by assuming that the beam states (deflections and rotations) can be described by polynomials of arbitrarily high order. This approach introduces a high number of degrees of freedom for the states and that high number is subsequently condensed by minimizing the elastic energy of the entire beam with constraints of prescribed states at the beam-ends. This approach indirectly results in shape functions, which are equal to the static deflection state for a beam with prescribed end conditions. The following equation shows the elastic strain energy of the beam.

$$2U = \int_0^L (\varepsilon^T K_s \varepsilon) dz'$$

where ε is the beam strain vector, and K_s is the cross-sectional stiffness matrix. The generalized strains of Timoshenko beam, ε , are expressed as

$$\{\varepsilon\}^T = \{\varepsilon_{x'}, \varepsilon_{y'}, \varepsilon_{z'}, \kappa_{x'}, \kappa_{y'}, \kappa_{z'}\} = \{u_{x'} - \theta_{y'}, -u_{y'} - \theta_{x'}, u_{z'}, \theta'_{x'}, \theta'_{y'}, \theta'_{z'}\}$$

The displacements and rotations can be expressed by an interpolating polynomial in terms of generalized degrees of freedom as follows

$$\varepsilon = B(z')\alpha$$

The elastic energy of the beam can be illustrated as follows

$$2U = \alpha^T \int_0^L B^T K_s B dz' \alpha$$

By applying boundary conditions at each end of the beam the nodal degrees of freedom are obtained as follows

$$\alpha = T_s d$$

Then, the strain energy is given as

$$U = \left(\frac{1}{2}\right) d^T T_s^T \int_0^L B^T K_s B dz' T_s d$$

where d is the beam displacement field described in the global coordinate system xyz , T_s is the transformation matrix, where s is the angle between the local beam element longitudinal direction, x' axis and x axis, whose value is calculated at the Gaussian integration point in finite element analysis.

Then,

$$U = \left(\frac{1}{2}\right) d^T K d$$

where K matrix, is the element stiffness matrix.

$$K = T_s^T \int_0^L B^T K_s B dz' T_s$$

The method to compute the element mass matrix is similar to the definition of the stiffness matrix.

The element mass matrix is obtained from the kinetic energy as follows:

$$T = \left(\frac{1}{2}\right) \iiint \rho \dot{r}^T r dV$$

Where ρ , \mathbf{r} , and V are the mass density, velocity of the material point inside the beam element, and volume of body, respectively. The velocity of the material point inside the beam element at the sectional coordinate, $\mathbf{r}' = \{x', y', 0\}^T$ can be expressed as

$$\dot{\mathbf{r}} = \dot{u} + \dot{\theta} * \mathbf{r}'$$

$$\dot{\mathbf{r}} = [I] - [\mathbf{r}' * I] \dot{q}$$

By applying the same shape function as the stiffness matrix, equation can be illustrated as follows:

$$\dot{\mathbf{r}} = [I] - [\mathbf{r}' * I] N(z') \dot{\alpha}$$

By substituting this into the kinetic energy equation which can be extended as follows:

$$T = \left(\frac{1}{2}\right) \iiint \rho \dot{\mathbf{r}}^T \mathbf{r} dV$$

$$T = \left(\frac{1}{2}\right) \int_0^L \left(\iint \rho \dot{\mathbf{r}}^T \dot{\mathbf{r}} dA \right) dz'$$

$$T = \left(\frac{1}{2}\right) \dot{\alpha} \int_0^L (N(z')^T M_s N(z')) dz' \dot{\alpha}$$

$$\alpha = T_s d$$

Then, $\dot{\alpha}$ can be obtained by differentiating α with respect to time as follows

$$\dot{\alpha} = T_s \dot{d}$$

Then,

$$T = \left(\frac{1}{2}\right) \dot{\alpha} \int_0^L (N(z')^T M_s N(z')) dz' \dot{\alpha} = \left(\frac{1}{2}\right) \dot{d} T_s^T \int_0^L (N(z')^T M_s N(z')) dz' T_s \dot{d}$$

$$T = \left(\frac{1}{2}\right) \dot{d}^T M \dot{d}$$

Where M is the element mass matrix.

5. Validation

In this section, several numerical results obtained by implementing the formulation have been discussed. The results for different cases by the present method are compared to the results from VABS (Variational Asymptotic Beam Section) analysis code [1, 3, 6, 7, 8]. The accuracy of the cross-sectional stiffness matrix depends on the size of the cross-section finite element mesh. A mesh convergence study has been performed in order to establish the minimum size of the cross-section finite element mesh to obtain realistic values. The cross-section coordinate system is given in Fig.5.1

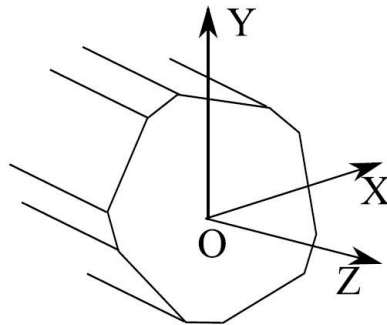


Figure.5.1. Cross-section coordinate system [5]

Firstly, in this section the convergence study to define the element length for the cross-sectional analysis is done. In order to verify whether the formulations are correct, we have taken three example of C-Channel section, I- section, Box beam section and ellipse section with isotropic material to compare the shear center and area under the section to that obtained from the tool. Then, the validation is done by comparing the cross-sectional properties obtained by the tool and those found in the literature.

The cases presented for the validation are chosen such that we have taken into account different materials and geometrical variations. The first case is the ellipse section with isotropic material. The second case chosen is an anisotropic square section made of T300/5208 Graphite epoxy. The aim in this case is to validate the tool can be implemented for different laminated configurations. The third case is a thin walled cylindrical crosssection which has been used as a benchmark case for various authors. The fourth validation case considered is the three cell cross-section, where the aim is to validate the results from tool for thin walled, multicelled, closed cross-sections with anisotropic material properties.

Then, the validation cases for the Timoshenko beam analysis are presented. The box beam model along with the airfoil model is considered for validation. In this validation, we only seek to validate the natural frequencies and mode shapes with the NASTRAN results and also from the literature.

Validations of the strain and stress recovery procedures implemented in framework are performed against a 3-D finite element model developed in NASTRAN [31] for a case of a solid prismatic beam of square cross-section made of graphite-epoxy material.

5.1. Convergence Test:

Before validating the stiffness results from the present method, a convergence test is performed to determine the minimum number of elements required for a relative error in the stiffness results less than 0.01. The dimensions and ply properties are given in Table.5.1. In Fig.5.3, a plot of several stiffness components is shown for increasing number of elements; using the layup given in Table 5.1. Fig.5.3 shows that 60 elements.

i.e an element size of 0.005in are sufficient to generate results with error below 0.01%. This shows that the method is suitable for the further simulation and analysis of the *mAEWing1* model.

Table.5.1. Dimensions and Material properties for the c/s in the figure 5.2.

Dimensions				
	a	0.53in		
	b	0.953in		
	t	0.03in		
Ply Properties				
	E ₁₁	20.59e6 psi		
	E ₁₂	1.42e6 psi		
	G ₁₂	8.7e5 psi		
	v ₁₂	0.3/0.42		
Layups				
Layup	Upperwall	Lower wall	Left Wall	Right wall
1	[15] ₆	[15] ₆	[15] ₆	[15] ₆



Figure.5.2. Rectangular box beam cross-section of the geometry.

Table.5.2.Different data sets for Cross-sectional Properties of the box beam geometry in figure 5.2.

Total number of elements	10 ⁴	2*10 ⁴	5*10 ⁴	6*10 ⁴	8*10 ⁴	10 ⁵
KS,11(lbs)	1.41E+06	1.42E+06	1.43E+06	1.43E+06	1.44E+06	1.44E+06
KS,14(lbs-in ²)	9.73E+04	9.96E+04	1.03E+05	1.07E+05	1.07E+05	1.07E+05
KS,22(lbs)	8.09E+04	8.56E+04	9.00E+04	9.29E+04	9.29E+04	9.29E+04
KS,25(lbs-in ²)	-4.98E+04	-5.14E+04	-5.28E+04	-5.43E+04	-5.44E+04	-5.44E+04
KS,33(lbs)	2.77E+04	2.97E+04	3.48E+04	3.83E+04	3.84E+04	3.84E+04
KS,36(lbs-in ²)	-4.89E+04	-5.06E+04	-5.36E+04	-5.65E+04	-5.66E+04	-5.66E+04
KS,44(lbs-in ²)	9.56E+03	1.02E+04	1.47E+04	1.65E+04	1.66E+04	1.66E+04
KS,55(lbs-in ²)	5.98E+04	6.01E+04	6.72E+04	6.73E+04	6.74E+04	6.74E+04
KS,66(lbs-in ²)	1.39E+05	1.50E+05	1.69E+05	1.73E+04	1.73E+05	1.73E+05

Table.5.3. Cross-sectional Properties of the box beam geometry in figure 5.2.

	PRESENT METHOD	VABS	PERCENTAGE ERROR (%)
KS,11 (lbs)	.1437E+07	.1432E+07	-0.04
KS,14 (lbs-in ²)	0.1073E+6	0.1060E+6	-0.16
KS,22 (lbs)	0.9293E+05	0.9018E+05	3.04
KS,25 (lbs-in ²)	-0.5438E+05	-0.5204E+05	-4.05
KS,33 (lbs)	.3838E+05	.3932E+05	-2.38
KS,36 (lbs-in ²)	-0.5662E+05	-0.5637E+05	-0.45
KS,44 (lbs-in ²)	0.1656E+05	0.1678E+05	-1.34
KS,55 (lbs-in ²)	.6735E+05	.6622E+05	1.71
KS,66 (lbs-in ²)	0.1731E+06	0.1726E+06	0.28

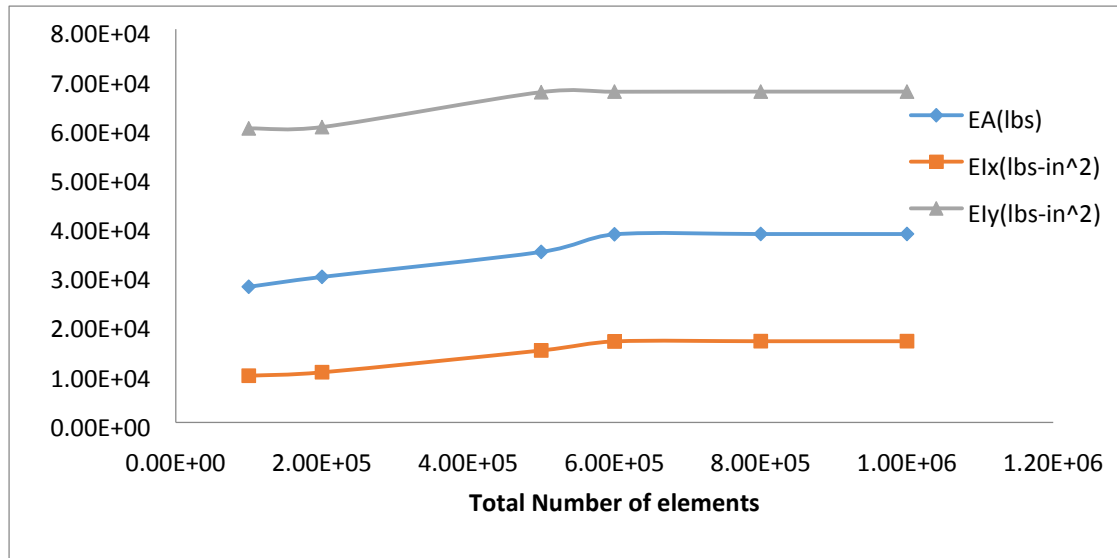


Figure.5.3. Plot of stiffness components with respect to number of elements

Furthermore, the relative error of the stiffness matrix of the present method w.r.t. the stiffness matrix from VABS is calculated. This error is a measure of how well the strain energy is captured by the present methods as compared to VABS.

In Table 5.2, the stiffness results for layout 1 are shown. In the case of the stiffness matrix, the present method overestimates the bending coefficients by 1.71 and 0.28 percent respectively. For the transverse shear coefficients, and coupling between transverse shear and bending, the present method has errors that are between -4.5 and 3%.

Based on the convergence test results, the size of the element is taken to be 0.005in. However sometimes, the arbitrary shape of the geometry dictates the mesh size and convergence test need to be performed in such a case.

5.2. Validation –Shear Center:

In this section, we have three cases in which the shear center obtained by the crosssectional analysis tool and by solving it explicitly are compared with the results from VABS to validate the tool. The first case is the channel section, second case is the I- section and third case is the box beam section.

5.2.1. C- Channel Section:

The dimension for the C- cross-section is given in the Fig. 5.4. The material properties are given in Table 5.4. The resulting shear center terms are then compared with the analytical solution. The results are shown in Table 5.5. They have a very good correlation.

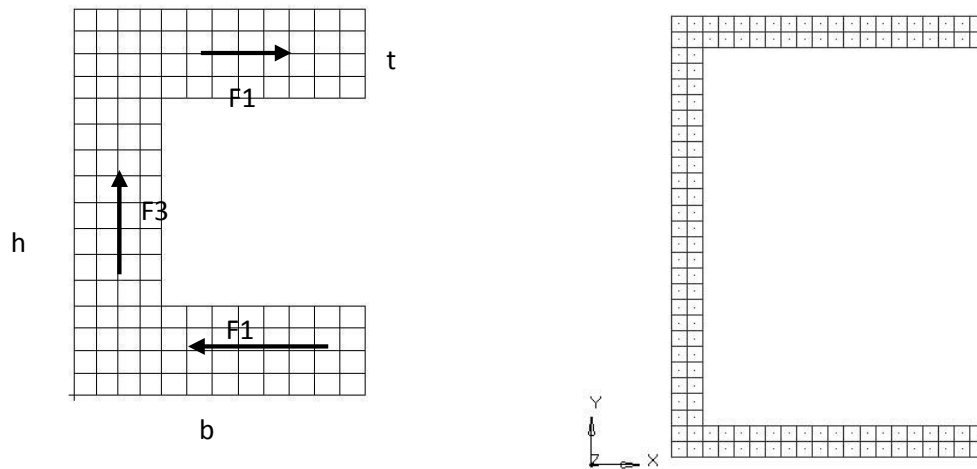


Figure.5.4. C- Section (Open section)

Tabel.5.4. Dimensions and Material properties for the cross section shown in figure.5.4.

Dimensions	
h	14m
b	10m
t	1m
w	1m
Material Properties	
E ₁₁	100GPa
E ₃₃	100GPa
G ₁₂	41.67GPa
G ₁₃	41.67GPa

$$F_1 = \left(\tau * \frac{a}{2} \right) * b * t$$

$$F_3 = \int_{-\frac{h}{2}}^{\frac{h}{2}} \tau * t * dy$$

$$F_1 * h = F * e$$

$$F = F_3$$

$$e = \frac{\frac{1}{2} * \tau * a * b * t * h}{F}$$

$$e = \frac{b1^2 * t * h^2}{4 I}$$

$$e = \frac{b1}{2 + (\frac{h}{3 * b * t})}$$

So, for the above example, the shear center comparison is given in the Table.5.4.

Table.5.5. Comparison of shear center for the C-section

Shear Center	Analytical	Present Method
x_s	5.02m	5.0245m
y_s	7m	6.998m

From this, we can say that the shear center for any cross-section lies on the longitudinal line parallel to the axis of the beam. The shear center comparison is done for the I-section and the box beam section as follows.

5.2.2. I- Channel Section:

The dimension for the I- cross-section is given in Fig.5.5. The material properties are given in Table.5.6. The resulting shear center terms are then compared with the analytical solution.

The results are shown in Table.5.7. They have very good correlation.

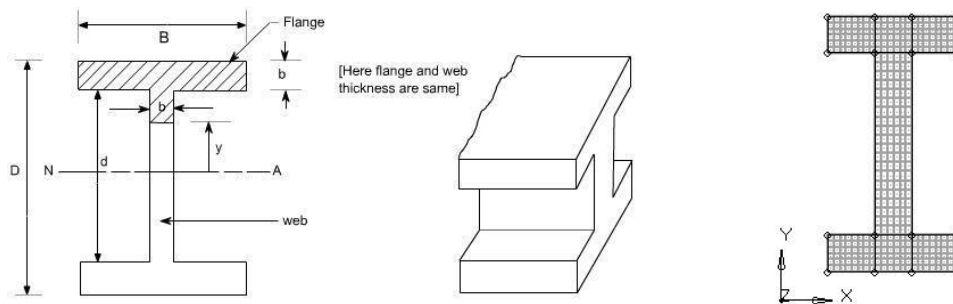


Figure.5.5. I- Section (Open section)

Table.5.6. Dimensions & Material properties for the I- section.

Dimensions	
D	14m
B	7.2m
d	10m
b	2m
Material Properties	
E ₁₁	100GPa
E ₃₃	100GPa
G ₁₂	41.67GPa
G ₁₃	41.67GPa

Table.5.7. Comparison of shear center for the I-section

Shear Center	Analytical	Present Method
x _s	3.56m	3.5689m
y _s	7m	6.998m

5.2.3 Box Beam Section:

The dimension for the box beam cross-section is given in Fig.5.6. The material properties are isotropic. The resulting shear center terms are then compared with the analytical solution. The results are shown in Table.5.9. They have a very good correlation.

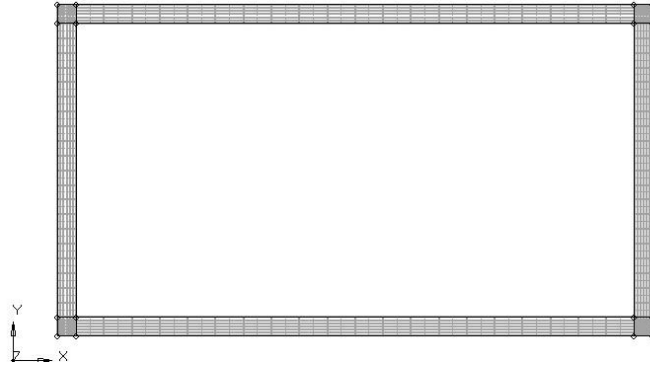


Figure.5.6. Rectangular Box Beam Section (Closed section)

Table.5.8. Material properties for the cross section shown in figure 5.6.

Material Properties	
E_{11}	100GPa
E_{33}	100GPa
G_{12}	41.67GPa
G_{13}	41.67GPa

Table.5.9. Comparison of shear center for the cross section shown in figure 5.6

Shear Center	Analytical	Present method
x_s	16.765mm	16.65mm
y_s	8.38mm	8.39mm

5.3. Validation –Cross-sectional Analysis:

5.3.1. Square Cross-section:

The dimension for the square cross-section is given in Fig.5.7. The material properties are given in Table 5.10. The resulting non zero terms for the cross-sectional stiffness matrix is compared from the VABS [1,8] . The results are shown in Table 5.11. The results have a very good correlation with the values from the VABS. For a square cross-section with isotropic materials, it is easier to find the cross-sectional properties analytically. The comparison between the current method and analytical gives us the confidence in the extraction of properties.

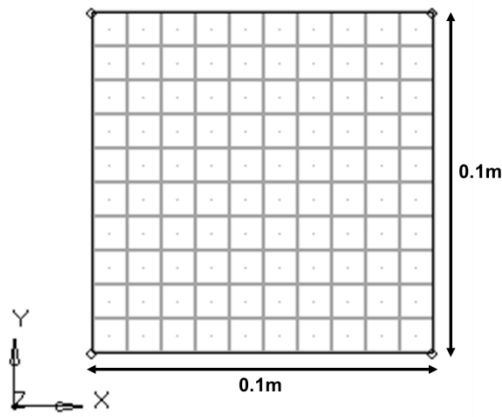


Figure.5.7. Square cross-section

Table.5.10. Material properties for the square cross section shown in figure 5.7.

Dimensions	
W	0.1m
H	0.1m
Material Properties	
E ₁₁	100GPa
E ₃₃	100GPa
G ₁₂	41.67GPa
G ₁₃	41.67GPa
G ₂₃	41.67GPa
V ₁₂ ; V ₁₃ ; V ₂₃ ;	0.2;0.2;0.2
ρ	1289 kg/m ³

Table.5.11. Cross-sectional properties for the cross section shown in figure 5.7

	Present Method	VABS	Analytical	PERCENTAGE ERROR (%)
K _{S,11} (GA _x)(N)*10 ⁹	3.49E-01	3.49E-01	0.34889	7.15E-04
K _{S,22} (GA _y) (N)*10 ⁹	3.49E-01	3.49E-01	0.34889	7.15E-04
K _{S,33} (EA) (N)*10 ⁹	1.00E+00	1.00E+00	1	0
K _{S,44} (EI _x) (Nm ²)*10 ⁹	8.34E-04	8.34E-04	0.0008334	0
K _{S,55} (EI _y) (Nm ²)*10 ⁹	8.34E-04	8.34E-04	0.0008334	0
K _{S,66} (GJ) (Nm ²)*10 ⁹	5.91E-04	5.91E-04	0.000591	0

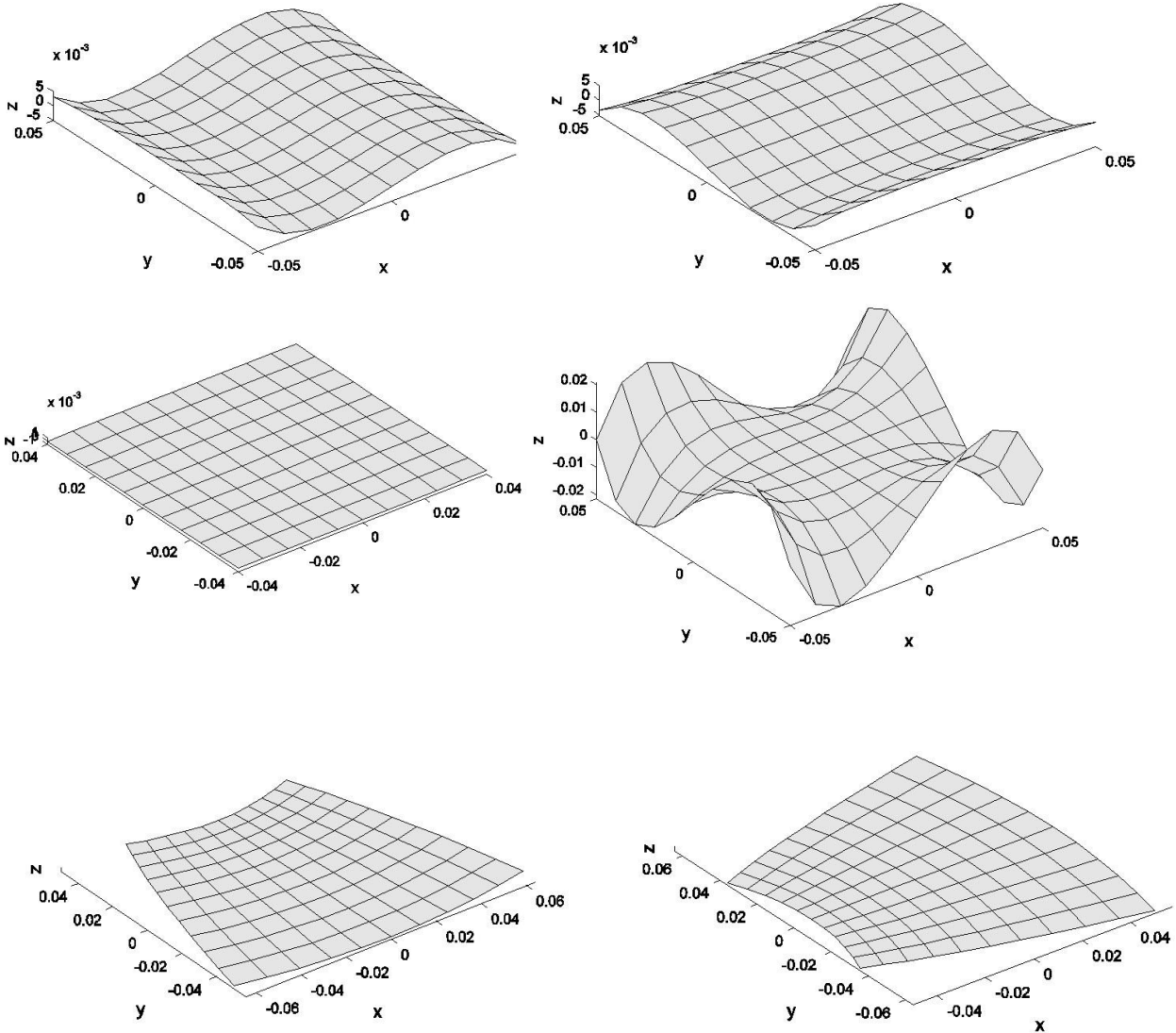


Figure.5.8. Square cross-section warping displacements

The shear strains, $\epsilon_x = 1$ and $\epsilon_y = 1$, induces a cross-section deformation shown in

Fig.5.8. The Poisson effect is visible in the results obtained for $\kappa_x = 1$ and $\kappa_y = 1$ with an in-plane expansion and contraction of the compression and tension sides, respectively.

This is presented above in Fig.5.8.

5.3.2. Cylindrical Shell:

In this section results are presented based on the cylindrical shell cross-section. The geometrical dimensions and the finite element mesh of the cylindrical shell cross-section

are presented in Fig. 5.9. The material considered is isotropic and is given in Table.5.12. As it is isotropic material, there are only diagonal terms. The results from the crosssectional analysis are indistinguishable from the results of VABS. This is shown in Table.5.12. [1, 6, 7].

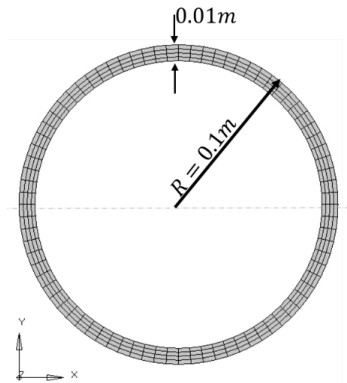


Figure.5.9. Cylindrical shell cross-section with isotropic materials.

Table.5.12. Material properties for the cross section shown in figure 5.9.

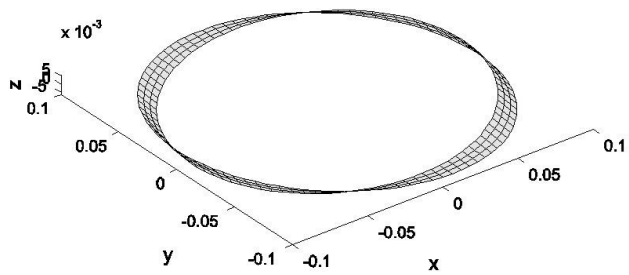
Dimensions	
Outer radius (R)	0.1 m
Thickness (t)	0.01 m
Material Properties	
E_{11}	100GPa
E_{33}	100GPa
G_{12}	41.67GPa
G_{13}	41.67GPa
G_{23}	41.67GPa
$\nu_{12} ; \nu_{13} ; \nu_{23} ;$	0.2;0.2;0.2
ρ	1289 kg/m ³

Table.5.13. Cross-sectional properties for the cross section shown in figure 5.9.

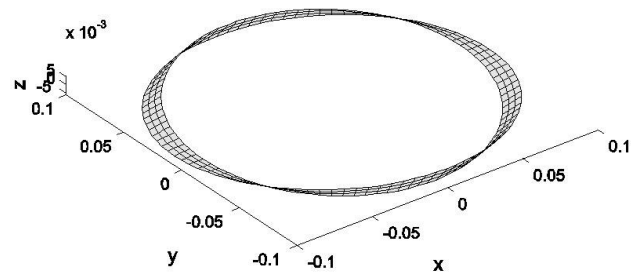
	PRESENT	VABS	PERCENTAGE ERROR
	METHOD		(%)
$K_{S,11} (GA_x)(N)*10^9$	1.25E-01	1.25E-01	7.20E-04
$K_{S,22} (GA_y) (N)*10^9$	1.25E-01	1.25E-01	7.20E-04
$K_{S,33} (EA) (N)*10^9$	5.97E-01	5.97E-01	1.68E-13
$K_{S,44} (EI_x) (Nm^2)*10^9$	2.70E-03	2.70E-03	5.59E-09
$K_{S,55} (EI_y) (Nm^2)*10^9$	2.70E-03	2.70E-03	5.59E-09
$K_{S,66} (GJ) (Nm^2)*10^9$	2.25E-03	2.25E-03	7.20E-04

As expected the shear strains are the only ones which induce out-of-plane deformation. Due to the axial symmetry, the torsion strain will not induce any out-of-plane deformation. The same holds for the shear and elastic positions, both of which coincide with the origin of the cross-section coordinate system. Thus, according both cross-sectional analysis and VABS $x_s = y_s = x_t = y_t = 0$.

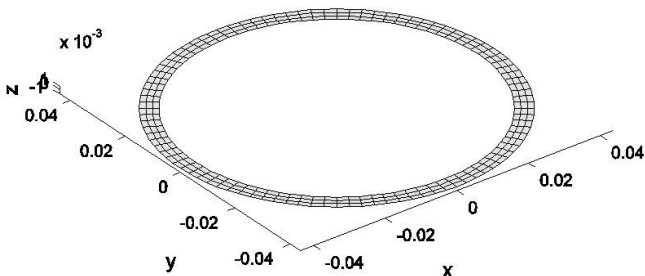
The warping displacements of the cross-section is shown in Fig. 5.10



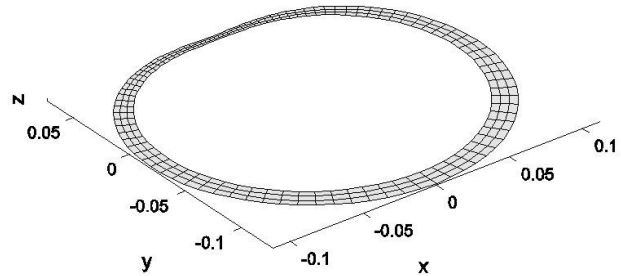
a. τ_x



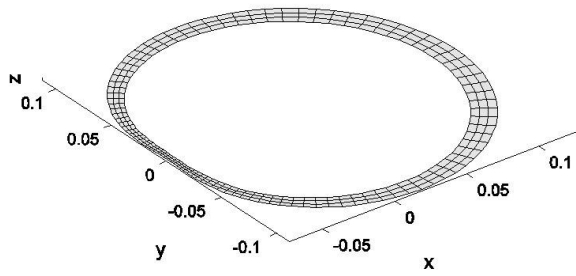
b. τ_y



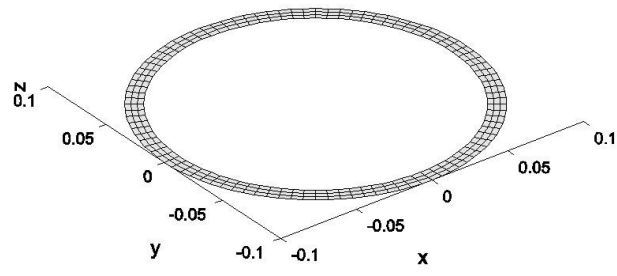
c. τ_z



d. κ_x



e. κ_y



f. κ_z

Figure.5.10. Circular cross-section warping displacements

5.3.3. Three Cell Cross-section:

In this section, a three cell sectional geometry is considered. The aim of this example is to illustrate the ability of the developed framework to correctly estimate the stiffness properties of the cross-sections regardless of the number of cells in the cross-section with the effect of material anisotropy in the model. The geometry, corresponding dimensions and finite element mesh for the three-cell cross-section are shown in Fig.5.11. The top faces of the three cells cross-section are laminated using the orthotropic material oriented at 45° . The vertical faces are made of isotropic material. The fibre plane lies parallel to the xz plane and rotates around the y axis. The material properties are given in Table 5.14 and the results comparison is given in Table 5.15 [1, 7].

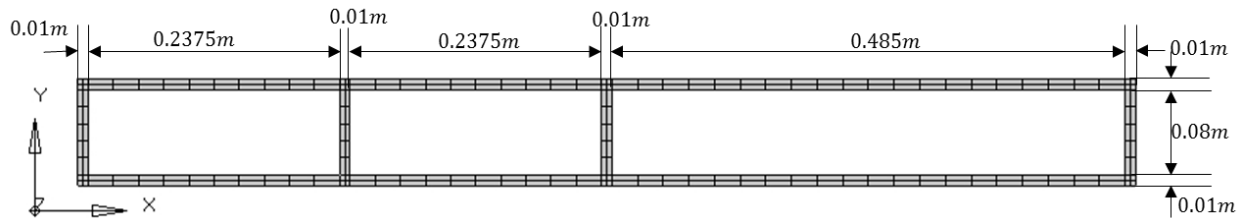


Figure.5.11 Three cell cross-section which has the top-bottom face of orthotropic material (P1) oriented at 45° and the vertical webs as isotropic material (P2).

Table 5.14. Material properties for the cross section shown in figure 5.11.

Material Properties (orthotropic) (P1)	
E_{11}	480 GPa
E_{22}	120GPa
E_{33}	120GPa
G_{12}	60GPa
G_{13}	60GPa
G_{23}	50GPa
$\nu_{12} ; \nu_{13} ; \nu_{23} ;$	0.19;0.19;0.26
ρ	1 kg/m ³
Material Properties (isotropic) (P2)	
E_{11}	100GPa
E_{33}	100GPa
G_{12}	41.67GPa
G_{13}	41.67GPa
G_{23}	41.67GPa
$\nu_{12} ; \nu_{13} ; \nu_{23} ;$	0.2;0.2;0.2
ρ	1kg/m ³

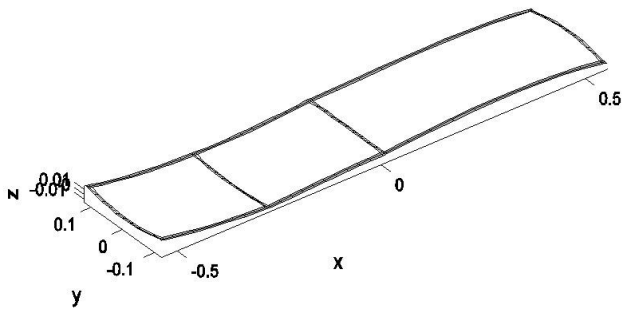
Table.5.15. Comparison of cross-sectional properties for the cross section shown in figure 5.11

	PRESENT METHOD	VABS	PERCENTAGE ERROR (%)
$K_{S,11} (N)*10^9$	1.79E+00	1.79E+00	5.58E-10
$K_{S,22} (N)*10^9$	3.22E-01	3.22E-01	1.24E-09
$K_{S,33} (N)*10^9$	4.37E+00	4.37E+00	2.29E-10
$K_{S,44} (Nm^2)*10^9$	5.23E-02	5.23E-02	7.65E-10
$K_{S,55} (Nm^2)*10^9$	3.81E-01	3.81E-01	-7.87E-10
$K_{S,66} (Nm^2)*10^9$	7.73E-02	7.73E-02	0.00E+00
$K_{S,13} (N)*10^9$	-8.48E-01	-8.48E-01	1.18E-10
$K_{S,15} (Nm^2)*10^9$	2.75E-03	2.75E-03	1.02E-08
$K_{S,24} (Nm^2)*10^9$	-3.13E-03	-3.13E-03	1.60E-09
$K_{S,26} (Nm^2)*10^9$	-1.49E-02	-1.49E-02	-2.68E-09
$K_{S,35} (Nm^2)*10^9$	5.64E-02	5.64E-02	-1.77E-10
$K_{S,46} (Nm^2)*10^9$	1.83E-02	1.83E-02	5.47E-10

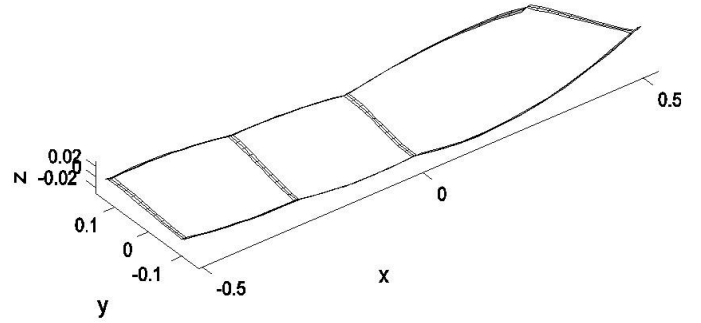
The resulting positions of the shear and elastic center are presented in Table 5.16. As before, the results from cross-sectional analysis approach and VABS are in a very good agreement for the estimation of the shear and elastic center. The warping displacements are given in Fig.5.12

Table.5.16. Comparison of mass properties for the cross section shown in figure 5.11

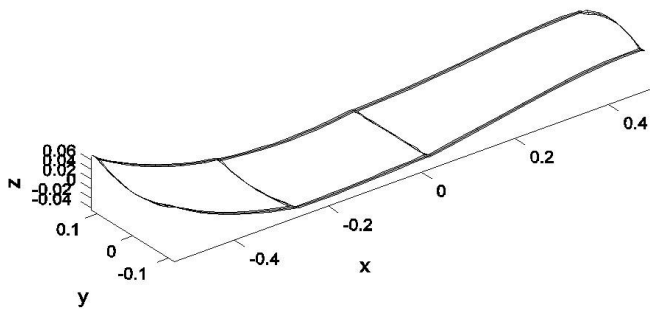
Shear & Elastic Center	VABS	PRESENT METHOD	Percentage Difference
x_s	-4.30E-02	-4.30E-02	0
y_s	0	0	0
x_t	-1.46E-02	-1.46E-02	0
y_t	0	0	0



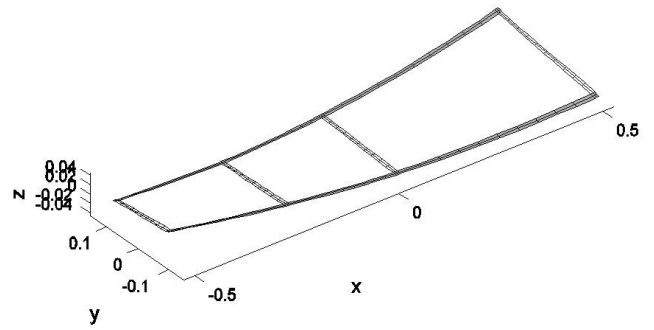
a. τ_x



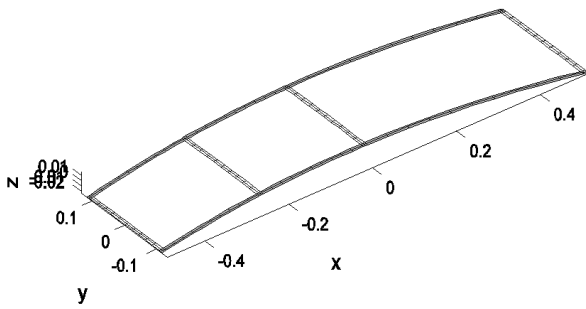
b. τ_y



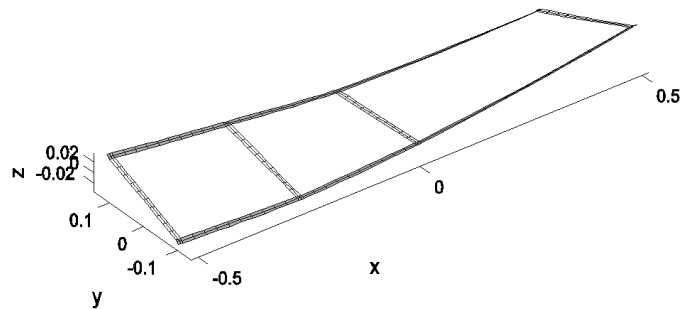
c. τ_z



d. κ_x



e. κ_y



f. κ_z

Figure.5.12. Three cell cross-section warping displacements

All results obtained using cross-sectional analysis tool developed in this study were found to be in perfect agreement with VABS for all the cross-sections analyzed. These results strongly indicate that the implementation is correct and can be used in a Timoshenko beam framework.

5.4. Validation –Timoshenko Beam Analysis:

5.4.1. Elliptical Beam:

The elliptical solid beam is considered for the validation. Beam was generated with a length of 10 meters using the cross-section from the Fig.5.13. The dimension for the elliptical cross-section is given in the Table 5.17. The material properties are given in Table 5.17. Eigenvalue computation is done in order to find the natural frequencies and mode shapes. To verify the static as well as normal mode solutions of this beam, an identical model was generated in NASTRAN using shell elements. For both the static and free vibrational analysis, the beam was fixed at its root. In addition, 30 evenly spaced elements were used along the length of the beam. In NASTRAN, the 3d model has 10,990 solid hex elements. The comparison of the natural frequencies is given in Table 5.19. The first six mode shapes is given in Fig.5.14

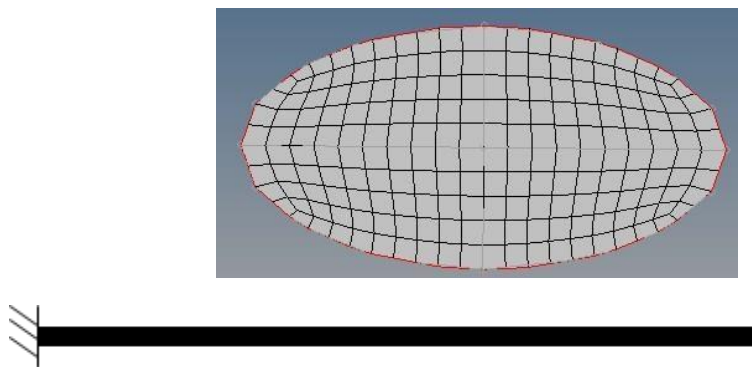


Figure.5.13. Elliptical cross- section cantilevered beam

Table.5.17. Dimension & material properties for the cross section shown in figure.5.13.

Dimensions	
2a	1m
2b	0.5m
Material Properties	
E ₁₁	100GPa
E ₃₃	100GPa
G ₁₂	41.67GPa
G ₁₃	41.67GPa
G ₂₃	41.67GPa
v ₁₂ ; v ₁₃ ; v ₂₃ ;	0.2;0.2;0.2
ρ	1 kg/m ³

Table.5.18. Cross-sectional properties for the cross section shown in figure 5.13

PRESENT METHOD	
K _{S,11} (N)*10 ⁹	6.39E-01
K _{S,22} (N)*10 ⁹	8.49E-01
K _{S,33} (N)*10 ⁹	1.10E+00
K _{S,44} (Nm ²)*10 ⁹	9.56E-04
K _{S,55} (Nm ²)*10 ⁹	9.56E-04
K _{S,66} (Nm ²)*10 ⁹	5.58E-04

Table.5.19. Comparison of natural frequencies with respect to NASTRAN for the cross section shown in figure 5.13

MODE	CURRENT MODEL[HZ]	MSC NASTRAN [HZ]	PERCENTAGE DIFFERENCE (%)
1	16.45	16.419	0.188449848
2	102.56	10.312	-0.546021841
3	288.6	289.15	-0.190575191
4	565.57	566.28	-0.125537069
5	935.09	934.89	0.021388316
6	1396.895	1392.58	0.30889938

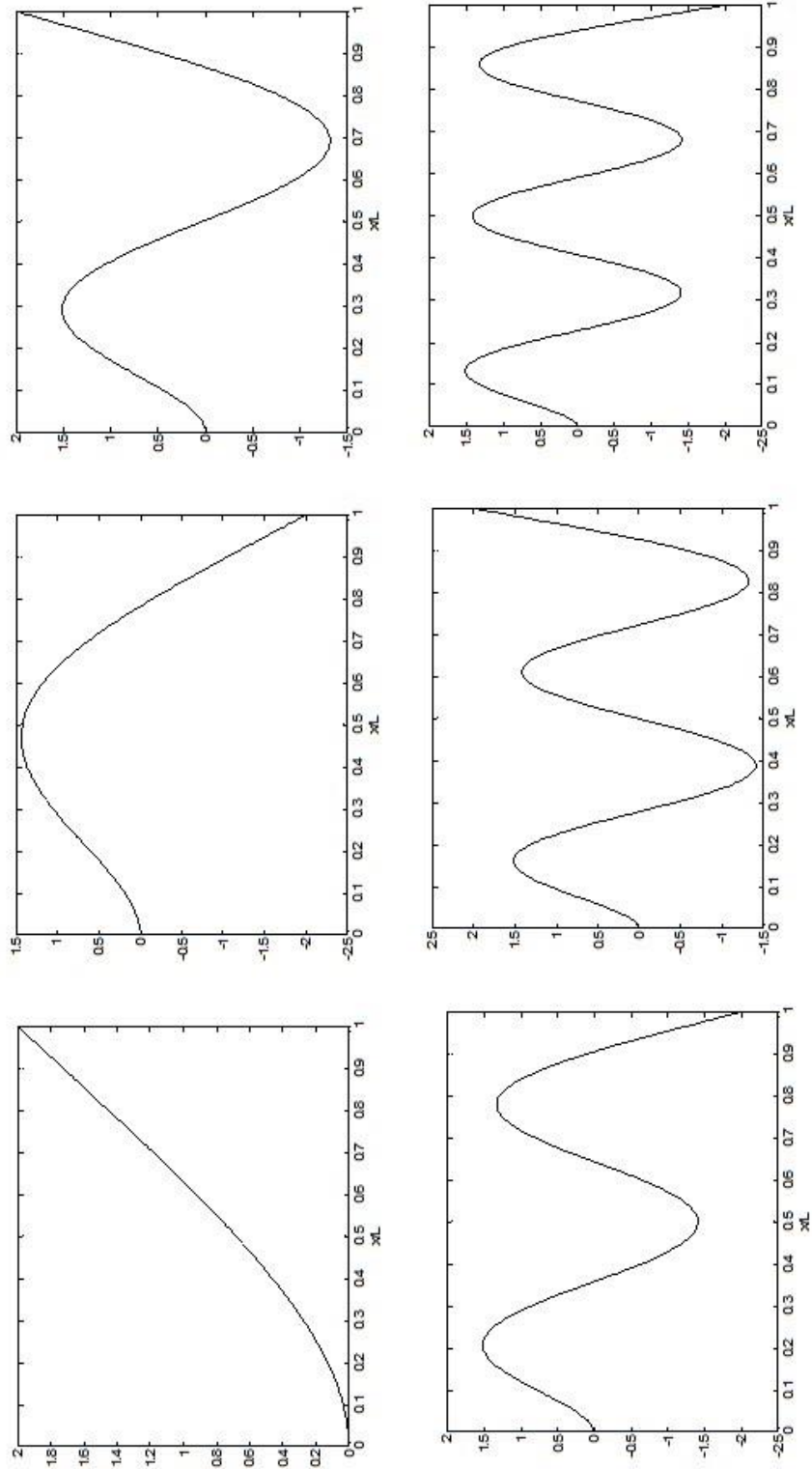


Figure.5.14. First six mode shapes of an elliptical cantilevered beam

5.4.2. Rectangular Box Beam:

The rectangular composite box beam is next considered for the validation. This is a standard example found in many research papers. Beam was generated with a length of 20 meters using the cross-section from the figure. The dimensions for the box beam crosssection are given in Fig.5.15. The material properties are given in Table.5.20. The fiber plane lies parallel to the xz plane and rotate around the y-axis .The resulting non zero terms for the cross-sectional stiffness matrix is compared from the VABS [1, 8]. The results are shown in Table 5.21. They have very good correlation with the values from the

VABS

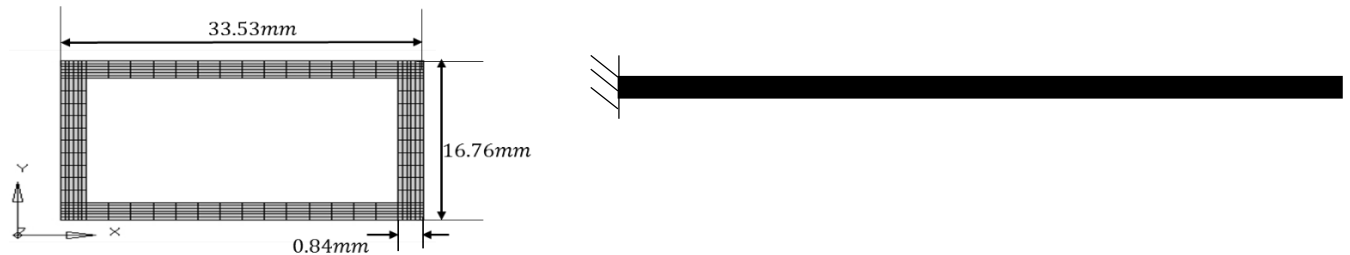


Figure.5.15. Rectangular box beam cross-section [20°/-70°/20°/-70°/-70°/20°] layups with T300/5208 Graphite [1, 8].

Table.5.20. Material properties for the cross section shown in figure 5.15

Material Properties (orthotropic)	
E_{11}	11.03 GPa
E_{22}	146.79GPa
E_{33}	146.79GPa
G_{12}	4.82GPa
G_{13}	6.20GPa
G_{23}	6.20GPa
$\nu_{12} ; \nu_{13} ; \nu_{23} ;$	0.28;0.28;0.26
ρ	1599kg/m ³

Table.5.21. Comparison of the cross-sectional properties for the cross section shown in figure 5.15

	CROSS-SECTIONAL PROPERTIES	VABS	PERCENTAGE ERROR (%)
$K_{s,11}(N)$	7.7345E+05	7.74E+05	5.58E-10
$K_{s,14}(Nm^2)$	8.3423E+03	8.33E+03	1.24E-09
$K_{s,22}(N)$	2.9587E+05	2.96E+05	2.29E-10
$K_{s,25}(Nm^2)$	9.0659E+03	9.07E+03	7.65E-10
$K_{s,33}(N)$	5.0614E+06	5.06E+06	-7.87E-10
$K_{s,36}(Nm^2)$	-1.7278E+04	-1.72E+04	0.00E+00
$K_{s,44}(Nm^2)$	2.46E+02	2.46E+02	1.18E-10
$K_{s,55}(Nm^2)$	7.44E+02	7.44E+02	1.02E-08
$K_{s,66}(Nm^2)$	1.50E+02	1.50E+02	1.60E-09

Eigenvalue computations are performed in order to find the natural frequencies and mode shapes. To verify the static as well as normal mode solutions of this beam, an identical model was generated in NASTRAN using shell elements. For both the static and normal mode case, the beam was fixed at its root. In addition, 40 evenly spaced elements were used along the length of the beam. In NASTRAN, the 2d model has 21,886 shell quad elements. The comparison of the natural frequencies is given in Table 5.22.

Table.5.22. Comparison of the natural frequency for the cross section shown in figure.5.15.

MODE	CURRENT MODEL[HZ]	HODGES (VABS)	MSC NASTRAN	PERCENTAGE DIFFERENCE (NASTRAN) (%)	PERCENTAGE DIFFERENCE (HODGES) (%)
1	3.00	3.00	2.98	0.666	0
2	5.19	5.19	5.12	1.348	0
3	18.79	19.04	18.65	0.745	1.330
4	32.41	32.88	32.02	1.203	1.450
5	52.57	54.69	52.17	0.761	4.0327
6	91.58		93.39	1.973	

From the above natural frequencies and mode shapes results it may be concluded that the beam model can capture the physical behaviors of a structurally coupled single body very well. The first six mode shapes are given in the Fig. 5.16.

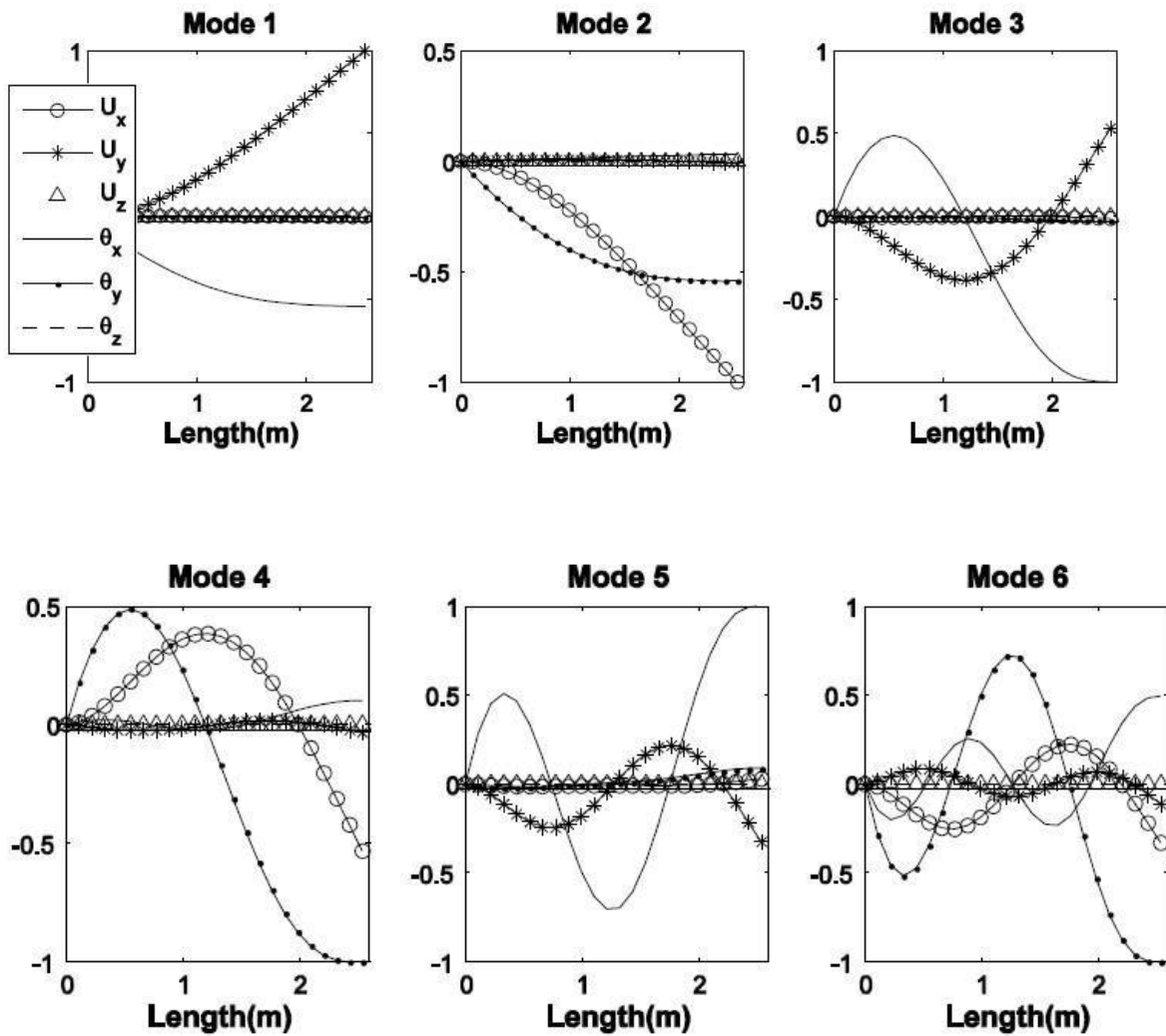


Figure.5.16. First six mode shapes of a cantilevered beam with box beam crosssection.

5.4.3. Airfoil Section:

The airfoil model beam is considered for the validation. This is a case found in many research papers by Yu [1, 6, 8, 19, 66]. Beam was generated with a length of 18 meters using the cross-section from the Fig. 5.17 The cross-sectional mesh used in the framework is given in Fig.5.18. Eigenvalue computation is performed in order to find the natural

frequencies and mode shapes. To verify the normal mode solutions of this beam, an identical model was generated in NASTRAN using shell elements. For normal mode analysis, the beam was fixed at its root. In addition, 20 evenly spaced elements were used along the length of the beam. In NASTRAN, the 2D model has 35,458 shell quad elements. The comparison of the natural frequencies is given in Table.5.24.



Figure.5.17. Mesh of the airfoil model in NASTRAN

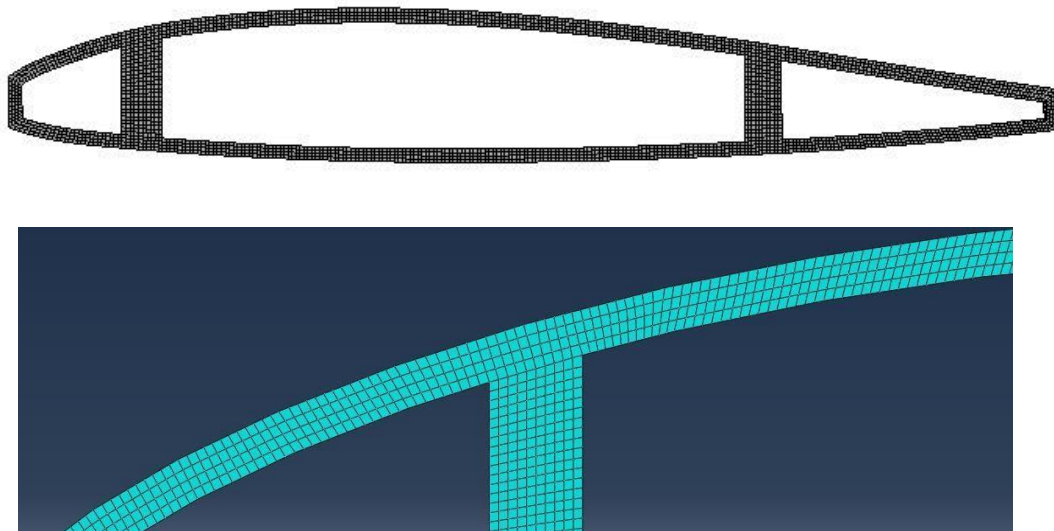


Figure.5.18. Cross-section mesh of the airfoil section used in the framework

Table.5.23. Comparison of the cross-sectional properties for the airfoil cross section.

	PRESENT METHOD	VABS	PERCENTAGE ERROR (%)
K _{S,11} (N)	4.47E+05	4.468E+05	5.58E-10
K _{S,22} (N)	3.840E+04	3.840E+04	1.24E-09
K _{S,33} (N)	1.586E+06	1.586E+06	2.29E-10
K _{S,44} (Nm ²)	5.0131E+01	5.017E+01	7.65E-10
K _{S,55} (Nm ²)	1.165E+01	1.165E+01	-7.87E-10
K _{S,66} (Nm ²)	0.145E+01	0.184E+01	0.00E+00
K _{S,13} (Nm ²)	5.666E+05	5.766E+05	1.18E-10
K _{S,46} (Nm ²)	-9.225E-01	-9.221E-01	1.02E-08

Table.5.24. Comparison of the natural frequencies for the airfoil cross section.

MODE	CURRENT MODEL[HZ]	VABS [HZ]	MSC NASTRAN	PERCENTAGE DIFFERENCE (NASTRAN) (%)	PERCENTAGE DIFFERENCE (HODGES) (%)
1	52.5	52.6	53.45	0.3256	0.002
2	209.7	209.8	209.95	0.25	0.005
3	326.1	326.3	327.8	0.258	0.058
4	899.3	899.8	900.58	0.487	0.258
5	1284.2	1284.9	1286.58	0.1896	0.587
6	1660.9	1661.3	1667.5	0.689	0.247

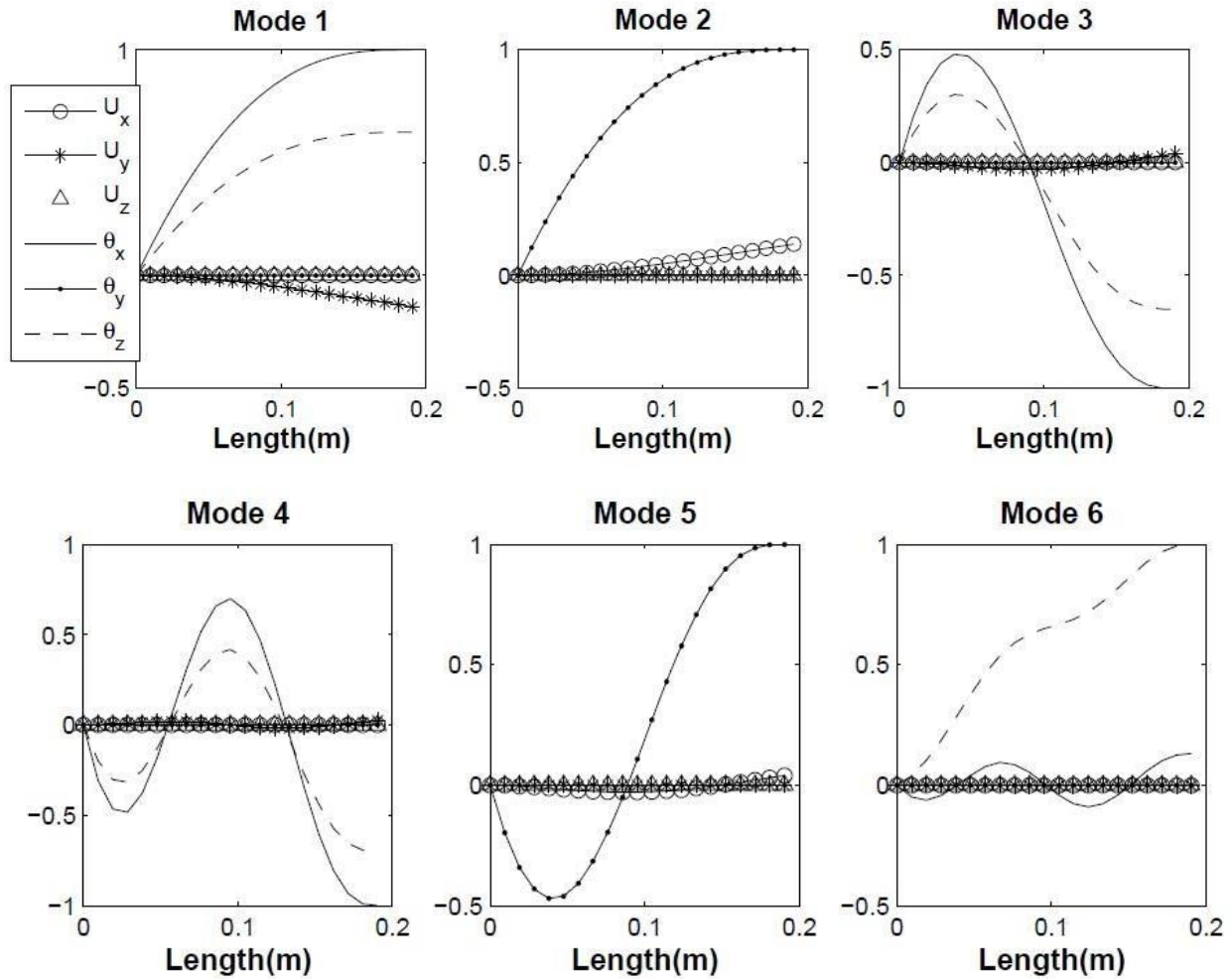


Figure.5.19. Mode shapes for the airfoil cross section.

It is clear to see that flap wise bending-torsion, KS_{46} , and axial-edgewise deflections, KS_{13} , are coupled for this structure from Table.5.23. The coupling effect on the structure can be captured through the mode shape analyses. Fig.5.19 shows the first 6 mode shapes. From the mode 1, 3, 4, and 6 it is shown that the u_y and ζ_x are coupled with the torsion related mode ζ_z . From the above results of natural frequencies and mode shapes, it can be concluded that the new beam model can capture the coupled physical characteristic behavior of complex cross sections.

5.5. Stress – Strain Validation:

Validations of the strain and stress recovery procedures implemented are compared against a 3-D finite element model developed in NASTRAN [31] for a case of a solid prismatic beam of square cross-section made of graphite-epoxy material. The beam is clamped at one end and load is applied at the free end in form of a tip force $F=1.0E5$ acting vertically (along the Y-axis), see Fig. 5.20. The cross-section of interest is in the middle of the beam, equidistant from both the constrained and the loaded beam-ends. The fiber planes in the entire beam cross-section are tilted by $\alpha = 17.5^\circ$ with respect to the XZ plane as given in Fig. 5.21. Additionally, all the fibers are biased by $\beta = 17.5^\circ$ away from the beam longitudinal Z axis. Geometrical and layup characteristics of the beam are given in Table 5.15. Graphite-epoxy material properties are given in Table 5.14.

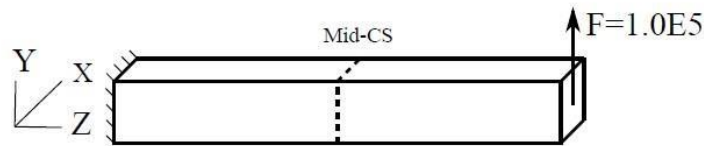


Figure.5.20. Square cross-section cantilevered beam

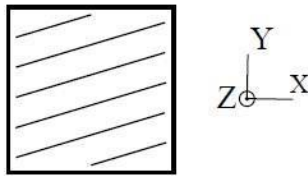
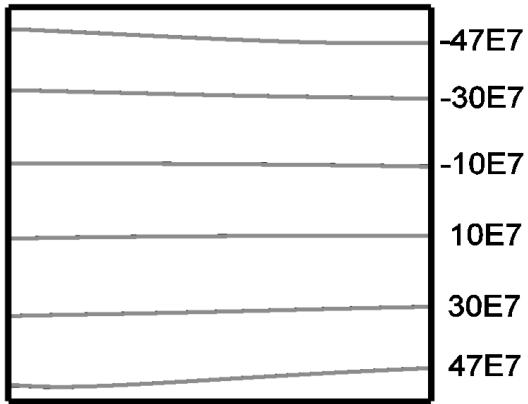


Figure.5.21. Fiber Plane coordinates system of the square cross-section.

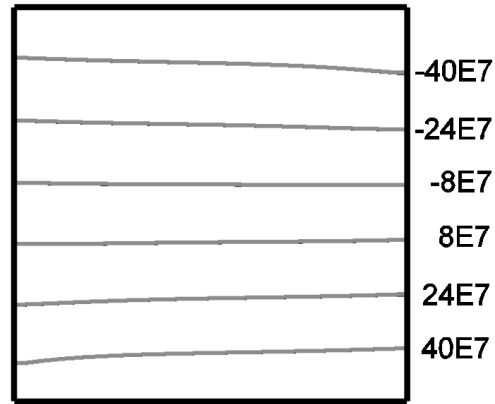
The beam cross-section of interest is meshed using 4-node elements. With the load F applied at the end of the beam, the mid-cross-section experiences a shear force F and a bending moment $M=FL/2$. The NASTRAN 3D FE model is meshed with 20-node SOLID elements

having 20x20 elements in the cross-section plane and 51 elements along the beam length. The tip load F is applied to the beam using an RBE3 element for master node configuration at the beam free end cross-section. The results for all six-stress components are given in the form of contour plots in Fig. 5.22.

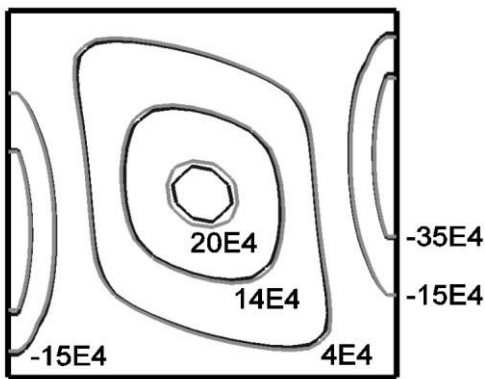
As it can be seen from the figures, the gray lines coincide with the dark lines, so it can be said that the results of the two models match very closely for all cases. Only for the ζ_{33} (Fig.5.22 c) the difference is noticeable, but very small.



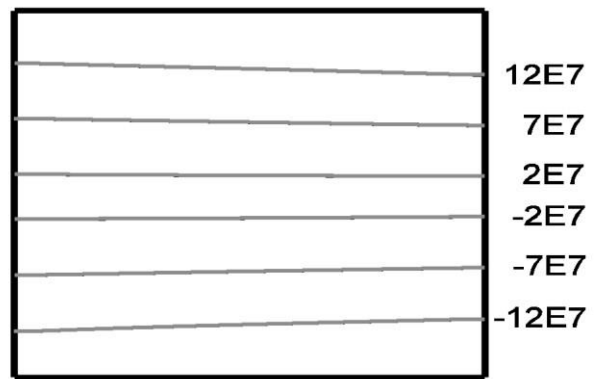
(a) ζ_{11}



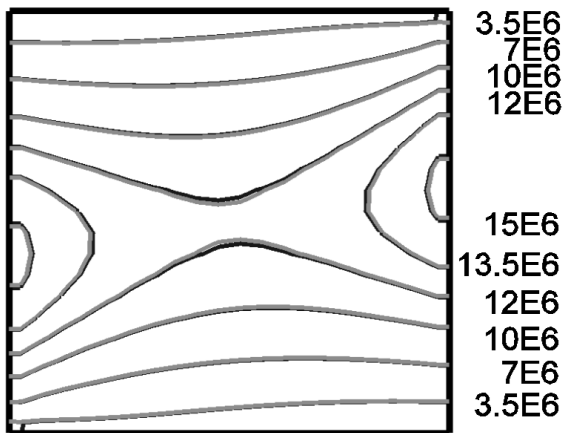
(b) ζ_{22}



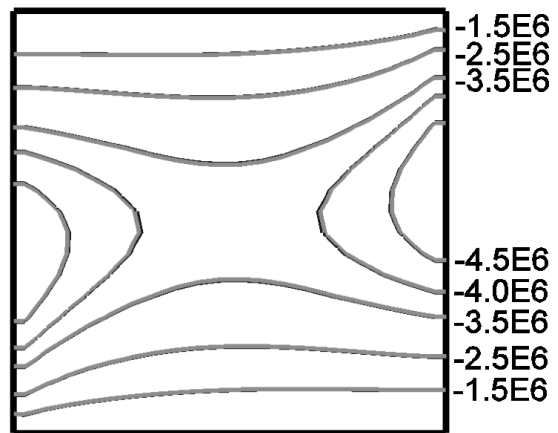
(c) ζ_{33}



(d) η_{13}



(e) η_{12}



(f) η_{23}

Figure.5.22. Stress contour of the cross-section. The light shaded lines are from the cross-sectional analysis tool, the dark lines indicate the stress from the NASTRAN model.

6. Natural Frequencies of a Drone

A 10-ft span unmanned aero vehicle named mAEWing1, which is shown in Fig.6.1, was designed, built and tested at the University of Minnesota (UMN). The wing of mAEWing1 is mainly composed of a solid spar. The solid spar was fabricated from a foam core with composite laminated reinforcements surrounding the core. The wing sets WS# 1 have larger stiffness properties for *mAEWing1*.

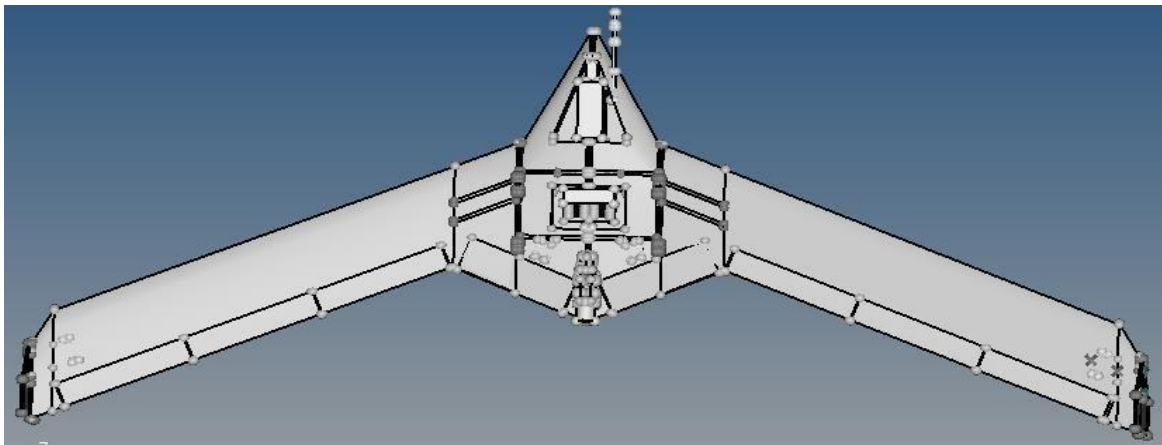


Figure.6.1. Geometry of the maewing1 model , (Credit: University of Minnesota) [79]

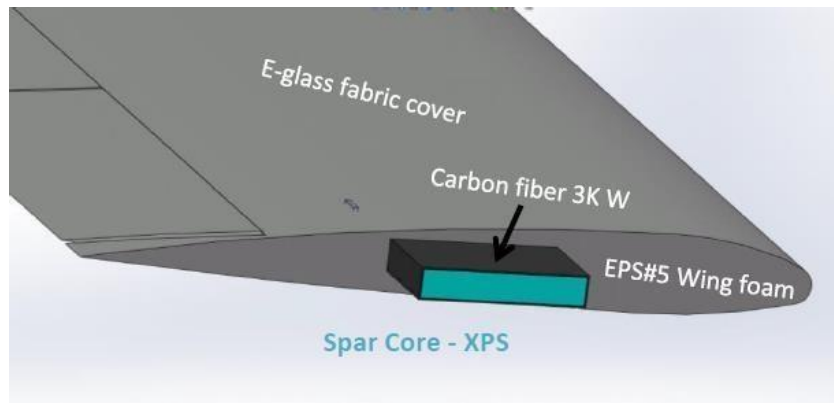


Figure.6.2. Depiction of the materials for the wing section of maewing1[70]

Spar core material is foam, XPS with density 2.3 lb/ft^3 . Reinforcement is carbon fiber lamination approximately $0.024''$ thick on all 4 sides. Outer lamination appears to be a unidirectional oriented to run along the spar. The spar was formed by laminating over a $2.75''$ by $0.25''$ foam plank. Based on limited measurements of the spar exterior a simple geometry was created and is shown in the top level drawing, a cross-section is shown in the Fig.6.2 [79].

The core material of the wing foam is EPS around 1.5 lb/ft^3 . There are ribs spaced within the foam core material near the actuator and hinge locations, none are externally visible so the construction is unknown. The wing foam is covered in fiberglass fabric, which is a plain weave with $0/90$ orientation and has $0.007''$ thickness. In the model, the wing foam cover is neglected, as it has very small thickness which has very little stiffness yet creates meshing problems. The hingeline is aligned to the upper wing surface. The control surface linkages are nylon horns with steel pushrods.

The center body is a framed structure from Carbon Fiber covered foam stock. Total thickness of structure stock is 0.25". The body is covered in carbon fiber fabric about 0.016" thick, single ply, oriented at ± 45 . A secondary bond of carbon fiber tape attaches the upper and lower surfaces. Control Surfaces were cut out. The lower surface is molded to approach the upper surface. The hingeline is aligned to the upper surface. The flight computer and battery bays were co-formed with the upper surface. The keel was formed separately and attached. There is also a separate cover for the flight computer bay that was formed separately.

Three sets of wings (Wing Set #1 (WS#1), WS#2 and WS#3) have been fabricated with different stiffness properties. The wingsets WS#1 and WS#3 have larger stiffness properties for *mAEWing1* and hence *mAEWing1* with WS#1 and WS#3 is called as stiff vehicle, and WS#2 has some slats in the wing foam and cover fabric to reduce the complete wing torsional stiffness to a lower value for a flexible wing. *mAEWing1* with WS#2 is named as flexible vehicle. In this report, we are considering WS#1 and WS#3 in order to implement the tool.

The solid spar is a main load-carrying member, and the solid spar has an uniform crosssectional area through the wing. The stiffness properties for the solid spar are obtained from the static test with one edge clamped and the other free. The properties for the beam for the solid spars are given in Table 6.1.

Table.6.1. Material properties of *mAEWing1*

Material Properties(WS1)(SOLID SPAR)	
Young's modulus E(psi) (Left)	3.80E+05
Shear modulus G(psi) (Left)	8.081E+04
Young's modulus E(psi) (Right)	3.389E+05
Shear modulus G(psi) (Right)	7.315E+04
Material Properties(WS3)(SOLID SPAR)	
Young's modulus E(psi) (Left)	3.80E+05
Shear modulus G(psi) (Left)	8.081E+04
Young's modulus E(psi) (Right)	3.254E+05
Shear modulus G(psi) (Right)	8.025E+04
Material Properties(Inner wing foam)	
Young's modulus E (psi)	2.300E+6
Shear modulus G (psi)	1.167E+5
Material Properties(Outer wing foam)	
Young's modulus E (psi)	2.559E+6
Shear modulus G (psi)	1.487E+5

The outer wing of *mAEWing1* is divided into 20 beam elements and a convergence study on the cross-sectional mesh is done for one of the sections to determine the element size, which was found to be .005". The inner wing of the *mAEWing1* is divided into 8 elements. The central body with mass elements is added with 6 elements with point loads at the node with respect to the geometry. This is shown in Fig.6.3. One of the crosssectional segment is shown in Fig.6.4. This model has 88 segments, and cross-sectional analysis tool is used in

order to find the stiffness properties of the cross-section. The cross-sectional properties of one of the segment are given in Table 6.2.

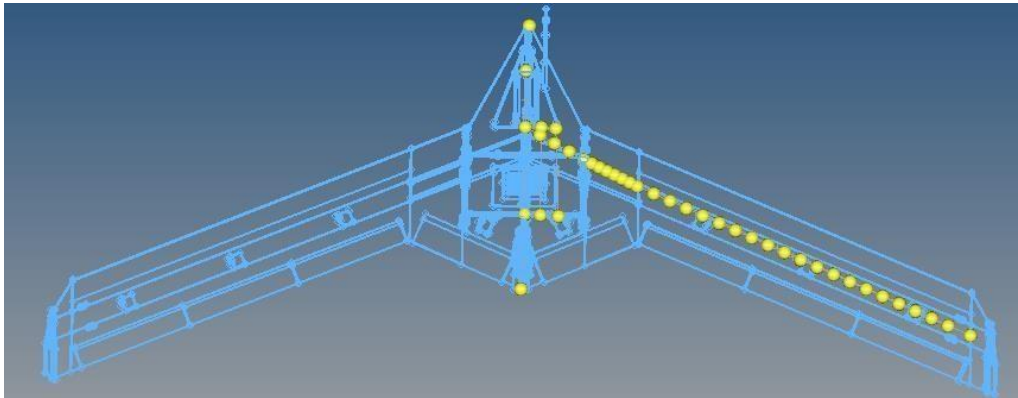


Figure.6.3. Depiction of the cross-section segments considered while modeling the beam

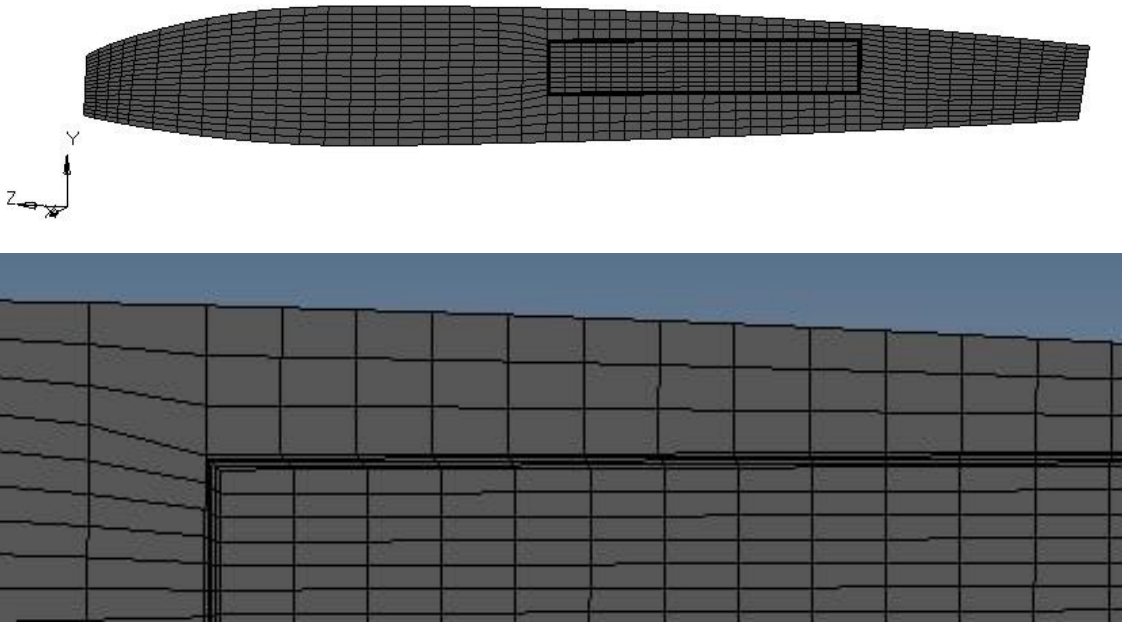


Figure.6.4. Airfoil mesh of maewing1 section 18.

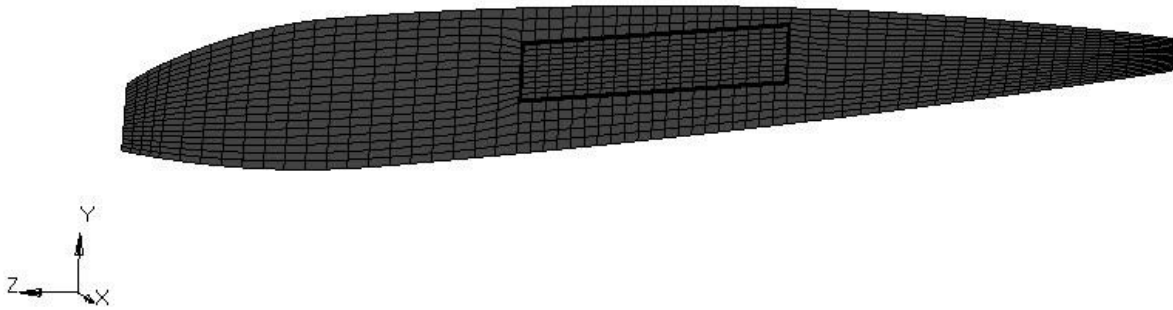


Figure.6.5. Airfoil mesh of maewing1 section 36 which is the intersection of the outer wing and inner wing.

Table.6.2. Cross-sectional properties of section12 of maewing1:

Present Method	
$K_{s,11}$ (lbs)	4.47E+05
$K_{s,22}$ (lbs)	3.840432E+04
$K_{s,33}$ (lbs)	1.5861568E+06
$K_{s,44}$ (lbs-in ²)	5.0.1313736E+01
$K_{s,55}$ (lbs-in ²)	1.1656606E+01
$K_{s,66}$ (lbs-in ²)	0.14567E+01
$K_{s,13}$ (lbs)	5.666750E+05
$K_{s,46}$ (lbs-in ²)	-9.22585E-01

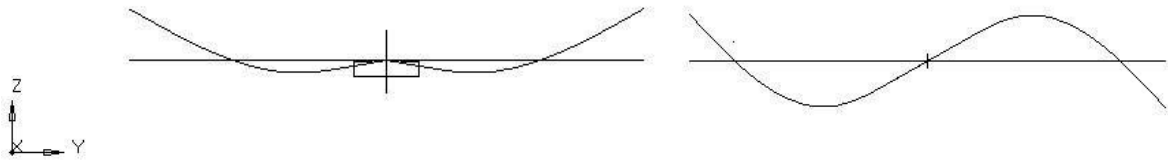
The centerbody of *maEWing1* is modeled as a rod attached with several point masses. The flight computer, propulsion battery, engine motor, body flaps, servos and accelerometers are all modeled as point masses. The mass of the wires in the centerbody and the combination of the foam and the cover fabric for the centerbody are modeled as a uniformly

distributed mass along the beam. While modeling the solid spar in the cross-sectional analysis the material is assumed to be isotropic with properties specified in the Table 6.1. Eigenvalue computation is done in order to find the natural frequencies and mode shapes. The natural frequencies for the *mAEWing1* WS#1 are given in Table 6.3. The natural frequencies for the *mAEWing1* WS#3 are given in the Table 6.4. The results are very comparable to the NASTRAN results. The difference in the results can be attributed to the fact that the cross-sectional properties are not constant along the length of the wing.

The results from NASTRAN are created by the beam model with equivalent properties. It has been created using beam elements in the NASTRAN along with rod elements for the center body. The modeling techniques used in the NASTRAN model is given in Ref.[70,71].

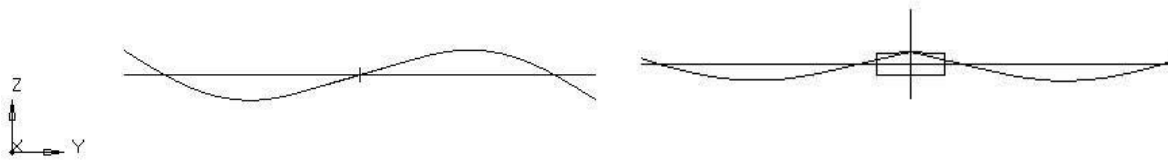
Table.6.3. Comparison of natural frequencies of the model with wingset WS#1

MODE	CURRENT MODEL[HZ]	MSC NASTRAN	PERCENTAGE DIFFERENCE (%)
1	7.025	6.95	1.0676
2	9.95	9.68	2.713
3	17.02	17.19	-0.998
4	16.89	16.74	0.888
5	20.35	20.94	-2.899
6	25.12	24.14	3.901



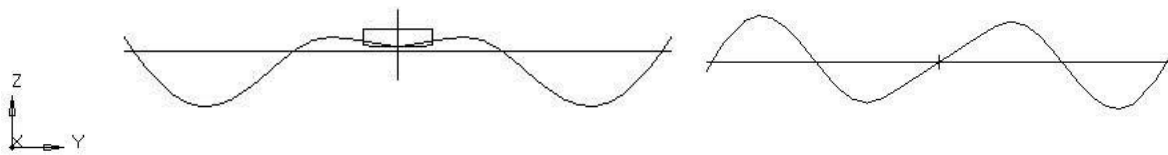
(a) Symmetric Bending Mode

(b) Antisymmetric Bending Mode



(c) Antisymmetric Torsion Mode

(d) Symmetric Torsion Mode



(e) Symmetric Bending Mode

(f) Antisymmetric Bending Mode

Figure.6.6. Six mode shapes of maewing1 WS#1

In the above Fig. 6.6, the first six mode shapes for WS#1 have been given. The Fig. 6.6.a represents the first symmetric bending mode. Fig. 6.6 (b) represents the first anti symmetric bending mode, (c) and (d) represents the first symmetric and antisymmetric torsion mode

respectively, and (e) and (f) represent the second symmetric bending mode and antisymmetric bending mode respectively.

The natural frequencies and mode shapes of WS#3 are given below. In Table 6.4, we can see that the results from the present analysis and NASTRAN using experimentally obtained equivalent properties are comparable. The mode shapes of the WS#3, extracted from the MATLAB are given in Fig.6.7

Table 6.4. Comparison of natural frequencies of the model with wingset WS#3.

MODE	CURRENT	MSC		PERCENTAGE
	MODEL[HZ]	NASTRAN		DIFFERENCE (%)
1	8.12	7.98	1.754	
2	13.85	13.21	4.844	
3	16.87	16.5	2.242	
4	19.82	19.44	0.964	
5	32.12	31.44	2.162	
6	42.87	41.96	1.929	

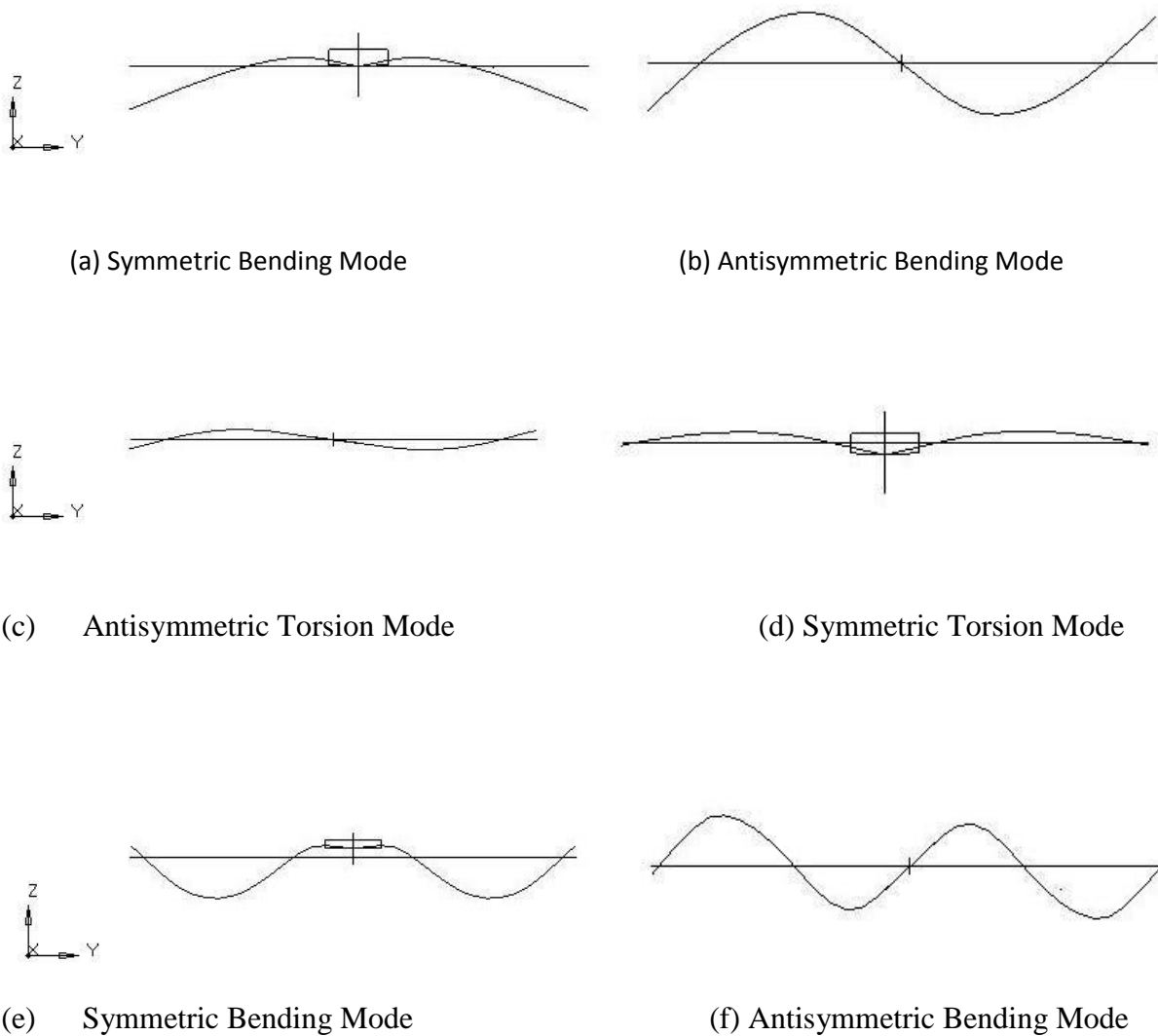


Figure.6.7. Six mode shapes of maewing1 WS#3

As it can be seen from the figure, the beam model has results which can be correlated to the NASTRAN model. The beam model is slightly stiffer than the NASTRAN model, so it has some discrepancies with the NASTRAN. From this, we can say that the framework for the Timoshenko beam model is verified and can be used for further modeling of *maewing2*, *xaewing3*.

7. Conclusion

This thesis presents a framework for a general, beam element that are being designed and built for static and free vibrational analysis of various drones whose wings have several couplings due to their cross-sectional geometry and material properties. A cross-section analysis tool has also been developed and validated in this thesis.

The theory underlying the evaluation of the cross-section stiffness properties has also been briefly described in this thesis. The numerical implementation of the theory has been thoroughly addressed. Finally, the validation of cross-sectional analysis was presented for various examples. The cross-section stiffness properties estimated have been compared against VABS (the Variation Asymptotic Beam Section Analysis by Yu et al[1]). Results are presented for different combinations of solid, thin-walled and open cross-sections, and isotropic and layered orthotropic materials. It is shown that the results from the proposed framework match closely with those of VABS in all cases. In particular, the proposed framework is able to correctly predict all geometrical and material induced couplings which are a great challenge for this type of tool. These results strongly suggest that the framework is efficient and robust, this framework will be able to handle a large range of section geometries and material properties.

The developed beam element is especially developed for *mAEWing1* and can be used for modeling wings with initial curvature (pre-bending), initial twist and taper. Originally, we had an idea to include warping of the beam element as degree of freedom. It was shown to be too ambitious and expensive. It will require a significant more research before it is possible to add such a capability to the multidisciplinary design optimization code.

The developed fully coupled beam element and the cross-section analysis tool has been validated against both numerical results and experiential measurements for wing of a drone *mAEWing*. Numerical validation has been performed against beam type calculations including Variational Asymptotical Beam Section analysis (VABS). The developed tool has been verified with *mAEWing1* mode results by comparing the present results with those calculated in NASTRAN.

References:

1. Hodges D., Nonlinear Composite Beam Theory, *Progress in Astronautics and Aeronautics Series*, 213, AIAA, 2006.
2. Jung S.N., Nagaraj, V.T. Chopra, I., Assessment Of Composite Rotor Blade Modeling Techniques, *Journal of the American Helicopter Society*, 4(3), 188- 205, 1999.
3. Volovoi V.V., Hodges D.H., Cesnik C.E.S., Popescu B., Assessment Of beaB Modeling Methods For Rotor Blade Applications, *Mathematical and Computer Modelling*, 33, 10991112, 2001.
4. Giavotto V., Borri M., Mantegazza P., Ghiringhelli G., Carmaschi V., Maffioli G.C., Mussi F., Anisotropic Beam Theory And Applications, *Composite Structures*, 16(1-4), 403413, 1983.
5. Blasques, J. P., Multi-Material Topology Optimization Of Laminated Composite Beams With Eigen Frequency Constraints. *Composite Structures* 2014, 111, 45-55.
6. Yu W., Volovoi, V.V., Hodges D.H., Hong X., Validation Of The Variational Asymptotic Beam Sectional Analysis (VABS), *AIAA Journal*, (40)10, 2105-2113.
7. Li L., Volovoi V. V., Hodges D. H., 2008, Cross-Sectional Design Of Composite Rotor Blades, *Journal of the American Helicopter Society*, 53(3), 240-251.
8. Hodges DH., Atilgan AR., Fulton MV., Rehfield LW., Free-Vibration Analysis Of Composite Beams, *Journal of the American Helicopter Society* 1991; 36(3): 36-47.
9. Issac M. D., Ori I., Engineering Mechanics Of Composite Materials, *Oxford*

University Press, 1994.

10. Kapania R K., Raciti S., Recent Advances In Analysis Of Laminated Beams and Plates: Part I. Shear Effects And Buckling; Part II. Vibrations And Wave Propagation, *AIAA Journal*, 1989; 27:923–46.
11. Chandrashekhara K, Krishnamurthy K, Roy S., Free Vibration Of Composite Beams Including Rotary Inertia And Shear Deformation, *Composite Structures* 1990; 14:269–79.
12. Bhimareddy A, Chandrashekhara K., Some Observations on the Modeling of Laminated Composite Beams With General Lay-Ups, *Composite Structures* 1991; 19:371–80.
13. Soldatos KP., Elishakoff I., A Transverse Shear and Normal Deformable Orthotropic Beam Theory, *Journal of Sound and Vibration* 1992; 154:528–33.
14. Abramovich H., Shear Deformation and Rotatory Inertia Effects of Vibrating Composite Beams, *Composite Structures* 1992; 20:165–73.
15. Krishnaswamy S., Chandrashekhara K., Wu WZB., Analytical Solutions to Vibration of Generally Layered Composite Beams, *Journal of Sound and Vibration* 1992; 159:85–99.
16. Chandrashekhara K., Bangera KM., Free Vibration of Composite Beams Using a Refined Shear Flexible Beam Element, *Computers and Structures* 1992; 43:719–27.
17. Abramovich H., Livshits A., Free Vibration of Non-Symmetric Crossply Laminated Composite Beams, *Journal of Sound and Vibration* 1994; 176:597– 612.
18. Khdeir AA., Reddy JN., Free Vibration of Cross-Ply Laminated Beams with

- Arbitrary Boundary Conditions, *International Journal of Engineering Science* 1994; 32:1971–80.
19. Maria AN., Yu W., Roy S., Two Finite Elements for General Composite Beams with Piezoelectric Actuators and Sensors, *Journal of finite elements in analysis and design*, Vol. 45, pp. 295- 304.
 20. Eisenberger M., Abramovich H., Shulepov O., Dynamic Stiffness Analysis of Laminated Beams using First Order Shear Deformation Theory, *Composite Structures* 1995; 31:265–71.
 21. Banerjee JR., Williams FW., Free Vibration of Composite Beams—An Exact Method Using Symbolic Computation, *Journal of Aircraft* 1995; 32:636–42.
 22. Teboub Y., Hajela P., Free Vibration of Generally Layered Composite Beams using Symbolic Computations, *Composite Structures* 1995; 33:123–34.
 23. Banerjee JR., Williams FW., Exact Dynamic Stiffness Matrix for Composite Timoshenko Beams with Applications, *Journal of Sound and Vibration* 1996; 194:573–85.
 24. Kant T., Marur SR., Rao GS., Analytical Solution to the Dynamic Analysis of Laminated Beams Using Higher Order Refined Theory, *Composite Structures* 1997; 40:1–9.
 25. Shimpi RP., Ainapure AV., Free Vibration Analysis of Two Layered Cross-ply Laminated Beams using Layer-wise Trigonometric Shear Deformation Theory, *Communications in Numerical Methods in Engineering* 1999; 15:651–60.
 26. Yildirim V., Sancaktar E., Kiral E., Free Vibration Analysis of Symmetric Crossply Laminated Composite Beams with the Help of the Transfer Matrix Approach, *Communications in Numerical Methods in Engineering* 1999; 15:651–60.

27. Yildirim V., Sancaktar E., Kiral E., Comparison of the In-Plane Natural Frequencies of Symmetric Cross-Ply Laminated Beams Based on the Bernoulli–Euler and Timoshenko Beam Theories, *Journal of Applied Mechanics* ,ASME 1999; 66:410-7.
28. Yildirim V.. Effect of the Longitudinal to Transverse Moduli Ratio on the InPlane Natural Frequencies of Symmetric Cross-Ply Laminated Beams by the Stiffness Method, *Composite Structures* 2000; 50:319–26.
29. Mahapatra DR., Gopalakrishnan S., Sankar TS., Spectral-Element Based Solutions For Wave Propagation Analysis of Multiple Connected Unsymmetric Laminated Composite Beams, *Journal of Sound and Vibration* 2000; 237:819–36.
30. Ghugal YM., Shimpi RP., A Review of Refined Shear Deformation Theories for Isotropic and Anisotropic Laminated Beams. *Journal of Reinforced Plastics and Composites* 2001;20:255–72.
31. Rao MK., Desai YM., Chitnis MR., Free Vibrations of Laminated Beams Using Mixed Theory, *Composite Structures* 2001; 52:149–60.
32. Chakraborty A., Mahapatra DR., Gopalakrishnan S., Finite Element Analysis of Free Vibration and Wave Propagation in Asymmetric Composite Beams with Structural Discontinuities, *Composite Structures* 2002; 55:23–36.
33. Mahapatra DR., Gopalakrishnan S., A Spectral Finite Element Model for Analysis of Axial Flexural-Shear Coupled Wave Propagation in Laminated Composite Beams, *Composite Structures* 2003; 59:67–88.
34. Chen WQ., Lu CF., Bian ZG., Elasticity Solution For Free Vibration of Laminated Beams, *Composite Structures* 2003; 62:75–82. 97
35. Chen WQ., Lu CF., Bian ZG., Free Vibration Analysis of Generally Laminated

- Beams Via State Space-Based Differential Quadrature, *Composite Structures* 2004; 63:417–25.
36. Ruotolo R., A Spectral Element For Laminated Composite Beams: Theory and Application to Pyro Shock Analysis, *Journal of Sound and Vibration* 2004; 270:149–69.
 37. Raveendranath P., Singh G., Pradhan B., Application of Coupled Polynomial Displacement Fields to Laminated Beam Elements, *Computers and Structures* 2000; 78:661–70.
 38. Yildirim V., Governing Equations of Initially Twisted Elastic Space Rods Made of Laminated Composite Materials, *International Journal of Engineering Science* 1999; 37:1007–35.
 39. Banerjee JR., Frequency Equation and Mode Shape Formulae for Composite Timoshenko Beams, *Composite Structures* 2001; 51:381–8.
 40. Banerjee JR., Explicit Analytical Expressions for Frequency Equation and Mode Shapes of Composite Beams, *International Journal of Solids and Structures* 2001; 38:2415–26.
 41. Bassiouni AS, Gad-Elrab RM, Elmahdy TH., Dynamic Analysis for Laminated Composite Beams., *Composite Structures* , 1999; 44:81–7.
 42. Shi G, Lam KY., Finite Element Vibration Analysis of Composite Beams Based on Higher Order Beam Theory, *Journal of Sound and Vibration* 1999; 219:707–21.
 43. Chen WQ., Lu CF., Bian ZG., A Semi-Analytical Method for Free Vibration of Straight Orthotropic Beams With Rectangular Cross-Sections., *Mechanics Research Communications* 2004; 31:725–34.

44. Aydogdu M., Vibration Analysis of Cross-Ply Laminated Beams with General Boundary Conditions by Ritz Method, *International Journal of Mechanical Sciences* 2005; 47:1740–55.
45. Murthy MVVS, Mahapatra DR, Badarinarayana K, Gopalakrishnan S., A Refined Higher Order Finite Element for Asymmetric Composite Beams, *Composite Structures* 2005; 7:27–35.
46. Numayr KS, Haddad MA, Ayoub AF., Investigation of Free Vibrations Of Composite Beams by Using the Finite-Difference Method, *Mechanics of Composite Materials* 2006; 42:231–42.
47. Subramanian P., Dynamic Analysis of Laminated Composite Beams Using Higher Order Theories And Finite Elements, *Composite Structures* 2006; 73:342–53.
48. Tahani M., Analysis of Laminated Composite Beams Using Layerwise Displacement Theories, *Composite Structures* 2007; 79:535–47.
49. Goyal VK, Kapania RK., A Shear-Deformable Beam Element For The Analysis Of Laminated Composites, *Finite Elements in Analysis and Design* ,2007; 43:463–77
50. Timoshenko SP., On the transverse vibration of bars of uniform cross-section. *Philosophical Magazine*, Series 6, Vol. 43, 2000, pp. 125-131.
51. Davis R, Henshell RD, Wanburton GB., A Timoshenko Beam Element. , *Journal of Sound and Vibration*, 1972; 22:475–87.
52. Thomas DL, Wilson JM, Wilson RR., Timoshenko Beam Finite Elements, *Journal of Sound and Vibration*, 1973;31:315–30.

53. Thomas J, Abbas BAH., Finite Element Model For Dynamic Analysis Of Timoshenko Beams, *Journal of Sound and Vibration*, 1975;41:291–9.
54. Levinson MA., A New Rectangular Beam Theory. , *Journal of Sound and Vibration*, 1981; 74:81–7.
55. Bickford WB., A Consistent High Order Beam Theory: Develop , *Journal of Applied Mechanics*, 1982;11:137–42.
56. Krishnamurthy AK., Toward a Consistent Beam Theory, *AIAA Journal*, 1984; 22:811–6.
57. Heyliger PR, Reddy JN., A High Order Beam Finite Element For Bending and Vibration Problems, *Journal of Sound and Vibration*, 1988; 126:309–26.
58. Kant T, Gupta A., A Finite Element Model For A High Order Shear Deformable Beam Theory, *Journal of Sound and Vibration*, 1988;125:193– 202.
59. Marur SR, Kant T. Free Vibration Analysis Of Fiber Reinforced Composite Beams Using Higher Order Theories And Finite Element Modeling, *Journal of Sound and Vibration*, 1996;194:337–51.
60. Kant T, Manut SR, Rao GS. Analytical Solution To The Dynamic Analysis Of Laminated Beams Using Higher Order Refined Theory, *Composite Structures*, 1988; 40:1–9.
61. Li Jun, Hua Hongxing , Shen Rongying, Dynamic Finite Element Method for Generally Laminated Composite Beams, *International Journal of Mechanical Sciences* 50 (2008); 466-480.
62. Kvaternik RG, Kaza KRV, Nonlinear Curvature Expressions for Combined

- Flapwise Bending, Chordwise Bending, Torsion, and Extension of Twisted Rotor Blades, *NASA TM X-73,997*, 1976.
63. Hodges DH., Nonlinear Equations for Dynamics of Pretwisted Beams Undergoing Small Strains and Large Rotations, *NASA TP 2470*, May 1985.
 64. Simo JC., A Finite Strain Beam Formulation: The Three Dimensional Dynamic Problem. Part I, *Computer methods in Applied Mechanics and Engineering*, Vol. 49, 1985, pp. 55-70.
 65. Simo JC, Vu-Quoc L., On the Dynamics in Space of Rods Undergoing Large Motion- A Geometrically Exact Approach, *Computer methods in Applied Mechanics and Engineering*, Vol. 66, 1988, pp. 125-161.
 66. Hodges DH., A Mixed Variational Formulation Based on Exact Intrinsic Equations for Dynamics of Moving Beams, *International Journal of Solids and Structures*, Vol. 26, No. 11, 1990, pp. 1253-1273.
 67. Bauchau OA., A Beam Theory for Anisotropic Materials, *Journal of Applied Mechanics*, Vol. 52, June 1985, pp. 416-422.
 68. Bauchau OA, Hong CH., Large Displacement Analysis of Naturally Curved and Twisted Composite Beams, *AIAA Journal*, Vol. 25, No. 11, 1987, pp. 1469-1475.
 69. Bauchau OA, Hong CH., Nonlinear Composite Beam Theory, *Journal of Applied Mechanics*, Vol. 55, March 1988, pp. 156-163.
 70. Zhao, W., Muthirevula, N., and Kapania, R. K., Finite Element Modeling of mAEWing1 in MSC PATRAN/NASTRAN, *Not published*, 2015.
 71. Zhao, W., Muthirevula, N., and Kapania, R. K., Finite Element Model Updating of a Small Flexible Composite UAV: mAEWing1 (Hati+WS3), *Not published*, 2016.

72. Smith, E. C., and Chopra, I. (1991), Formulation and Evaluation of an Analytical Model for Composite Box-Beams, *Journal of the American Helicopter Society*, Vol. 36, pp. 23-35.
73. Pai. F., and Nayfeh, A. H. (1992), A Nonlinear Composite Beam Theory, *Nonlinear Dynamics*, Vol. 3, pp. 273–303.
74. Song, O., and Librescu, L. (1993), Free Vibration of Anisotropic Composite ThinWalled Beams of Closed Cross-Section Contour, *Journal of Sound and Vibration*, Vol. 167, pp. 129–147.
75. Loughlan, J., and Ata, M. (1997), The Behavior of Open and Closed Section Carbon Fibre Composite Beams Subjected to Constrained Torsion, *Composite Structures*, Vol. 38, pp. 631–647.
76. Massa, J. C., and Barbero, E. J. (1998), A Strength of Materials Formulation for Thin Walled Composite Beams with Torsion, *Journal of Composite Materials*, Vol. 32, pp. 1560–1594.
77. Johnson, E. R., Vasiliev, V. V., and Vasiliev, D. V. (2001), Anisotropic Thin - Walled Beams with Closed Cross-Sectional Contours, *AIAA Journal*, Vol. 39, pp. 2389–2393.
78. Jung, S. N., Nagaraj, V. T., and Chopra, I. (2002), Refined Structural Model for Thin-and Thick-Walled Composite Rotor Blades, *AIAA Journal*, Vol. 40, pp. 105–116.
79. Regan, C., Static Test Of *maewing I* Spars and Foam, Not published, 2015

Appendix:

Matlab code:

Arrays:

```
function [ array ] = Arrays1( varargin ) options = varargin{ 1 }; originalFolder = pwd;
array.foldername=options.foldername; cd (array.foldername)
npos=load('N2D.in'); elconn=load('E2D.in'); emat=load('EMAT.in');
array.matprops=load('MATPROPS.in'); cd(originalFolder)
array.ne_2d=size(elconn,1); array.nn_2d=size(npos,1);
array.nmat=size(array.matprops,1); argin = elconn(:,2:end); vecform =
reshape(argin,[],1); idx_vecform_zeros = vecform==0; idx_vecform_nonzeros =
~idx_vecform_zeros; vecform_nonzeros = vecform(idx_vecform_nonzeros);
idxmap_nonzeros(unique(vecform_nonzeros))=1:size(unique(vecform_nonzeros),1);
aaa = idxmap_nonzeros(vecform_nonzeros); bbb = zeros(numel(vecform),1);
bbb(idx_vecform_nonzeros) = aaa; argout = reshape(bbb,[],size(argin,2));
array.el_2d = [(1:size(elconn,1))' argout]; array.elabel = elconn(:,1);
array.mapen_labls2int(elconn(:,1),1)=array.el_2d(:,1); mapnn =
idxmap_nonzeros(npos(:,1));
[B,IX] = sort(mapnn); array.nl_2d =
[mapnn(IX)' npos(IX,2:end)]; array.nlabel =
npos(IX,1); array.mapnn_labls2int(:,1) =
idxmap_nonzeros; array.emat = emat;
```

```

[ array ] = EBM_Q4_array( array ); array.max_ngpoints =
max([array.element(:).gpnts]); array.max_nnpe_2d =
max([array.element(:).nnpe_2d]); array.max_mdim_2d =
max([array.element(:).mdim_2d]);
array.etype(1:array.ne_2d)=1;
[array.iQ,array.jQ,array.vQ,array.iQm,array.jQm,array.vQm,array.density]=EBM_RotateElementM
aterialConstMatrix(array);
[array.pr_2d]=EBM_ReorderNodalPositions(array);
End

```

```

function [ Ag, Rg, Lg, Mg, Cg, Eg, Dg ] = EBM_Assemble_Ks( array ) nMECsum=0;
for e=1:array.ne_2d    nMECsum = nMECsum +
(array.element(array.etype(e)).mdim_2d)^2; end iM=zeros(nMECsum,1);
jM=zeros(nMECsum,1); vM=zeros(nMECsum,1);
iE=zeros(nMECsum,1); jE=zeros(nMECsum,1); vE=zeros(nMECsum,1);
iC=zeros(nMECsum,1); jC=zeros(nMECsum,1);
vC=zeros(nMECsum,1); nQ=(6)*(6); ind=1; for e=1:array.ne_2d
nnpe_2d = array.element(array.etype(e)).nnpe_2d;    mdim_2d =
array.element(array.etype(e)).mdim_2d;
    Qe=sparse(array.iQ((e-1)*nQ+1:e*nQ),array.jQ((e-1)*nQ+1:e*nQ),array.vQ((e-
1)*nQ+1:e*nQ));

```



```

[Me,Ee,Ce] = EBM_Q4(e,Qe,array);
edof_2d=zeros(mdim_2d,1);      for
i=1:nnpe_2d

    for j=1:mdim_2d/nnpe_2d      edof_2d(mdim_2d/nnpe_2d*(i-1)+j) = mdim_2d /
nnpe_2d * (array.el_2d(e,i+1)-1)+j;
    end
end

nMEC=(nnpe_2d*3)^2;   iM(ind : ind + nMEC-
1)=reshape(kron(edof_2d(:),ones(size(Me,1),1)),size(Me,1)*size(Me,2),1);   jM(ind : ind + nMEC-
1)=reshape(kron(edof_2d(:),ones(1,size(Me,1))),size(Me,1)*size(Me,2),1);   vM(ind : ind +
nMEC-1)=reshape(Me,size(Me,1)*size(Me,2),1);   iE(ind : ind + nMEC-
1)=reshape(kron(edof_2d(:),ones(size(Ee,1),1)),size(Ee,1)*size(Ee,2),1);   jE(ind : ind + nMEC-
1)=reshape(kron(edof_2d(:),ones(1,size(Ee,1))),size(Ee,1)*size(Ee,2),1);   vE(ind : ind + nMEC-
1)=reshape(Ee,size(Ee,1)*size(Ee,2),1);   iC(ind : ind + nMEC-
1)=reshape(kron(edof_2d(:),ones(size(Ce,1),1)),size(Ce,1)*size(Ce,2),1);   jC(ind : ind + nMEC-
1)=reshape(kron(edof_2d(:),ones(1,size(Ce,1))),size(Ce,1)*size(Ce,2),1);   vC(ind : ind + nMEC-
1)=reshape(Ce,size(Ce,1)*size(Ce,2),1);   ind = ind + nMEC; end

Mg=sparse(iM,jM,vM);

Eg=sparse(iE,jE,vE);

Cg=sparse(iC,jC,vC);

[ Zg ] = EBM_Zg( array );

Rg=sparse(Cg'*Zg);

Lg=sparse(Mg*Zg);

```

```
Ag=sparse(Zg'*Mg*Zg);
```

```
Dg = Zg';
```

```
end
```

```
function [ Ms ] = EBM_Assemble_Ms( Mass, xm, ym, Ixx, Iyy, Ixy )
```

```
Ms11=[ Mass    0    0 ;
```

```
    0    Mass    0 ;
```

```
    0    0    Mass];
```

```
Ms12=[ 0    0  -Mass*ym;
```

```
    0    0    Mass*xm;
```

```
    Mass*ym  -Mass*xm  0  ];
```

```
Ms22=[ Ixx  -Ixy    0  ;
```

```
  -Ixy  Iyy    0  ;
```

```
    0    0    Ixx+Iyy];
```

```
Ms=[Ms11 Ms12;
```

```
  -Ms12 Ms22];
```

```
end
```

```
function [ AlphaPrincipleAxis_Ref, AlphaPrincipleAxis_ElasticCenter ]
```

```
=EBM_CalcOrientationElasticAxes( Ks, ElasticX, ElasticY ) ksub=Ks(4:5,4:5);
```

```
[ mod, val ] = eig(ksub); [
```

```
val, ind ] = sort(diag(val));
```

```
mod = mod(:,ind);
```

```

AlphaPrincipleAxis_Ref=atan(mod(2,1)/mod(1,1));

p=[ ElasticX ElasticY ]; alpha=EBM_rad2deg(
0 );

[ Ksprime ] = EBM_TransformCrossSectionMatrix( Ks, p, alpha );
ksub=Ksprime( 4:5, 4:5 ); [ mod, val ] = eig( ksub ); [ val, ind ] =
sort(diag(val)); mod = mod(:,ind);

AlphaPrincipleAxis_ElasticCenter=atan(mod(2,1)/mod(1,1)); end

function[ Mass, xm, ym, Ixx, Iyy, Ixy, Ax, Ay, Axx, Ayy, Axy, Area, MassPerMaterial ] =
EBM_CalcSectionMassProps( array )

Ixx=0;Iyy=0;Ixy=0;

Mass=0; xm=0;ym=0;

Axx=0;Ayy=0;Axy=0;Area=0;

Ax=0;Ay=0;

MassPerMaterial=zeros(1,max(array.emat(:,2))); for
e=1:array.ne_2d

[Ixxe,Iyye,Ixye,Axxe,Ayye,Axye,Areae,Axe,Aye,Masse,MassXe,MassYe]=EBM_Q4_ElementMas
sProps(e,array);

    Ixx=Ixx+Ixxe;

    Iyy=Iyy+Iyye;

    Ixy=Ixy+Ixye;

xm=xm+MassXe;

ym=ym+MassYe;

```

```

Mass=Mass+Masse;

Axx=Axx+Axxe;

Ayy=Ayy+Ayye;

Axy=Axy+Axye;

Area=Area+Areae;

Ax=Ax+Axex;

Ay=Ay+Ayey;

MassPerMaterial(array.emat(e,2))=MassPerMaterial(array.emat(e,2))+Masse; end

xm=xm/Mass; ym=ym/Mass; Ax=Ax/Area; Ay=Ay/Area; end function [ ShearX,
ShearY, ElasticX, ElasticY ] =EBM_CalcShearAndElasticCenter( Ks ) F=Ks\eye(6);

z=1;

ShearX = (-F(6,2)+F(6,4)*(1-z))/F(6,6);

ShearY = (F(6,1)+F(6,5)*(1-z))/F(6,6);

ElasticX = -(F(4,4)*F(5,3)+F(4,5)*F(4,3))/(F(4,4)*F(5,5)-F(4,5)^2);

ElasticY = -(F(4,3)*F(5,5)-F(4,5)*F(5,3))/(F(4,4)*F(5,5)-F(4,5)^2);

end function [ Ks, solvec]=EBM_Constitutive_Ks(
array )

[Ag,Rg,Lg,Mg,Cg,Eg,Dg] = EBM_Assemble_Ks(array);

[Ks,solvec.dX,solvec.dY,solvec.X,solvec.Y] = EBM_SolveLin(Mg,Cg,Eg,Rg,Lg,Ag,Dg);

end function [ Ms ] = EBM_Constitutive_Ms( utils )

[Mass,xm,ym,Ixx,Iyy,Ixy]=EBM_CalcSectionMassProps(utils);

[Ms]=EBM_Assemble_Ms(Mass,xm,ym,Ixx,Iyy,Ixy); end

function [props] = EBM_CrossSectionProps(Ks,array)

[ props.ShearX, props.ShearY, props.ElasticX, props.ElasticY ]

```

```

=EBM_CalcShearAndElasticCenter( Ks );

[ props.MassTotal, props.MassX, props.MassY, props.Ixx, props.Iyy, props.Ixy,props.AreaX, props.AreaY,
props.Axx, props.Ayy, props.Axy, props.AreaTotal, props.MassPerMaterial ]

=EBM_CalcSectionMassProps( array );

[ props.AlphaPrincipleAxis_Ref, props.AlphaPrincipleAxis_ElasticCenter ] =
EBM_CalcOrientationElasticAxes( Ks, props.ElasticX, props.ElasticY );

End function [ R1 ] = EBM_CrossSectionRotationMatrix( alpha )

c=cosd(alpha); s=sind(alpha); R11=[c s 0;
-s c 0;
0 0 1];

R1=[R11 zeros(3); zeros(3) R11]; end function [ T2 ]
= EBM_CrossSectionTranslationMatrix( p )

T2=eye(6);

T2(1,6)=p(2);T2(2,6)=-p(1);T2(3,4)=-p(2);T2(3,5)=p(1); end function [
Qm, Sm ] = EBM_ElementMaterialConstitutiveMatrix( array, e )

E1=array.matprops(array.emat(e,2),1);
E2=array.matprops(array.emat(e,2),2);
E3=array.matprops(array.emat(e,2),3);
G12=array.matprops(array.emat(e,2),4);
G13=array.matprops(array.emat(e,2),5); G23=array.matprops(array.emat(e,2),6);
nu12=array.matprops(array.emat(e,2),7);
nu13=array.matprops(array.emat(e,2),8);
nu23=array.matprops(array.emat(e,2),9);

Sm = [ 1/E1 -nu12/E1 -nu13/E1 0 0 0 ;

```

$$\begin{array}{cccccc}
-\nu_{12}/E_1 & 1/E_2 & -\nu_{23}/E_2 & 0 & 0 & 0 & ; \\
-\nu_{13}/E_1 & -\nu_{23}/E_2 & 1/E_3 & 0 & 0 & 0 & ; \\
0 & 0 & 0 & 1/G_{23} & 0 & 0 & ; \\
0 & 0 & 0 & 0 & 1/G_{13} & 0 & ; \\
0 & 0 & 0 & 0 & 0 & 1/G_{12} &];
\end{array}$$

Qm=Sm\eye(6);

edof=[6 1 2 3 5 4];

Qm(edof,edof)=Qm; Sm(edof,edof)=Sm; end function [

Qf] = EBM_ElemRotateFiberPlane(Qm, c, s) t1 = (c ^

2); t3 = (s ^ 2); t7 = 2 * Qm(1,3) * c * s; t8 = Qm(1,1) *

t1 + Qm(1,2) * t3 + t7; t14 = 2 * Qm(3,3) * c * s; t15 =

Qm(3,1) * t1 + Qm(3,2) * t3 + t14; t16 = s * t15; t17 = c

* t8 + t16; t19 = c * t15; t24 = 2 * Qm(2,3) * c * s; t25 =

Qm(2,1) * t1 + Qm(2,2) * t3 + t24; t27 = t19 + s * t25;

t32 = Qm(1,1) * t3 + Qm(1,2) * t1 - t7; t36 = Qm(3,1) *

t3 + Qm(3,2) * t1 - t14; t37 = s * t36; t38 = c * t32 + t37;

t40 = c * t36; t43 = Qm(2,1) * t3 + Qm(2,2) * t1 - t24;

t45 = t40 + s * t43; t56 = -0.10e1 * t3 + 0.10e1 * t1; t58 = -0.10e1 *

Qm(1,1) * c * s + 0.10e1 * Qm(1,2) * c * s + Qm(1,3) * t56; t67 = -0.10e1 *

Qm(3,1) * c * s + 0.10e1 * Qm(3,2) * c * s + Qm(3,3) * t56; t68 = s * t67;

t69 = c * t58 + t68; t71 = c * t67; t79 = -0.10e1 * Qm(2,1) * c * s + 0.10e1 *

Qm(2,2) * c * s + Qm(2,3) * t56; t81 = t71 + s * t79; t88 = 0.10e1 *

Qm(1,4) * c + 0.10e1 * Qm(1,5) * s; t94 = 0.10e1 * Qm(3,4) * c + 0.10e1 *

$$\begin{aligned}
& Qm(3,5) * s; t95 = s * t94; t96 = c * t88 + t95; t98 = c * t94; t103 = 0.10e1 * \\
& Qm(2,4) * c + 0.10e1 * Qm(2,5) * s; t105 = t98 + s * t103; t112 = -0.10e1 * \\
& Qm(1,4) * s + 0.10e1 * Qm(1,5) * c; t118 = -0.10e1 * Qm(3,4) * s + 0.10e1 \\
& * Qm(3,5) * c; t119 = s * t118; t120 = c * t112 + t119; t122 = c * t118; t127 \\
& = -0.10e1 * Qm(2,4) * s + 0.10e1 * Qm(2,5) * c; t129 = t122 + s * t127; \\
& t133 = s * Qm(3,6); \\
& t134 = c * Qm(1,6) + t133; t136 = c * Qm(3,6); t138 = t136 + s * Qm(2,6); \\
& t205 = 2 * Qm(4,3) * c * s; t206 = Qm(4,1) * t1 + Qm(4,2) * t3 + t205; t212 \\
& = 2 * Qm(5,3) * c * s; t213 = Qm(5,1) * t1 + Qm(5,2) * t3 + t212; t218 = \\
& Qm(4,1) * t3 + Qm(4,2) * t1 - t205; t222 = Qm(5,1) * t3 + Qm(5,2) * t1 - \\
& t212; t232 = -0.10e1 * Qm(4,1) * c * s + 0.10e1 * Qm(4,2) * c * s + Qm(4,3) \\
& * t56; t241 = -0.10e1 * Qm(5,1) * c * s + 0.10e1 * Qm(5,2) * c * s + Qm(5,3) \\
& * t56; t248 = 0.10e1 * Qm(4,4) * c + 0.10e1 * Qm(4,5) * s; t254 = 0.10e1 * \\
& Qm(5,4) * c + 0.10e1 * Qm(5,5) * s; t261 = -0.10e1 * Qm(4,4) * s + 0.10e1 * \\
& Qm(4,5) * c; t267 = -0.10e1 * Qm(5,4) * s + 0.10e1 * Qm(5,5) * c; t295 = 2 \\
& * Qm(6,3) * c * s; Qf(1,1) = t17 * c + t27 * s; \\
& Qf(1,2) = t38 * c + t45 * s; \\
& Qf(1,3) = (t69 * c + t81 * s); \\
& Qf(1,4) = (t96 * c + t105 * s); \\
& Qf(1,5) = (t120 * c + t129 * s); \\
& Qf(1,6) = t134 * c + t138 * s; \\
& Qf(2,1) = (-s * t8 + t19) * s + (-t16 + c * t25) * c; \\
& Qf(2,2) = (-s * t32 + t40) * s + (-t37 + c * t43) * c;
\end{aligned}$$

$$Qf(2,3) = (-(-s * t58 + t71) * s + (-t68 + c * t79) * c);$$

$$Qf(2,4) = (-(-s * t88 + t98) * s + (-t95 + c * t103) * c);$$

$$Qf(2,5) = (-(-s * t112 + t122) * s + (-t119 + c * t127) * c);$$

$$Qf(2,6) = (-(-s * Qm(1,6) + t136) * s + (-t133 + c * Qm(2,6)) * c);$$

$$Qf(3,1) = -t17 * s + t27 * c;$$

$$Qf(3,2) = -t38 * s + t45 * c;$$

$$Qf(3,3) = (-t69 * s + t81 * c);$$

$$Qf(3,4) = (-t96 * s + t105 * c);$$

$$Qf(3,5) = (-t120 * s + t129 * c);$$

$$Qf(3,6) = -t134 * s + t138 * c;$$

$$Qf(4,1) = c * t206 + s * t213;$$

$$Qf(4,2) = c * t218 + s * t222;$$

$$Qf(4,3) = (c * t232 + s * t241);$$

$$Qf(4,4) = (c * t248 + s * t254);$$

$$Qf(4,5) = (c * t261 + s * t267);$$

$$Qf(4,6) = c * Qm(4,6) + s * Qm(5,6);$$

$$Qf(5,1) = -s * t206 + c * t213;$$

$$Qf(5,2) = -s * t218 + c * t222;$$

$$Qf(5,3) = (-s * t232 + c * t241);$$

$$Qf(5,4) = (-s * t248 + c * t254);$$

$$Qf(5,5) = (-s * t261 + c * t267);$$

$$Qf(5,6) = -s * Qm(4,6) + c * Qm(5,6);$$

$$Qf(6,1) = Qm(6,1) * t1 + Qm(6,2) * t3 + t295;$$

$$Qf(6,2) = Qm(6,1) * t3 + Qm(6,2) * t1 - t295;$$

$$Qf(6,3) = (-0.10e1 * Qm(6,1) * c * s + 0.10e1 * Qm(6,2) * c * s + Qm(6,3) * t56);$$

$$Qf(6,4) = (0.10e1 * Qm(6,4) * c + 0.10e1 * Qm(6,5) * s);$$

$$Qf(6,5) = (-0.10e1 * Qm(6,4) * s + 0.10e1 * Qm(6,5) * c);$$

$$Qf(6,6) = Qm(6,6); \text{ end function [Qp] =}$$

$$\text{EBM_ElemRotateLayer(Qm, c, s)}$$

$$t1 = (c ^ 2); t5 = 2 * Qm(1,4) * c * s; t6 = s ^ 2; t8$$

$$= Qm(1,1) * t1 - t5 + Qm(1,6) * t6; t13 = 2 *$$

$$Qm(4,4) * c * s; t15 = Qm(4,1) * t1 - t13 +$$

$$Qm(4,6) * t6; t16 = s * t15; t17 = c * t8 - t16; t19 =$$

$$c * t15; t23 = 2 * Qm(6,4) * c * s; t25 = Qm(6,1) *$$

$$t1 - t23 + Qm(6,6) * t6; t27 = t19 - s * t25; t31 = s$$

$$* Qm(4,2); t32 = c * Qm(1,2) - t31; t34 = c *$$

$$Qm(4,2); t36 = t34 - s * Qm(6,2); t43 = 0.10e1 *$$

$$Qm(1,3) * c - 0.10e1 * Qm(1,5) * s; t49 = 0.10e1 *$$

$$Qm(4,3) * c - 0.10e1 * Qm(4,5) * s; t50 = s * t49;$$

$$t51 = c * t43 - t50; t53 = c * t49; t58 = 0.10e1 *$$

$$Qm(6,3) * c - 0.10e1 * Qm(6,5) * s; t60 = t53 - s *$$

$$t58; t68 = -0.10e1 * t6 + 0.10e1 * t1; t73 = 0.10e1$$

$$* Qm(1,1) * c * s + Qm(1,4) * t68 - 0.10e1 *$$

$$Qm(1,6) * c * s; t82 = 0.10e1 * Qm(4,1) * c * s +$$

$$Qm(4,4) * t68 - 0.10e1 * Qm(4,6) * c * s; t83 = s *$$

$$t82; t84 = c * t73 - t83; t86 = c * t82; t94 = 0.10e1$$

$$* Qm(6,1) * c * s + Qm(6,4) * t68 - 0.10e1 *$$

$$\begin{aligned}
& Qm(6,6) * c * s; t96 = t86 - s * t94; t103 = 0.10e1 \\
& * Qm(1,3) * s + 0.10e1 * Qm(1,5) * c; t109 = \\
& 0.10e1 * Qm(4,3) * s + 0.10e1 * Qm(4,5) * c; t110 \\
& = s * t109; t111 = c * t103 - t110; t113 = c * t109; \\
& t118 = 0.10e1 * Qm(6,3) * s + 0.10e1 * Qm(6,5) * \\
& c; t120 = t113 - s * t118; t125 = Qm(1,1) * t6 + t5 \\
& + Qm(1,6) * t1; t129 = Qm(4,1) * t6 + t13 + \\
& Qm(4,6) * t1; t130 = s * t129; t131 = c * t125 - \\
& t130; \\
& t133 = c * t129; t136 = Qm(6,1) * t6 + t23 + Qm(6,6) * t1; t138 = t133 - s * \\
& t136; t144 = 2 * Qm(2,4) * c * s; t171 = 2 * Qm(3,4) * c * s; t173 = \\
& Qm(3,1) * t1 - t171 + Qm(3,6) * t6; t178 = 2 * Qm(5,4) * c * s; t180 = \\
& Qm(5,1) * t1 - t178 + Qm(5,6) * t6; t190 = 0.10e1 * Qm(3,3) * c - 0.10e1 * \\
& Qm(3,5) * s; t196 = 0.10e1 * Qm(5,3) * c - 0.10e1 * Qm(5,5) * s; t206 = \\
& 0.10e1 * Qm(3,1) * c * s + Qm(3,4) * t68 - 0.10e1 * Qm(3,6) * c * s; t215 = \\
& 0.10e1 * Qm(5,1) * c * s + Qm(5,4) * t68 - 0.10e1 * Qm(5,6) * c * s; t222 = \\
& 0.10e1 * Qm(3,3) * s + 0.10e1 * Qm(3,5) * c; t228 = 0.10e1 * Qm(5,3) * s \\
& + 0.10e1 * Qm(5,5) * c; t233 = Qm(3,1) * t6 + t171 + Qm(3,6) * t1; t237 = \\
& Qm(5,1) * t6 + t178 + Qm(5,6) * t1; \\
& Qp(1,1) = t17 * c - t27 * s; \\
& Qp(1,2) = t32 * c - t36 * s; \\
& Qp(1,3) = (t51 * c - t60 * s); \\
& Qp(1,4) = (t84 * c - t96 * s);
\end{aligned}$$

$$Qp(1,5) = (t111 * c - t120 * s);$$

$$Qp(1,6) = t131 * c - t138 * s;$$

$$Qp(2,1) = Qm(2,1) * t1 - t144 + Qm(2,6) * t6;$$

$$Qp(2,2) = Qm(2,2);$$

$$Qp(2,3) = (0.10e1 * Qm(2,3) * c - 0.10e1 * Qm(2,5) * s);$$

$$Qp(2,4) = (0.10e1 * Qm(2,1) * c * s + Qm(2,4) * t68 - 0.10e1 * Qm(2,6) * c * s);$$

$$Qp(2,5) = (0.10e1 * Qm(2,3) * s + 0.10e1 * Qm(2,5) * c);$$

$$Qp(2,6) = Qm(2,1) * t6 + t144 + Qm(2,6) * t1;$$

$$Qp(3,1) = c * t173 - s * t180;$$

$$Qp(3,2) = c * Qm(3,2) - s * Qm(5,2);$$

$$Qp(3,3) = (c * t190 - s * t196);$$

$$Qp(3,4) = (c * t206 - s * t215);$$

$$Qp(3,5) = (c * t222 - s * t228);$$

$$Qp(3,6) = c * t233 - s * t237;$$

$$Qp(4,1) = t17 * s + t27 * c;$$

$$Qp(4,2) = t32 * s + t36 * c;$$

$$Qp(4,3) = (t51 * s + t60 * c);$$

$$Qp(4,4) = (t84 * s + t96 * c);$$

$$Qp(4,5) = (t111 * s + t120 * c);$$

$$Qp(4,6) = t131 * s + t138 * c;$$

$$Qp(5,1) = t173 * s + t180 * c;$$

$$Qp(5,2) = Qm(3,2) * s + Qm(5,2) * c;$$

$$Qp(5,3) = (t190 * s + t196 * c);$$

$$Qp(5,4) = (t206 * s + t215 * c);$$

```

Qp(5,5) = (t222 * s + t228 * c);
Qp(5,6) = t233 * s + t237 * c;
Qp(6,1) = (s * t8 + t19) * s + (t16 + c * t25) * c;
Qp(6,2) = (s * Qm(1,2) + t34) * s + (t31 + c * Qm(6,2)) * c;
Qp(6,3) = ((s * t43 + t53) * s + (t50 + c * t58) * c);
Qp(6,4) = ((s * t73 + t86) * s + (t83 + c * t94) * c);
Qp(6,5) = ((s * t103 + t113) * s + (t110 + c * t118) * c); Qp(6,6) = (s * t125
+ t133) * s + (t130 + c * t136) * c; end function EBM_PrintResults(const,
props, array ) Filename='EBM_cc12.out'; fid = fopen(Filename,'w+'); sk =
size(const.Ks); fprintf(fid,'\n'); fprintf(fid,'Stiffness matrix w.r.t. to the
crosssection reference point \n'); fprintf(fid,'K=\n');
fprintf(fid,[repmat('%19.12g\t',1,sk(2)-1) '%19.12g\n'],full(const.Ks).');
fprintf(fid,'\n'); fprintf(fid,'Compliance matrix w.r.t. to the cross section
reference point \n'); fprintf(fid,'F=\n');
fprintf(fid,[repmat('%19.12g\t',1,sk(2)-1) '%19.12g\n'],full(inv(const.Ks)).');
fprintf(fid,'\n'); fprintf(fid,'Mass matrix w.r.t. to the cross section reference
point \n'); fprintf(fid,'M=\n'); fprintf(fid,[repmat('%19.12g\t',1,sk(2)-1)
'%19.12g\n'],full(const.Ms).'); fprintf(fid,'\n'); fprintf(fid,'Shear center;\n');
fprintf(fid,'ShearX=%19.12g \n', props.ShearX);
fprintf(fid,'ShearY=%19.12g \n', props.ShearY);

fprintf(fid,'\n'); fprintf(fid,'Elastic center:\n');
fprintf(fid,'ElasticX=%19.12g \n', props.ElasticX);
fprintf(fid,'ElasticY=%19.12g \n', props.ElasticY);

```

```

fprintf(fid,'Mass center:\n');
fprintf(fid,'MassX=%19.12g \n',props.MassX);
fprintf(fid,'MassY=%19.12g \n',props.MassY);
fprintf(fid,'\n'); fprintf(fid,'Mass per unit
length:\n'); fprintf(fid,'Mass=%19.12g
\n',props.MassTotal);
fprintf(fid,'\n'); fprintf(fid,'Mass moments of
inertia:\n'); fprintf(fid,'Ixx=%19.12g
\n',props.Ixx); fprintf(fid,'Iyy=%19.12g
\n',props.Iyy); fprintf(fid,'Ixy=%19.12g
\n',props.Ixy); fprintf(fid,'\n'); fprintf(fid,'Area
center:\n'); fprintf(fid,'AreaX=%19.12g
\n',props.AreaX); fprintf(fid,'AreaY=%19.12g
\n',props.AreaY);
fprintf(fid,'\n'); fprintf(fid,'Area per unit
length:\n'); fprintf(fid,'Area=%19.12g
\n',props.AreaTotal); fprintf(fid,'Area
moments:\n'); fprintf(fid,'Ixx=%19.12g
\n',props.Axx); fprintf(fid,'Iyy=%19.12g
\n',props.Ayy); fprintf(fid,'Ixy=%19.12g
\n',props.Axy); p=[props.ShearX
props.ShearY]; theta=0;
[Ksprime]=EBM_TransformCrossSectionMatrix(const.Ks,p,theta);

```

```

fprintf(fid,'\n'); fprintf(fid,'Stiffness matrix with respect to shear
center:\n'); fprintf(fid,[repmat('%19.12g\t',1,sk(2)-1)
'%19.12g\n'],full(Ksprime).'); p=[props.ElasticX props.ElasticY];
theta=EBM_rad2deg(0);
[Ksprime]=EBM_TransformCrossSectionMatrix(const.Ks,p,theta);
fprintf(fid,'\n'); fprintf(fid,'Stiffness matrix with respect to the elastic
center:\n'); fprintf(fid,[repmat('%19.12g\t',1,sk(2)-1)
'%19.12g\n'],full(Ksprime).'); p=[props.MassX props.MassY]; theta=0;
[Msprime]=EBM_TransformCrossSectionMatrix(const.Ms,p,theta);
fprintf(fid,'\n'); fprintf(fid,'Mass matrix with respect to mass center\n');
fprintf(fid,[repmat('%19.12g\t',1,sk(2)-1) '%19.12g\n'],full(Msprime).');
fclose('all');

end function [ Me, Ee, Ce ] = EBM_Q4( enum, Qe,
array )

gw=zeros(array.element(array.etype(enum)).gpoints,1);
SNa=zeros(6*array.element(array.etype(enum)).gpoints,12);
Ba=zeros(6*array.element(array.etype(enum)).gpoints,12);

ng=0; for
n=1:array.element(array.etype(enum)).gpoints
xsg = array.element(array.etype(enum)).xxg(n);
yys = array.element(array.etype(enum)).yyg(n);
wg = array.element(array.etype(enum)).wg(n);

[ iJ, detJ ] = EBM_Q4_Jacobian( xxs, yys, array.pr_2d(:,enum) );

```

```

[ SN ] = EBM_Q4_SNe( xxs, yys );
[ B ] = EBM_Q4_Be( xxs, yys, iJ );
ng=ng+1;
SNa(1+(ng-1)*6:ng*6,:)=SN;
Ba(1+(ng-1)*6:ng*6,:)=B;
gw(ng)=wg*detJ; end
Qa=blkdiag(Qe*gw(1),Qe*gw(2),Qe*gw(3),Qe*gw(4));
Me=(Qa*SNa)*SNa;
Ee=Ba*Qa*Ba; Ce=Ba*Qa*SNa; end function [ array ] = EBM_Q4_array( array )
array.element(1).nnpe_2d=4; array.element(1).mdim_2d=12;
array.element(1).gpoinst=4; array.element(1).xxg = [ -0.577350269      -
0.577350269      0.577350269
0.577350269];
array.element(1).yyg = [ -0.577350269      0.577350269      -0.577350269
0.577350269]; array.element(1).wg = [1 1 1 1];
array.element(1).vertex_connection = [1 2 3 4];
array.element(1).gpoinstOrder = [1 3 4 2]; end
function [ B ] = EBM_Q4_Be( xxs, yys, iJ )
B=zeros(6,12); t1 = -1 + yys; t3 = -1 + xxs; t5 =
(iJ(1,1) * t1) / 0.4e1 + (iJ(1,2) * t3) / 0.4e1; t7 = -1
- xxs; t9 = -(iJ(1,1) * t1) / 0.4e1 + (iJ(1,2) * t7) /
0.4e1; t10 = 1 + yys; t13 = (iJ(1,1) * t10) / 0.4e1 -
(iJ(1,2) * t7) / 0.4e1; t16 = -(iJ(1,1) * t10) / 0.4e1 -

```

$$\begin{aligned}
& (iJ(1,2) * t3) / 0.4e1; t19 = (iJ(2,1) * t1) / 0.4e1 + \\
& (iJ(2,2) * t3) / 0.4e1; t22 = -(iJ(2,1) * t1) / 0.4e1 + \\
& (iJ(2,2) * t7) / 0.4e1; t25 = (iJ(2,1) * t10) / 0.4e1 - \\
& (iJ(2,2) * t7) / 0.4e1; t28 = -(iJ(2,1) * t10) / 0.4e1 - \\
& (iJ(2,2) * t3) / 0.4e1;
\end{aligned}$$

$$B(1,1) = t5;$$

$$B(1,4) = t9;$$

$$B(1,7) = t13;$$

$$B(1,10) = t16;$$

$$B(2,2) = t19;$$

$$B(2,5) = t22;$$

$$B(2,8) = t25;$$

$$B(2,11) = t28;$$

$$B(3,1) = t19;$$

$$B(3,2) = t5;$$

$$B(3,4) = t22;$$

$$B(3,5) = t9;$$

$$B(3,7) = t25;$$

$$B(3,8) = t13;$$

$$B(3,10) = t28;$$

$$B(3,11) = t16;$$

$$B(4,3) = t5;$$

$$B(4,6) = t9;$$

$$B(4,9) = t13;$$


```

B(4,12) = t16;

B(5,3) = t19;

B(5,6) = t22;

B(5,9) = t25; B(5,12) = t28; end function [ Ixx, Iyy, Ixy,Axx, Ayy, Axy, Area,
Ax, Ay,Mass, MassX, MassY ] =
EBM_Q4_ElementMassProps( enum, array )

Ixx=0;Iyy=0;Ixy=0;

Axx=0;Ayy=0;Axy=0;Area=0;

Ax=0;Ay=0;

Mass=0;MassX=0;MassY=0;

for n=1:array.element(array.etype(enum)).gpoints
xxs = array.element(array.etype(enum)).xxg(n);
yys = array.element(array.etype(enum)).yyg(n);      wg
= array.element(array.etype(enum)).wg(n);

[ xxb, yyb ] = EBM_Q4_InterpPos( array.pr_2d( :, enum ), xxs, yyb );
[ iJ, detJ ] = EBM_Q4_Jacobian( xxs, yyb, array.pr_2d( :, enum ) );

Iyy = Iyy + xxb^2*array.density(enum)*wg*detJ;

Ixx = Ixx + yyb^2*array.density(enum)*wg*detJ;

Ixy = Ixy + xxb*yyb*array.density(enum)*wg*detJ;

Ayy = Ayy + xxb^2*wg*detJ;

Axx = Axx + yyb^2*wg*detJ;

Axy = Axy + xxb*yyb*wg*detJ;

Area = Area + wg*detJ;

Ay = Ay + yyb*wg*detJ;

```

$Ax = Ax + xxb * wg * detJ;$

$Mass = Mass + array.density(enum) * wg * detJ;$

$MassX = MassX + xxb * array.density(enum) * wg * detJ;$

$MassY = MassY + yyb * array.density(enum) * wg * detJ;$

end

$J(1,1) = -(t1 * pr(1)) / 0.4e1 + (t1 * pr(3)) / 0.4e1 + (t4 * pr(5)) / 0.4e1 - (t4 * pr(7)) / 0.4e1; J(1,2)$

$= -(t1 * pr(2)) / 0.4e1 + (t1 * pr(4)) / 0.4e1 + (t4 * pr(6)) / 0.4e1 - (t4 * pr(8)) / 0.4e1; J(1,3) =$

$0.0e0;$

$J(2,1) = -(t13 * pr(1)) / 0.4e1 - (t15 * pr(3)) / 0.4e1 + (t15 * pr(5)) / 0.4e1 + (t13 * pr(7)) / 0.4e1; J(2,2)$

$= -(t13 * pr(2)) / 0.4e1 - (t15 * pr(4)) / 0.4e1 + (t15 * pr(6)) / 0.4e1 + (t13 * pr(8)) / 0.4e1;$

$J(2,3) = 0.0e0;$

$J(3,1) = 0.0e0;$

$J(3,2) = 0.0e0;$

$J(3,3) = 0.1e1;$

$detJ = J(1,1) * J(2,2) - J(1,2) * J(2,1);$

$iJ = eye(3); iJ(1,1) = 1 / detJ * J(2,2); iJ(1,2) = -$

$1 / detJ * J(1,2); iJ(2,1) = -1 / detJ * J(2,1);$

$iJ(2,2) = 1 / detJ * J(1,1); end function [SN$

$] = EBM_Q4_SNe(xxs, yys)$

$SN = zeros(6,12); t1 = 1 - xxs; t2 = 1 - yys;$

$t4 = (t1 * t2) / 0.4e1; t5 = 1 + xxs; t7 = (t5$

$* t2) / 0.4e1; t8 = 1 + yys; t10 = (t5 * t8) /$

$0.4e1; t12 = (t1 * t8) / 0.4e1; SN(4,1) = t4;$

```

SN(4,4) = t7;

SN(4,7) = t10;

SN(4,10) = t12;

SN(5,2) = t4;

SN(5,5) = t7;

SN(5,8) = t10;

SN(5,11) = t12;

SN(6,3) = t4;

SN(6,6) = t7;

SN(6,9) = t10; SN(6,12) = t12; end function [ varout ] = EBM_rad2deg( varin )

varout=varin*180/(pi); end function [pr_2d]=EBM_ReorderNodalPositions(array)

pr_2d=zeros((array.max_nnpe_2d-1)*2+2,array.ne_2d); for ii=1:array.ne_2d    nnpe_2d =
array.element(array.etype(ii)).nnpe_2d;    pr_2d(1:nnpe_2d*2,ii) = reshape(array.nl_2d(
array.el_2d(ii,2:nnpe_2d+1),2:3)',[],1); end end function [ iQg, jQg, vQg, iQm, jQm, vQm,
density ]=EBM_RotateElementMaterialConstMatrix(
array ) nQ=(6)*(6);

iQg=zeros(array.ne_2d*nQ,1);

jQg=zeros(array.ne_2d*nQ,1);

vQg=zeros(array.ne_2d*nQ,1)

iQm=zeros(array.ne_2d*nQ,1)

jQm=zeros(array.ne_2d*nQ,1)

jQm=zeros(array.ne_2d*nQ,1)

density=zeros(array.ne_2d,1);

```

```

[ Qm, Sm ] = EBM_ElementMaterialConstitutiveMatrix( array, e );
cf=cosd(-array.emat(e,3));   sf=sind(-array.emat(e,3));
[Qg]=EBM_ElemRotateLayer(Qm,cf,sf);
cp=cosd(-array.emat(e,4));   sp=sind(-array.emat(e,4));
[Qg]=EBM_ElemRotateFiberPlane(Qg,cp,sp);
Qm=(Qm+Qm')./2;   Qg=(Qg+Qg')./2;
iQm((e-1)*nQ+1:e*nQ)=reshape(kron((1:6)',ones(size(Qm,1),1)),size(Qm,1)*size(Qm,2),1);
jQm((e-1)*nQ+1:e*nQ)=reshape(kron((1:6)',ones(1,size(Qm,1))),size(Qm,1)*size(Qm,2),1);
vQm((e-1)*nQ+1:e*nQ)=reshape(Qm,size(Qm,1)*size(Qm,2),1);
iQg((e-1)*nQ+1:e*nQ)=reshape(kron((1:6)',ones(size(Qg,1),1)),size(Qg,1)*size(Qg,2),1);
jQg((e-1)*nQ+1:e*nQ)=reshape(kron((1:6)',ones(1,size(Qg,1))),size(Qg,1)*size(Qg,2),1);
vQg((e-1)*nQ+1:e*nQ)=reshape(Qg,size(Qg,1)*size(Qg,2),1);
end
end

```